A PIEZOELECTRIC FORCE MEASURING SYSTEM FOR HUMAN MOBILITY ANALYSIS

by

Paul Norman Estey

B.Sc.M.E., Queen's University
(1976)

SUBMITTED IN PARTIAL FULFILLMENT

OF THE REQUIREMENTS FOR THE

DEGREE OF

MASTER OF SCIENCE

at the

MASSACHUSETTS INSTITUTE OF TECHNOLOGY

(June 1978)

Signature of Author Signature redacted
Department of Mechanical Engineering, February 1978

Certified by Signature redacted
Thesis Supervisor

Accepted by Signature redacted
Chairman, Departmental Committee on Graduate Studies

A PIEZOELECTRIC FORCE MEASURING SYSTEM FOR HUMAN MOBILITY ANALYSIS

by

PAUL NORMAN ESTEY

Submitted to the Department of Mechanical Engineering on February 28, 1978, in partial fulfillment of the requirements for the Degree of Master of Science.

ABSTRACT

In response to the need to measure the foot-floor reaction forces in human mobility analysis studies, a system was designed using a matrix of force sensitive plates.

A state-of-the-art review of foot-floor force instrumentation and of the desirable attributes of an idealized system, one which would not compromise the path freedom or influence the natural gait of the subject, led to the invention of this new concept.

The system conceived consists of a "pathway" of rows and columns of 17.3 cm high, equilateral triangular shaped, aluminum plates, mounted on piezoelectric crystals. The crystals transduce the normal and shear forces exerted on them into an electric charge. Each plate measures the total forces and moments exerted on it, as well as the point of application of these forces.

Amplifiers to convert the piezoelectric charge into a voltage proportional to the stress applied to the crystal were designed and tested. Much stringent experimentation and attendant revision of the crystals, method of electrical and mechanical mounting and of the amplifiers resolved all but one difficulty, the voltage output produced lags the force input to the crystal in what appears to be a first order lag.

Some ideas are presented for the calculation of the resultant forces, moments and trajectory of the points of force application as a subject walks on the "pathway".

A performance and cost comparison is made of this triangle-pathway design with a commercially available biomedical force platform. Recommendations are made for the future development of the "pathway".

Thesis Supervisor: R.W. Mann
Title: Whitaker Professor of Biomedical Engineering

ACKNOWLEDGEMENTS

I wish to thank Professor Mann for giving me the opportunity to conduct this study and his endless patience with my constant ineptitude. I am also grateful to all the members of the Mobility Facility, both staff and students, who's encouragement, advice and compatriotism helped me along. Special thanks must be given Ralph Burgess who's many hours of guidance and teaching were invaluable to me.

I cannot leave out my office mates and friends; Jon for struggling along together with me, Dave for his expert advice in producing this thesis and Erik who's witticisms and comments made for a relaxed working atmosphere. Many thanks gents.

Last and far from least I would like to extend my gratitude to all the members of the MIT Varsity Hockey teams of 1976-77 and 1977-78, most especially; "Stag", Barry, Don, Lou, and Al, without whom it is questionable whether I would have survived my two years here. Sorry for all those cheap goals but I'm glad to have helped the team along and wish you good luck in the future.

TABLE OF CONTENTS

LIST OF FIGURES

CHAPTER 2

CHAPTER 3

LIST OF TABLES

CHAPTER 1 INTRODUCTION

1.1 Introduction

Studies of human mobility require the measurement of several parameters of the body in motion. Such information, can produce analyses of the forces and moments at various skeletal joints in the body. Data sought includes the displacements, velocities and accelerations of the limbs and body segments and the activity of relevant muscle groups, usually employing electromygraphic measurements. To supplement these measurements, information on the foot-floor reaction is desired, normally using a force plate measuring system. This thesis is a report of a design study of a novel force measurement system for human mobility analysis. The work was done in the Mobility Facility of the MIT Mechanical Engineering Department and supervised by Professor R.W. Mann.

Much of the research in the Mobility Laboratory addresses how to best augment handicapped humans with limb and sensory protheses. The general approach is man-interactive computer simulation. In a typical experiment, a person is mobile in the 10 by 30 meter Mobility Facility space. By means of a kinematic data acquisition system called TRACK, the computer is continually updated, in real-time, on the position and orientation of portions of the person's body pertinent to the experiment. The computer is preprogrammed to detect and respond to significant features of the person's movement or trajectory, by relaying via telemetry to the person and/or to his prosthesis information germane to the experiment. The TRACK system then records the human's behaviorial response.

Specific examples of the use of this system would include, for

example, detecting the knee flexion angle of an above-knee prosthesis wearer in combination with other physical and biological signs (i.e., foot-floor force, muscle electromyographic activity, etc.). Upon receiving this data, and subject to an experimental hypothesis, the computer would change the artificial knee characteristics during a stride. Or, as another example, for the study of optimal presentation of surrogate sensory information to a blind traveller, the computer informed by TRACK of the proximity of the traveller and an obstacle could stimulate a tactile and/or auditory display on the human and then record the traveller's path change.

Such a mobility facility offers a powerful and flexible design capability in the search for and evaluation of optimal cybernetic protheses. Beyond these on-line, real-time studies the Mobility Facility is engaged in biomechanical studies of human gait using off-line analyses of stored data.

A full complement of instrumentation for the Mobility Facility must include; beyond the TRACK system which establishes the 6 degrees of freedom of up to ten body segments, and the EMG telemetry system which transmits data from fourteen muscles, a foot-floor force measuring system superior to conventional force plates. Such devices, approximately 40 cm square plates flush with the floor, produce force and moment information when stepped on. Since however, the subject must be somehow steered onto the plate, by guides, visual signs, or otherwise, the naturalness of the experiment is inescapably compromised. The foot-floor force measuring system should not influence the freedom of the subject

any more than our totally unrestricted TRACK and EMG systems do. This thesis is concerned with developing such a foot-floor measuring system.

The force measuring system proposed in this thesis consists of rows and columns of small (20 cm on the side) equilateral triangular shaped force plates. Each plate would measure the foot-floor reaction forces in three orthogonal directions: vertical force, fore-aft and lateral horizontal forces. Each plate would also establish the point of application of the external force vector and the moments about the three axes through this center of force.

Several force transducers were considered. However, piezoelectric crystals were the most extensively studied. These crystals develop a charge proportional to the stress exerted on them. Instrumentation was designed, constructed and tested to convert the piezoelectric charge into a voltage suitable for data acquisition and computation. Consideration was given to a system of data collection and reduction from a matrix consisting of several of the plates. Finally, the design concept was compared with a presently available commercial force plate measurement system.

1.2 Organization of the Thesis

This thesis is divided into five chapters. The introduction, Chapter 1, gives a brief overview of the project. The remaining chapters are outlined below.

1.2.1 Chapter 2

Chapter 2 reviews force measuring systems and techniques used by

prior researchers. It is divided into sections according to the approach to force measurement. Section 2.2 deals with measuring pressure at a certain point on the foot. Section 2.3 discusses foot-mounted transducing systems and schemes where an attempt was made to obtain a distribution of the forces over the foot. The next part, 2.4 covers large force plates. It is further subdivided into divisions each dealing with one of the four most common force transducers used: springs, strain gauges, linear variable differential transformers and piezoelectric crystals.

1.2.2 Chapter 3

This chapter introduces the triangle-pathway concept. It reviews the requirements of a force sensing system for use in human mobility and gait analysis and the development of the basic idea. Analyses of triangle size, mass and dynamic performance are presented, as well as some preliminary ideas on data collection and reduction. The chapter ends by introducing the transducing elements considered for the pathway.

1.2.3 Chapter 4

Chapter 4 is devoted primarily to piezoelectric crystals. A description of the piezoelectric effect is presented. Amplifier designs for use with the crystals and their development are described. Problems encountered with the crystals are reviewed. Two following sections describe other force transducing methods which measure the deflection of an elastic member to determine the force. The first method uses strain gauges and the second uses linear variable differential transformers.

Again the underlying theory of operation of each device is presented. A comparison of force transducers is made in the last section.

1.2.4 Chapter 5

The final chapter describes a presently available force plate manufactured by the Kistler Corporation (32). This plate is then compared with the triangle-pathway system giving the advantages and disadvantages of each system.

CHAPTER 2 A BRIEF HISTORY OF FORCE SENSING SYSTEMS FOR BIOMEDICAL USE

2.1 Introduction

For many years now, researchers have developed methods of quantifying the force in the foot-floor reactions occuring in human ambulation and other activities. As early as 1872, Murey and Caret (as reported by Cunningham (14) and Bresler and Frankel (5)) used a pneumatic load cell on the sole of a shoe.

Generally there are three areas in the overall study of human movement that require knowledge of the foot-floor reaction forces; 1) gait analysis, 2) energy studies of the working human, 3) biomechanical studies of sport.

Elftman (18,19) was the first to use force studies in his gait analysis work in 1934. He constructed a spring scale force plate and used it in conjunction with movies of persons walking across the force plate. Jacobs and Skorecki (29) used a "gait machine" built by Skorecki in 1972 to study the behaviour of normal and pathological gait. Hargraves and Scales (24) used a foot mounted transducer in their studies of the effects of corrective surgery on walking. Gait studies are underway now at numerous institutions using various force measuring devices and systems.

Lareau (35) was the first to use a force plate to study the exertion of the body in performing work. He used his force plate to investigate bricklaying, bending and stooping, operating a lathe and office tasks. Since then, Greene (23) built a "force platform" which was improved upon by Whetsel (67) and then Hearn and Konz (26). This platform was used to study body position as well as forces required to achieve a certain task. Whitney (68) used his force plate to study the differences in foot placement, and grasp height and type in lifting a horizontal bar.

Much use has been made of force plates in the study of sport. Payne (48) used a force plate while studying weight lifting, sprinting, tennis, hurdling and shot-putting. Ramey (52) examined the long jump using a force plate of his own design. Cooper and Ward (11,12) examined various sporting activities, including the golf swing.

Different approaches have been taken in the investigation of the foot-floor reaction, ranging from obtaining the force at a particular point, Hennacy (27), to pressure distribution throughout the foot, Arcan and Brull (1), to the more common determination of the total forces and moments exerted by one and possibly two feet using a large force plate.

In view of this variety, this chapter is divided into 3 sections. The first deals with the analysis of force at a point, the next with pressure distribution and foot-mounted force sensing systems and the next with large sized force plates. The latter subject is divided into 4 parts according to the method of force transduction, there being 4 popular techniques; springs, strain gauges, linear variable differential transformers and piezoelectric crystal transducers.

2.2 Pressure at a Point

One method of obtaining the force at a particular point on the foot is through the use of small piezoelectric crystals taped to the location the force measurement is desired, as described by Richard Hennacy (27) in his 1975 paper in the Journal of American Podiatry Association.

Piezoelectricity is described fully in section 4.1. However, briefly it is an effect found in certain crystals whereby when subjected to a stress the crystal develops a charge which can be measured. Since this charge is

proportional to the force exerted on the crystal, a crystal, with the proper electronics, can become a force transducer.

Heannacy used a crystal .953 mm in diameter and .51 mm thick with a voltage follower amplifier to sense the forces. He claims linearity in sensing forces up to 456 Newtons both statically and dynamically although no figure for the deviation from a straight line is given. The crystals and appropriate lead-in cable were attached to the foot by using a spray adhesive and tape. The six areas of interest to his group were: the 1^{st}, 3^{rd} and 5^{th} metatarsal, the navicular, lateral heel and medial heel. Socks were worn over the transducers to minimize the sensation due to their presence.

2.3 Pressure Distribution and Foot Mounted Transducers

2.3.1 Early Attempts

The first attempts at measuring the actual pressure distribution across the foot was made by Beely in 1882 (from Cunningham (14), Stokes (63) and Scranton (57)) who made footprint impressions of his subjects as they walked on a thin bag filled with plaster of paris. Morton (41) in 1935 and Elftman (19) in 1934 used rubber mats with smooth upper surfaces and either triangular corrugations (Morton) or pyramidal shaped projections (Elftman) on the lower surface which sat on a plate of glass. A movie was taken through the glass as a footstep occured thereby giving a qualitative analysis of the pressure distribution with time during the foot-floor interaction.

2.3.2 Liquid Crystals

More recently quantitative data has been sought. This is not an easy

task since the method must not affect normal gait. The technique invented by Scranton and McMaster (57) in 1976, although not fully quantitative at the time of reporting, holds promise. It used the recently discovered "Liquid Crystals", commonly used as displays in digital watches. These crystals are lypotrophic and cholesteric substances that change colour from light blue to dark blue when a pressure is exerted on them. The crystals were encased in a flexible 23 by 30 cm plastic sheet lying on top of a plexiglass plate. A camera and suitable lighting under the plate (as shown in Figure 2.3.1) recorded the footfall as the subject stepped on the sheet. Quantitative analysis of the wavelength change of light reflected from the crystals has yet to be done, but is planned.

2.3.3 Load Distribution Across the Foot by Multiple Beams

Stokes, Stott and Hutton developed a quasi pressure determining force plate in 1974 (63,64). Their system consisted of a 7 m walkway in the middle of which was inserted a load measuring area 144 mm by 400 mm. The load sensing device, as shown in Figure 2.3.2, was constructed of 12 beams 11 mm wide and 400 mm long, each with knife edge supports and a reduced section at each end. Strain gauges were mounted on both the top and bottom of each reduced section wired in a full bridge circuit such that the sum of the bending movements was obtained, this sum being proportional to the vertical load exerted on the beam. They report linearity of force transduction of $\pm$ 2% for vertical loads up to 500 Newtons with less than 2% variation of output for different loading locations on the beam. Sensitivity to horizontal forces was down 18 db from that for vertical forces. The measured unloaded natural frequency of a beam was 350 hz; with a 70 kg load the

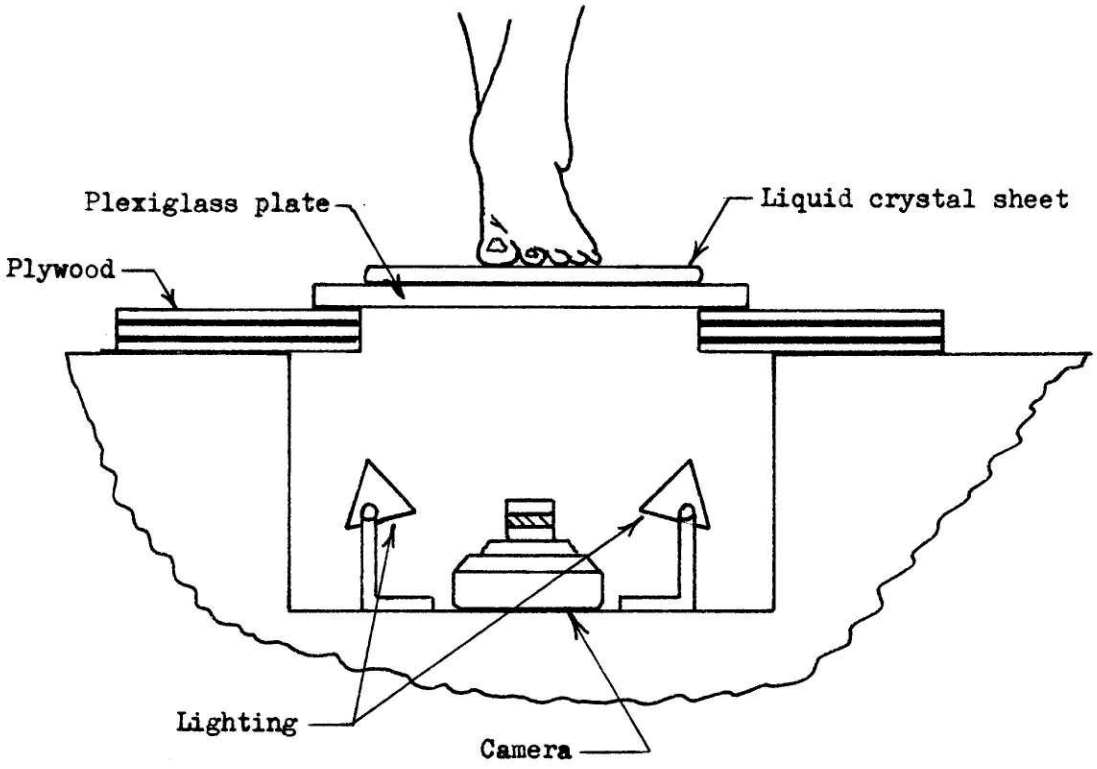

Figure 2.3.1 The use of liquid crystals for obtaining the pressure distribution across the foot.

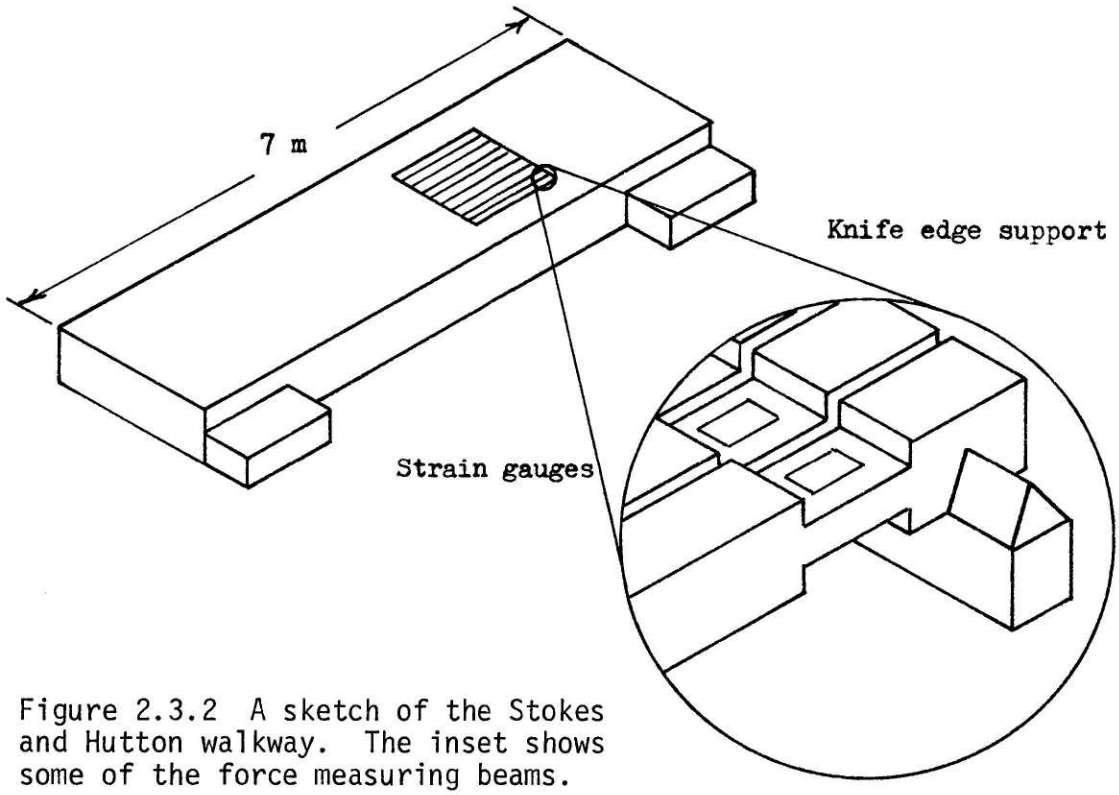

Figure 2.3.2 A sketch of the Stokes and Hutton walkway. The inset shows some of the force measuring beams.

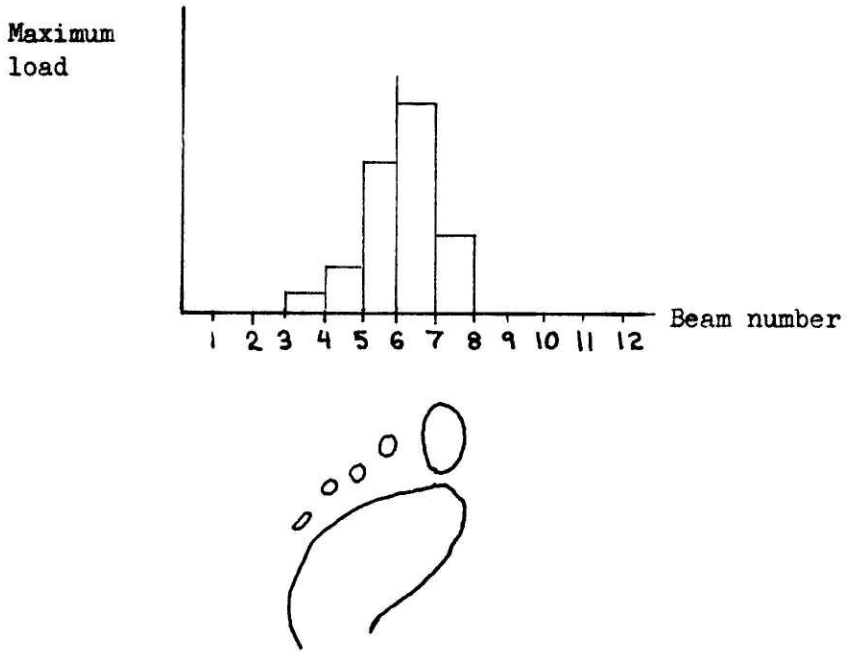

Figure 2.3.3 A comparison of maximum load with position.

natural frequency was 150 hz.

The outputs from the 12 bridge curcuits was recorded by an Ultraviolet recorder giving a load versus time trace. Also, these signals were put through analog circuitry capable of storing the maximum voltage from each circuit, thus a record of maximum load was obtained. During tests the force measuring area was covered with a piece of plastic with the underside inked. Below this was placed a piece of paper, so that when the subject walked over it, a permanent record was made of his footfall. The subjects walked over the force sensing area barefoot to make a better impression. The comparison of maximum force and foot position was said to help in the diagnosis of patients (Figure 2.3.3).

2.3.4 A Force-Sensing Leather Sole

Along the lines of the Elftman and Morton rubber mats was the Arcan and Brull (1) leather sole, on which were mounted hemispherically shaped solids. The amount of deflection of the solids indicated the loading in the following manner. The system consisted of three parts; a platform, an imaging system and the leather sole. The platform was constructed in four layers (refer to Figure 2.3.4); a stiff transparent plate, optical filters, optically sensitive elastic material and a reflective layer. The imaging system was composed of a light source, a mirror at 45^{o} to the plane of the platform and either a T.V. camera connected to a recorder or a movie camera.

As the subject transversed the platform, the solids deflected the photo elastic sheet according to their applied force distribution, causing circular interference patterns to form, which were recorded. Knowing the re-

lationship of diameter of interference fringe versus load, the load can be calculated by measuring the diameter of the interference pattern created from each solid. Unfortunately, the calibration curve of diameter of interference pattern versus load was distinctly nonlinear especially at high loads. However, at low loads the nonlinearity was not so great as to lead to large error thus by increasing the number of solids per unit area, the authors claim adequate accuracy was possible. A second problem encountered was that in order to obtain a pressure distribution each solid area needed to be measured, which was a tedious job. Work was being done to interface the T.V. camera with a computer to automate the calculations.

2.3.5 Force Transducing Insoles

Holden and Muncey (28) developed a force transducing insole that was based on a change of capacitance indicating force. Their transducer consisted of a double condensor arrangement using layers of foil and rubber mat, pimpled as on table tennis bats, as shown in Figure 2.3.5. Overall the assembly was 3.2 mm thick and had a 3.2 sq cm pressure sensitive area. Using the "gauge" as a capacitor in an oscillator circuit, the change in capacity was measured as force was exerted on the assembly compressing the rubber and reducing the distance between the plates. The oscillator circuitry was strapped to the subject's leg during experiments, and connected to a discriminator which deflected a cathode ray tube spot, which was photographed. No information on sensitivity or linearity was given in their report, however they claim a "high frequency response limit" of 2000 hz.

Another foot mounted transducing scheme was that used by Hargraves and

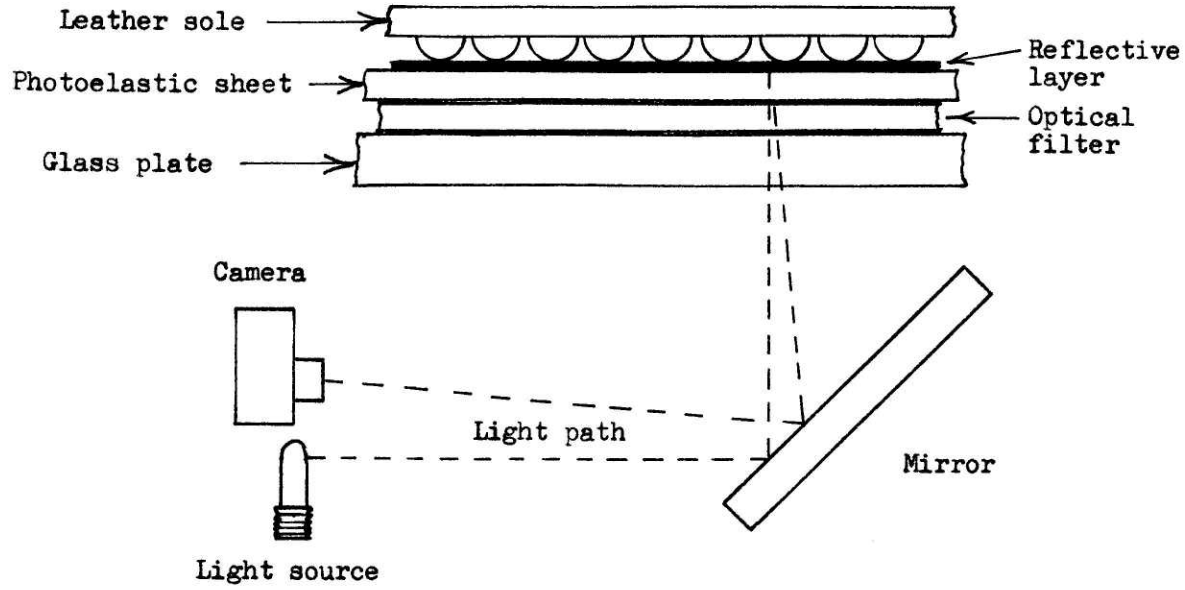

Figure 2.3.4 The light system used by Arcan and Brull.

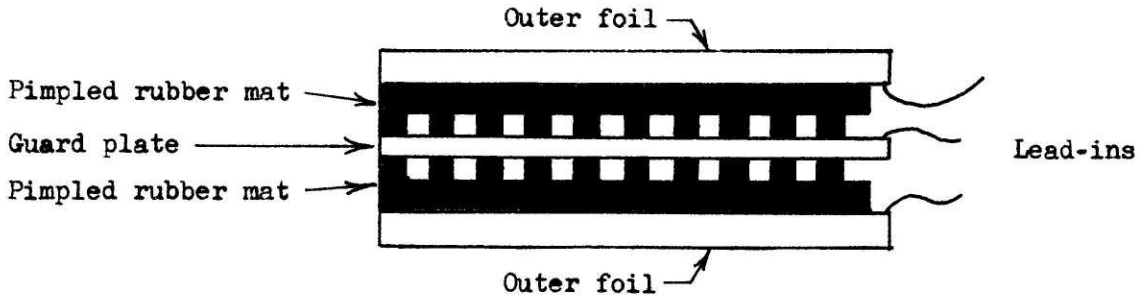

Figure 2.3.5 The capacitive force "gauge".

Scales (24). They describe a sandwich transducer which was used to replace the insole of a canvas sports shoe. The force information was telemetried out to receivers which processed it. No information was given on the actual construction of the transducer, although it was believed to be a variable capacitor similar to that of Holden and Muncey.

A foot mounted scheme, using a strain gauged, Belleville spring actuated transducer was developed by Rick Levin and his colleagues (38) at Harvey Mudd College. A sketch of the transducer is shown on Figure 2.3.6. Four such transducers were mounted in a leather sandal at the great toe, the 1^{st} and 5^{th} metatarsal and the heel. As the load was applied to the top of the transducer, the Belleville spring would be flattened, exerting force at its edge on the transducer plate, thus causing it to bend. With the semiconductor strain gauges mounted at the reduced section as shown, this bending was measured giving an output proportional to force. Problems were encountered with the output voltage not being linear to the force applied, but this nonlinearity was reduced sufficiently to allow the use of the sandal in the diagnosis of patients.

2.4 Force Plates

2.4.1 Springs as Transducers

Herbert Elftman's work (18) in 1934 was the first done with what is now called a force plate, a large floor mounted plate onto which the subject steps in order to obtain the forces in the foot-floor reaction. A sketch of the system devised by Elftman is shown on Figure 2.4.1. The total force and center of force was obtained by using the vertical displacement at points 1,2,3 and using moment calculations. The upper plate rolled on

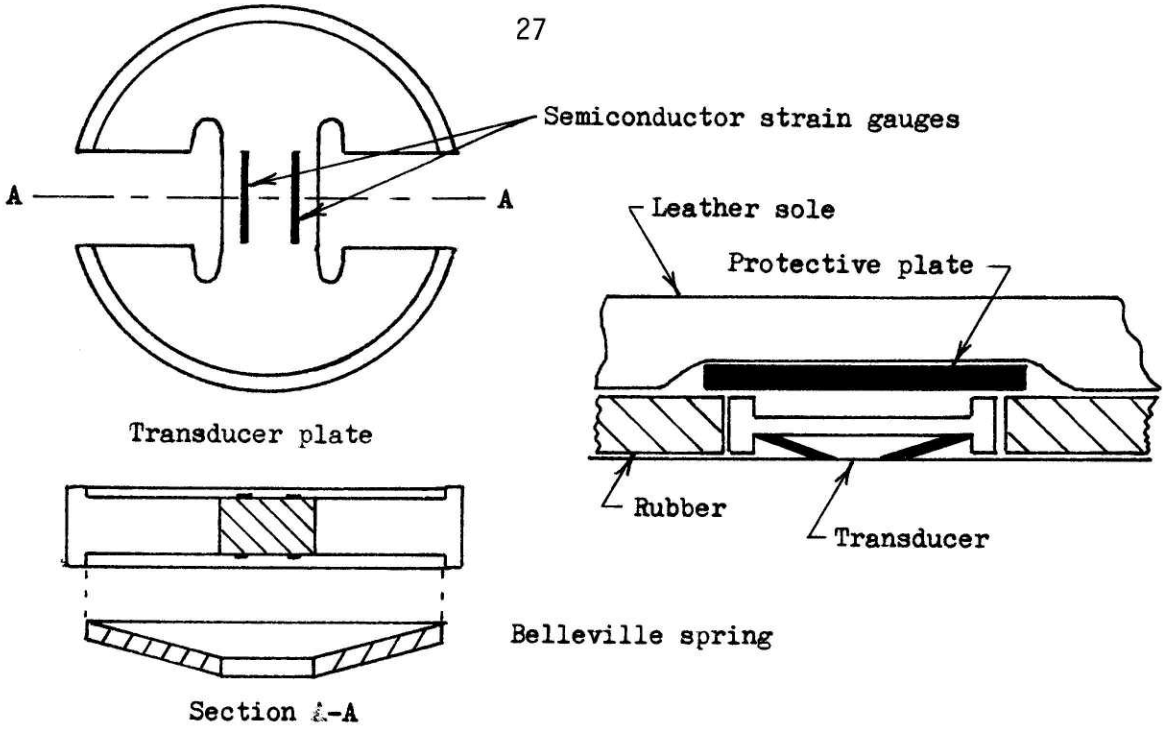

Figure 2.3.6 A sketch of the Levin transducer.

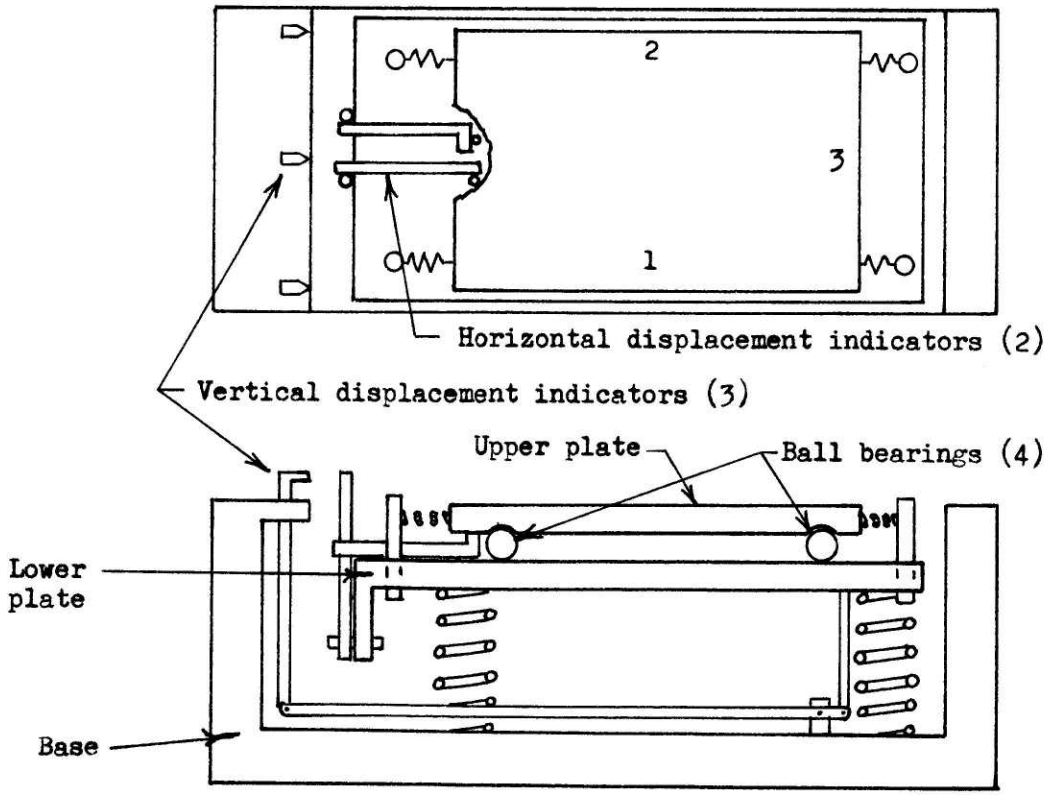

Figure 2.4.1 The spring scale force plate used by Elftman.

ball bearings on top of the lower plate and was restrained by springs attached to the lower plate. The frontal and lateral displacements were measured by indicating levers which amplified the actual motion. Movie pictures were made of the position of the levers as the subject walked across the plate. A pendulum swung in the field of view of the camera was used to time the data.

Since this work, most force plate transducers have used more modern techniques as described in further sections however a plate designed by Patel (46) in 1971 used the displacement of U-shaped springs to measure forces. In this design an aluminum plate was mounted on top of the inverted U-springs with a ball bearing race sandwiched in between thus allowing horizontal movement. This horizontal motion was restrained by coil springs in one direction and rubber blocks in the other. The horizontal displacements of the U-springs as a vertical force was exerted on them were sensed by a wire-potentiometer arrangement.

2.4.2 Strain Gauged Transducing Elements

Many researchers have used elastic members with bonded strain gauges to determine the deflection of the transducer element and thus the force exerted. This approach is described more fully in Section 4.2. Various load cell configurations have employed columns, cantilever beams, circular tubes and proving rings. Examples of these methods are reviewed in the next 5 subsections.

2.4.2.1 Columns as Load Cells

A classic example of the use of a strain gauged column to detect forces

on a plate attached to the column is the force plate designed by Cunningham and Brown (14) at the University of California. A diagram of the essential elements of the system is shown on Figure 2.4.2. The plate was .38 m by .5 m cast aluminum rigidly bolted in the four corners to 13.3 cm high 16 mm diameter tubular aluminum columns, that were in turn fixed to a steel base plate. Vertical load, and the coordinates of the point of application of force on the plate were measured with 6 gauges on each column. Horizontal forces in both directions were calculated from the strains measured by four gauges per column and torques about a vertical axis obtained from the strains in 2 gauges per column. The natural frequency of the plate was 105 hz in the horizontal direction, resulting in resonance in this mode when a load was applied. To overcome this problem, a damping system was constructed using a viscous oil film between the top plate and bottom plate. Linearity of the system was stated to be 6% in the vertical mode and 2% in shear and torque. The Cunningham and Brown plate was used by Bressler and Frankel (5) in their gait studies. This basic design was modified by Paul (47) and Payne (48).

Another common configuration using columns, illustrated by Figure 2.4.3, incorporates a central column supporting a top plate and attached to a lower plate. From the strain in this column, measurement of torque, shear forces and center of application of force could be made. The lower plate was supported on three other vertical columns which measured the total vertical force. This basic scheme was used independently by Cooper (11,12) and Endo (20).

Yamashita (69) used only the three point supported lower plate design with a large right angled isosceles triangular shaped plate, thus only

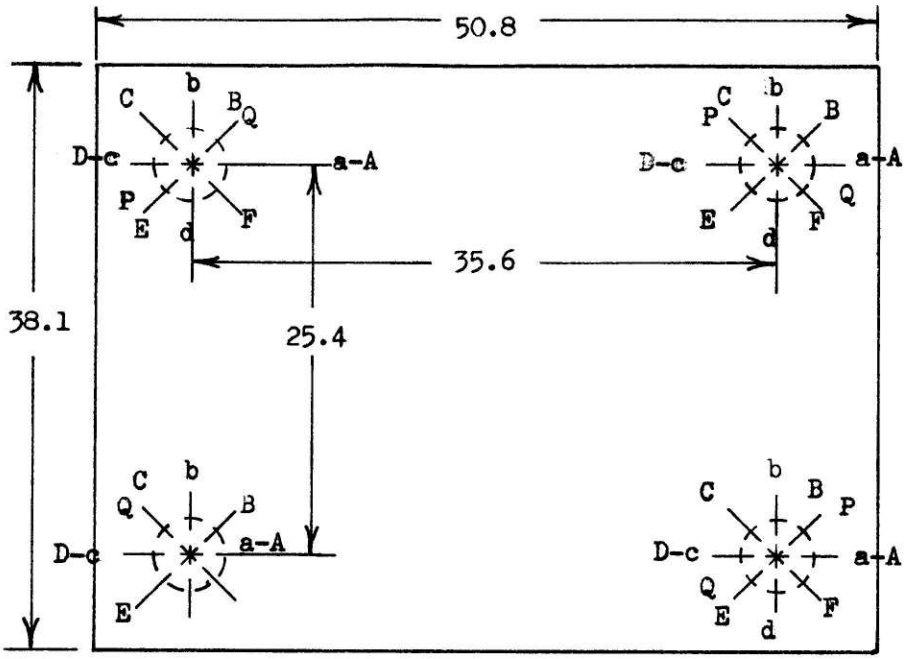

All figures in centimeters.

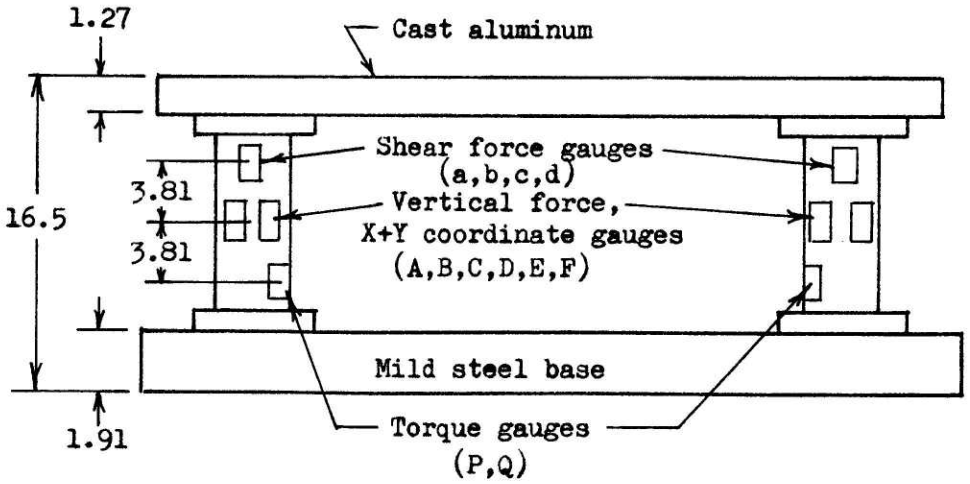

Figure 2.4.2 The Cunningham and Brown plate.

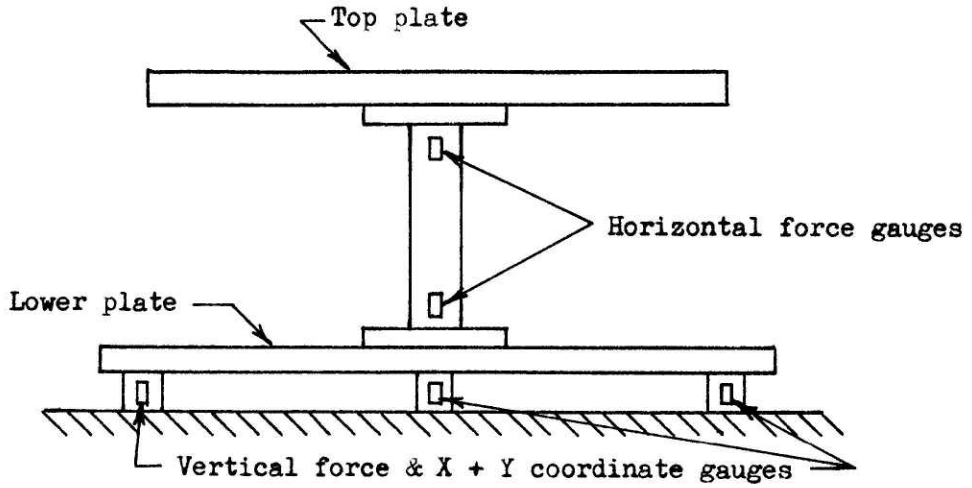

Figure 2.4.3 A sketch of the central column technique.

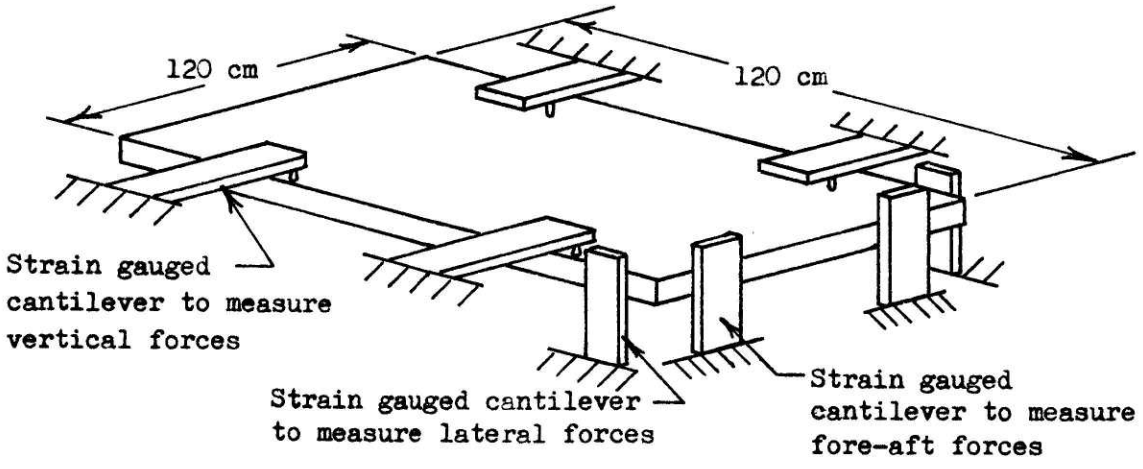

Figure 2.4.4 A sketch of a force plate using cantilever beams.

vertical forces were obtained. The 2.2 m long hypotenuse of the triangle was used as a walkway for the subjects. The study was aimed at discovering the point of application of the vertical force during level walking.

2.4.2.2 Cantilever Beams

The force plate designed by Whitney (68) used four cantilever beams to support a 123 cm on the side square plate in the vertical mode and eight beams (two in each corner) to restrain the plate's horizontal motion. This design is pictorially presented in Figure 2.4.4. The plate was actually a box-girder style platform made of dural which weighed 40 kg. Damping was provided at the corners for all three modes of vibration using oil filled bellows because the undamped natural frequency of the structure was 37 hz in the vertical mode and 25 hz in the horizontal mode. A total of 40 gauges were used and connected in bridge circuits to give six channels of information: three forces and three moments about the axes. The linearity of measurement was .1% in the vertical mode and cross sensitivity was reported as negligible.

Carlsoo (7) at Stockholm University used a design in which the plate was supported by four vertical flat springs, 50 mm long, 12 mm wide and .4 mm thick, as shown in Figure 2.4.5. The springs were instrumented with eight strain gauges, wired to give the three orthogonal forces and moments. Carlsoo was interested in studying walking on different surfaces.

2.4.2.3 Horizontal Tubes Supporting Plates

Ramey (52) was the first to report using circular tubes laid horizontally as the elastic member from which forces are determined. His design

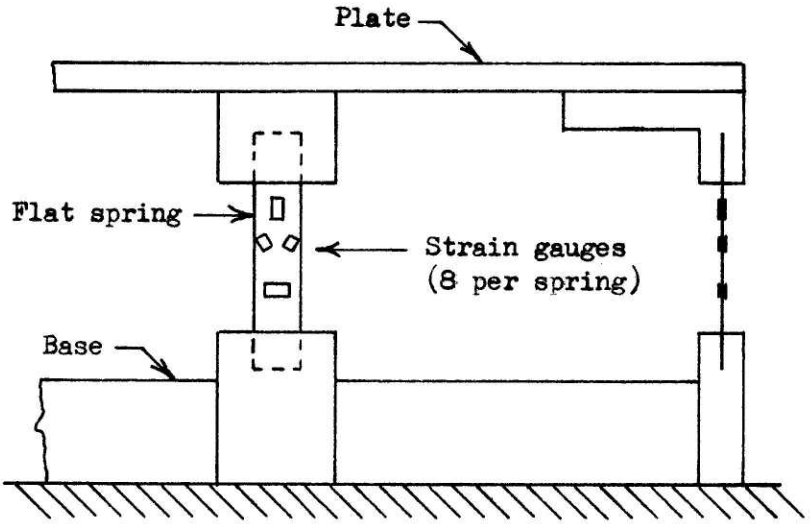

Figure 2.4.5 The force plate system used by Carlsoo.

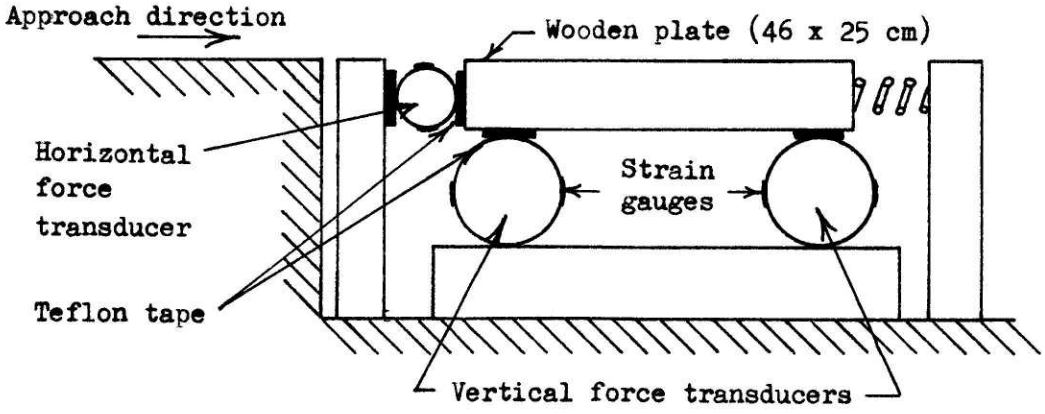

Figure 2.4.6 The Ramey designed force plate.

(Figure 2.4.6) used three tubes in all, 10.2 cm in diameter for vertical supports and 7.6 cm diameter for the longitudinal supports, upon which a 25 by 46 cm plate was placed. To suppress cross talk, the plate-tube interface was Teflon tape, allowing free sliding to occur. Unfortunately, lateral forces could not be measured. The strain gauges measured the distortion of the tubes with force.

2.4.2.4 Proving Rings

The final common configuration using strain gauges as elastic force transducers is the use of proving rings. A proving ring, as shown in Figure 2.4.7 is usually octagonal in shape and is normally used to support a corner of the plate. Cavanagh (8) used this scheme with two proving rings oriented along the x axis (frontal axis) and two along the y axis (lateral axis). In this way it was possible to determine the three orthogonal forces and moments. While Kirkpatrick (34) used much the same scheme, he supported the plate on top of the transducers with ball-vee grooves. The purpose was to reduce cross-talk by allowing motion in the direction of the vee and transmission of force in a direction transverse to the vee. Unfortunately, the decrease in cross-talk also decreased the natural frequency in the horizontal mode to 38 hz (34).

2.4.3. Linear Variable Differential Transformers as Force Transducers

The linear variable differential transformer (abbreviated LVDT) is a device which measures movement by a change in inductance. This device is described fully in Section 4.3. For use with force plate systems, an elastic member is used to support or restrain the plate and the deflection of

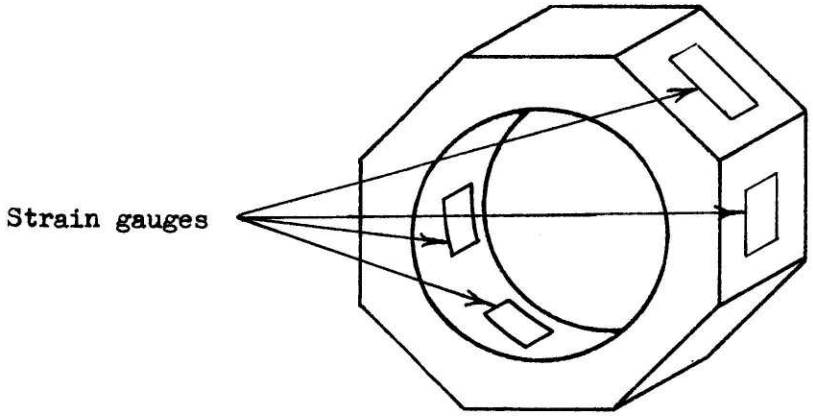

Figure 2.4.7 A proving ring with strain gauges.

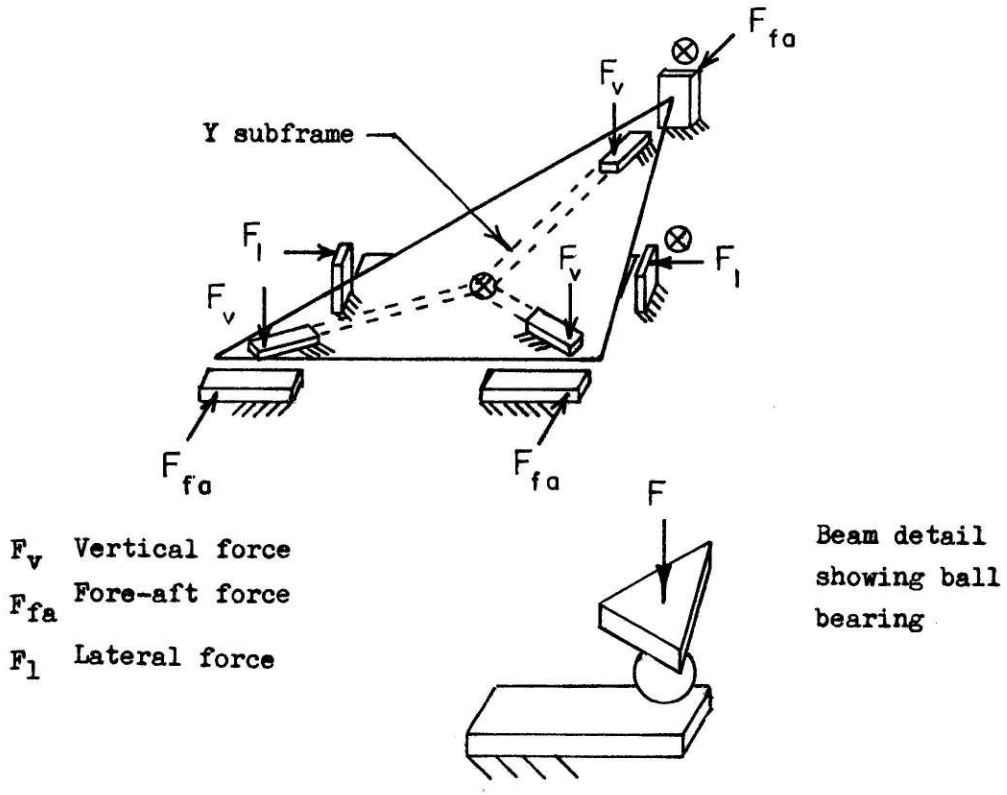

Figure 2.4.8 The Greene and Morris concept.

this member is measured to give the indication of the force exerted on the member. In this respect then, this system is similar to strain gauges.

Greene and Morris (23) were the first to use LVDT measurements in a force plate. Their plate was a triangular shaped piece of plywood, 12.7 mm thick, supported by a Y-shaped tubular steel frame. The frame's movement was resisted by three high strength cantilever beams, one in each corner, for the vertical mode and five cantilevers for the horizontal modes. This is diagrammed in Figure 2.4.8. Each cantilever, as shown by the detail from Figure 2.4.8, contacted the Y subframe with steel ball bearings, partially recessed into triangular shaped steel plates. Only three LVDTs were used, one at the center of gravity of the triangle, one at the midpoint of one side and the last at the apex of the triangle. Using this scheme only the total forces; vertical, frontal and lateral could be measured. The voltage from each LVDT was recorded by a strip chart recorder.

Whetsel (as reported by Hearn (26)) added another triangle on top of the Greene and Morris design to form a hexagon. He also preloaded the vertical beams thus allowing equal response up and down. However, Hearn reports that dynamic force measurements were not equal to the same force applied statically. At a loading frequency of 2 hz, there was a 10% increase in sensitivity in the vertical mode and 30% in lateral and 50% in frontal shear modes.

Hearn (26) continued improving this basic design. He fabricated the hexagon of cast aluminum and increased its size from 30 to 38 cm per side. As well, two LVDTs were added per axis to give torque readings about each axis. The reported natural frequency was 100 hz for vertical vibrations and 2500 hz for the frontal and lateral axes. The platform as described

above was used in the evaluation of the forces and body positions concerned with the performance of various tasks.

2.4.4 Piezoelectric Platforms

2.4.4.1 The Effort Detector

The piezoelectric effect as mentioned in Section 2.2 and described in detail in Section 4.1 was first used in a force plate called an "Effort Detector" by Larau (35) in 1957. His plate a sketch of which is shown in Figure 2.4.9, used three quartz piezoelectric transducers between two triangular shaped plates to measure the vertical forces. The horizontal forces were measured by two transducers rigidly connected to the base at the apex and along one side, "in close contact" with both triangular plates. The crystals were connected to an electrometer with an input resistance of 10^{15} ohms. The output of the electrometer was connected to a two stage amplifier and recorded by an oscillograph. Unfortunately, only dynamic forces could be measured by his amplifier. This system also was used to study man performing work.

2.4.4.2 The Kistler Plate

Technological improvements in the piezoelectric crystal method now permits the measurement of static as well as dynamic forces. The plate manufactured by the Kistler Corporation (32) for biomechanical studies is an example of a modern "Effort Detector". This plate described more fully in Chapter 5, measures 40 by 60 cm with transducers in each corner. These transducers are able to detect forces in all three orthogonal directions due to piezoelectric crystals that respond to normal or shear forces.

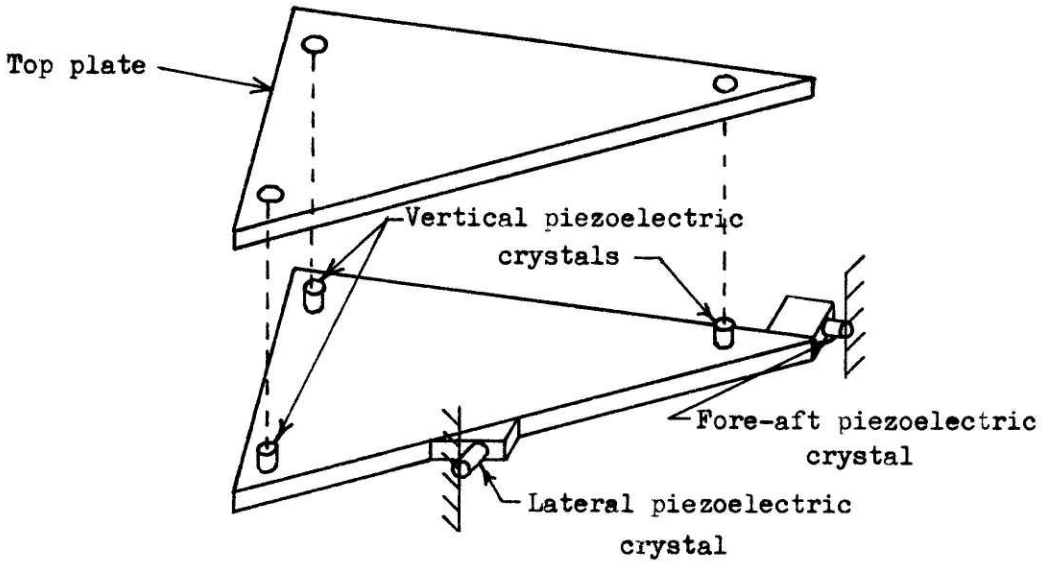

Figure 2.4.9 The Larau piezoelectric force plate.

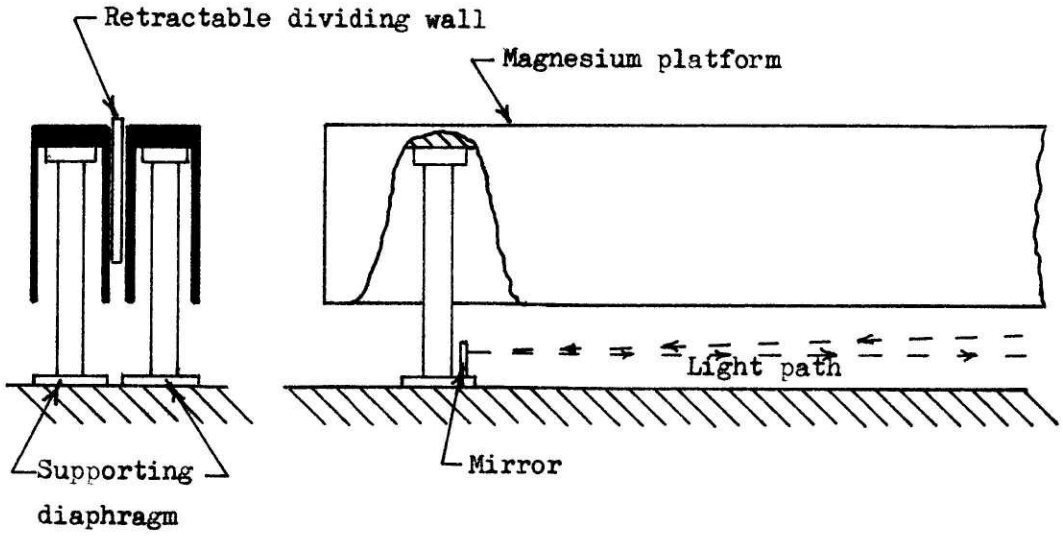

Figure 2.4.10 The "gait machine".

Thus all three orthogonal forces can be detected as well as the three moments and point of application of the force. The natural frequency of greater than 200 hz, excellent linearity ($\leq$ 1%) and low cross talk ($\leq$ 2%) make it useful for many biomechanics studies (52).

2.4.5 The Gait Machine

One force transducing system that falls into none of the above categories is the "Gait Machine" designed and built by Skorecki (59) at the University of Manchester. His system consisted of two magnesium platforms in the shape of inverted channel beams 50.8 cm deep, 2.8 m long and 17.8 cm wide, mounted side by side, each beam supported near the ends by columns which were attached to diaphragms (Figure 2.4.10). The diaphragms were 15.2 cm in diameter, 2.33 mm thick and deflected with applied load. The spring constant of the diaphragm was 8.76×10^3 N/mm. As each diaphragm deflected, it reflected an ultraviolet light beam proportionally to the deflection onto photosensitive paper thus reproducing the load variation. The diaphragm was damped by the use of an adjustable orifice through which motor oil (SAE 20) was forced. The system was supported from moving transversely by leaf springs attached to the base. Thus only vertical force measurements were made but since there were two beams and they were so long, it was possible to obtain force-time records of both feet for several paces.

2.5 Conclusion

This has been a brief review of the methods and systems employed for the measurement of the foot-floor reaction forces. It is not intended to be a complete and comprehensive report but rather a summary of examples

of the different techniques employed by scientists and medical doctors to date. The next two chapters describe and analyze a different approach taken by the author to determine the magnitude, location and direction of the forces in the interaction of the foot and floor.

CHAPTER 3 THE TRIANGLE-PATHWAY APPROACH

3.1 Introduction

Many different designs have been considered for force measuring systems useful for researchers and medical doctors in their research and/or diagnosis. The previous chapter has described some of these methods and identified problems experienced. This chapter describes the approach adopted by the author at the Mobility Facility of the MIT Mechanical Engineering Department. The students and faculty in this laboratory are involved in a number of human mobility studies which would benefit from foot-floor reaction force measurement.

"Force Plate Meetings" comprised of these individuals influenced this design. A comment at one of these meetings describes the ideal force sensing system:

> The perfect force plate would be an aerosol spray, that we would spray onto the subject's feet. This spray would transduce the force at every point on the foot, telemeter the data to the computer which would give us the pressure distribution throughout the foot. Such a system would be absolutely linear and have an infinite frequency response (22).

Indeed, such a force measuring technique would be ideal for the studies contemplated. However, at this time (1978) this notion is not technologically feasible. What is considered feasible is the triangle-pathway design arrived at and analyzed in this study.

3.2 The Design Requirements

While requirements of a biomedical force transducing system are few, they are not necessarily easily satisfied. As defined by the personnel of the Facility, the requirements are as follows:

The system must allow free movement of the subject, both while wearing shoes and in bare feet. In particular the system must not require "lining-up" the subject with the force sensing area as is necessary with most of the systems described in Chapter 2. Such pre-orientation of the subject inevitably prejudices natural unfettered movement and places in question the validity of the force measurements. This compromising of the subject is especially troubling with pathological cases, including children. Furthermore, since this laboratory is concerned with general mobility, not just gait analysis, the direction of travel cannot be preordained. Further it is important to collect data from two consecutive strides of the subject, that is both feet striking the sensitive area twice. This presumably redundant data will increase confidence in its validity and repeatability. If possible, it would be desirable to obtain a pressure distribution over each foot.

Maximum load levels of 2224 Newtons in the vertical direction, 112 N in the lateral and 622 N in the fore-aft directions were set for the system. Such large loads, which are roughly twice those expected for the normal gait of a 100 kg man, were chosen to allow for the possible case of people jumping on the plate.

Finally, as high a natural frequency of the measurement system as possible was desired in order that peak dynamic forces can be measured accurately. As can be observed from Chapter 2, the undamped natural frequency of many systems was low enough that when stepped upon, they tended to resonate at their natural frequency, thus confusing the actual force data. Holden and Muncey (28) report frequency components as high as 500 Hz in heel strike.

3.3 Early Concepts

The requirement of bare footed walking combined with freedom of movement negated the use of foot-mounted transducers such as Holden's (28) or Levin's (38). These transducing systems tended to hinder normal gait if for no other reason than that the subjects were not accustomed to the feel of the shoes attached to the transducers (28). Although these foot mounted systems did allow taking data on stairs, ramps and uneven surfaces, this was not considered a promising enough feature to counterbalance the special shoe requirement. Similarly a large, floor mounted force plate was rejected because this requires that a definite target be hit by the subject, a restriction that was to be avoided at all costs.

The idea of numerous small plates, placed on the floor, was then considered. The size and shape of such plates was the next hurdle to cross. To obtain any kind of pressure distribution across the foot many small sensors would be required in a mat-like matrix on the floor. This idea led into the transducer problem, since most standard force transducers were not small enough to fit the size need, ideally a matrix of 5 mm or smaller square sensors. The only force sensing element small enough were piezoelectric ceramic crystals, which are described fully in Chapter 4. These were available in discs or squares down to 1 mm in diameter or 1 mm on the side. Also since a crystal could be capable of detecting normal or shear forces acting on the crystal surface, a column of crystals three high could theoretically measure the forces in the three orthogonal directions.

An idea was conceived where a matrix of these small load cells would be connected together by flexible mylar sheets with a grid of conducting paths laid on them such that every crystal would lie at an intersection

point. In just mulling this idea around it was realized that this scheme would be very difficult if not impossible to implement. Despite each unit cell's low cost, it would be prohibitively expensive due to the multiplicity of cells.

As a result, the requirement for the measurement of the pressure distribution across the foot was relaxed and it was decided to try larger, discrete plates. The decision as to what shape was easily overcome since it was felt that, because of the non-redundancy of supporting a plane on three points, a triangular shaped plate would be optimum.

3.4 The Triangle

3.4.1 Size Calculations

The size, mass and mounting of such a plate was tackled next. Since the idea of obtaining the pressure distribution was partially abandoned, the size trade-off became that plate of maximum size which would collect information from one foot only, while reducing the possibility of the two feet landing on the same plate. Adjacent or nearby plates would gather the data from the other foot.

To determine the optimum triangle size, information on foot sizes and stride dimensions was obtained. Figure 3.4.1 shows a sketch of a typical stride with the pertinent dimensional parameters labelled. Using data from Murray's (43,44) and Donath's studies (17), stride length and width were calculated. Table 3.4.1 gives the average stride lengths and widths of normal and post knee-operation men and women.

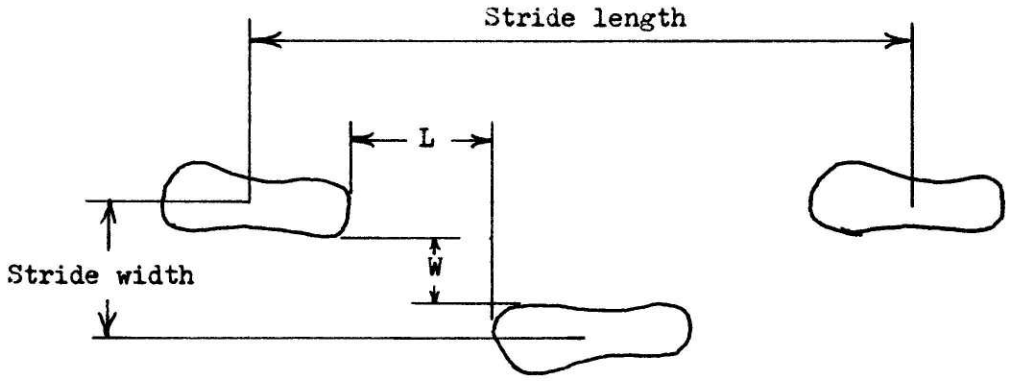

Figure 3.4.1 A typical stride.

TABLE 3.4.1

Stride Data for Normals and Post Knee-Operation Patients

Normals[1]

		Stride Length (cm)	Stride Width (cm)	L (cm)	W (cm)
Men:	Short (167 cm)	150.8	8.2	50.0	-.98
	Medium (175.5 cm)	156.2	8.6	51.4	-1.05
	Tall (183 cm)	162.5	7.2	53.4	-2.87
Women:	Medium (163 cm)	133.0		41.9	

Post-Operation Patients[2]

Men:	Average Ht. 174 cm	103.6		25.35
Women:	Avg. Ht. 165 cm	93.4		21.8

1 - Averaged from data on 70 Men, 40 Women
2 - Averaged from data on 20 Men, 34 Women

TABLE 3.4.2

Body segment parameters for normal humans

Men:
Foot Width = .055 x Height
Foot Length = .152 x Height

Women:
Foot Width = .057 x Height
Foot Length = .151 x Height

Using data from this table and Contini's (10) body dimensions in Table 3.4.2 the minimum distances L and W were calculated using

L = .5 x Stride Length - Foot Length

W = Stride width - Foot width

These values are tabulated in Table 3.4.1 in the rightmost two columns. In this table, the blanks reflect the absence of necessary data to calculate the appropriate values.

The L dimension always exceeds 20 cm. The negative values of W indicate that one foot tends to fall in front of the other. Thus using a conservative approach, a side length of the triangle of 20 cm was chosen with an equilateral shape to allow close packing. It was felt that this dimension and shape combination would ensure that no two feet would contact the same plate at the same time, during normal or abnormal gait, and indeed one foot could easily contact more than one plate at the same time, giving some semblance of a pressure distribution.

Using many plates in rows and columns a pathway could be constructed. The row dimension (overall width) was selected to be four triangles, a width of 69 cm, considered adequate to avoid the need of guiding the subject towards the force sensing area. The column dimension (overall length) would be as long as possible given resources and data handling and storage capability. Two rows were considered to be the absolute minimum, providing data from only one footfall. A pathway 223 cm long would provide data from a minimum of two steps. Such a pathway would require 66 tiles in all. Figure 3.4.2 illustrates some of the pathway.

3.4.2 Plate Static Analysis

The thickness of the plate is based upon deflection and stress analysis. For a flat plate equilateral triangle simply supported on all edges with a uniform load over a circle of radius r at the centroid of the triangle, the maximum stress in the plate, also at the centroid is obtained

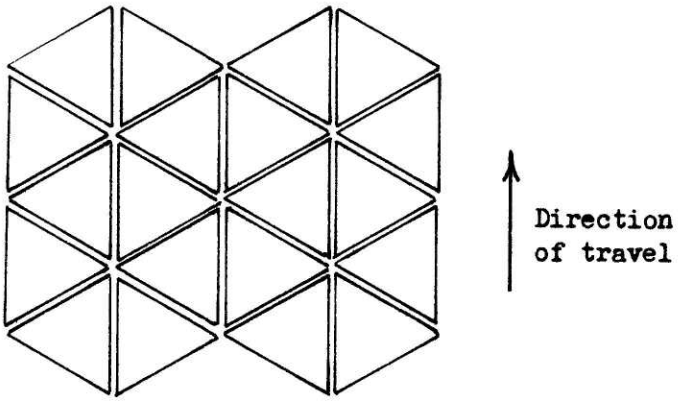

Figure 3.4.2 The triangle pathway.

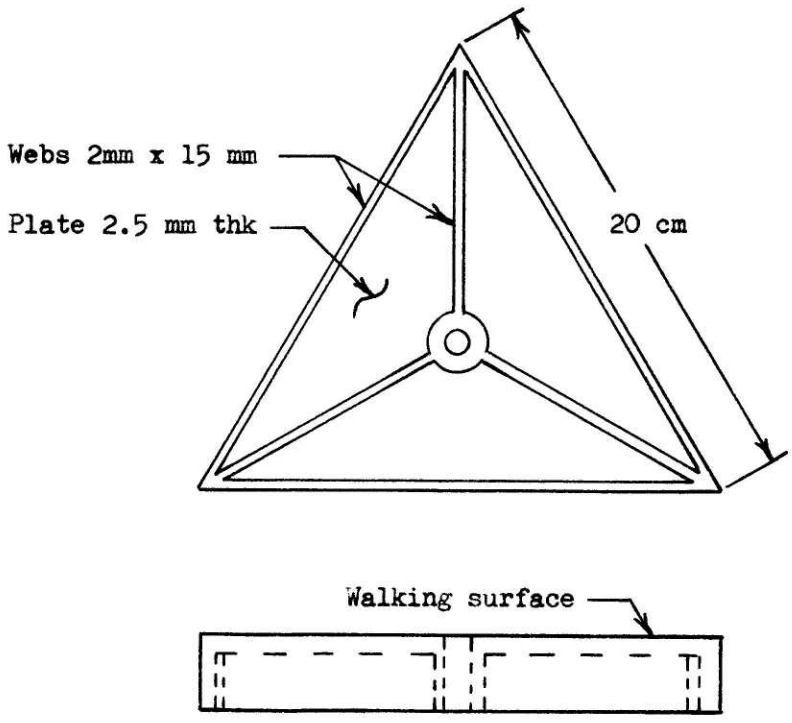

Figure 3.4.3 The triangle.

from (53)

$$\sigma_{max} = \frac{3W}{2\pi t^2} \left[(1 + \nu) \ln \left(\frac{.378a}{r}\right) + 1\right]$$

where σ_{max} - maximum stress, due to bending

t - plate thickness

W - load applied

ν - Poisson's ratio of the material

Also the maximum deflection is calculated from (53)

$$Y_{max} = \frac{0.069W\ (1-\nu^2)\ a^4}{Et^3}$$

where a - height of the triangle

E - Young's modulus for the material

Assuming thicknesses of 2.5 mm and 5.0 mm and a force of 500 N, using wrought aluminum 2014-T6 having a yield strength of 413 MN/m^2 (2) gives:

2.5 mm thick	= 526 MN/m^2	= 5.0 mm
5.0 mm thick	= 131 MN/m^2	= .62 mm

Despite these large stresses and deflections, it is believed that a 2.5 mm thick plate with proper webbing on the underside, along each side and toward the centroid as in the diagram of Figure 3.4.3, would be adequate.

The cross-section of the webs can only be estimated. Considering the side web as a simply supported beam 2 mm by 15 mm, stressed with a force of 500 N at the middle, the maximum bending stress is calculated to be 400 MN/m^2, close to the yield strength. These plate dimensions then are considered an adequate first approximation to proceed with the studies. Ultimately the plate design must be optimized to achieve minimum weight and

adequate stiffness under realistic loadings.

3.4.3 Dynamic Analysis

A force plate can be modelled as a second order system consisting of a mass, a damper and a spring as in Figure 3.4.4. The equation of motion of the system using Laplace transforms is (4)

$$\frac{X_0(s)}{F_i} = \frac{\frac{1}{k_s}}{\frac{s^2}{\omega_n} + \frac{2\zeta s}{\omega_n} + 1}$$

where ω_n = undamped natural frequency $= \sqrt{\frac{k_s}{M}}$

ζ = damping coefficient $= \sqrt{\frac{B}{2\ K_s M}}$

For a step input q_{is} this second order system responds according to (4)

$$q_0 \left(\frac{s^2}{\omega_n^2} + \frac{2\zeta s}{\omega_n} + 1\right) = K q_{is}$$

The step response of such a system consisting of three cases; underdamped, critically damped and overdamped is shown in nondimensional form in Figure 3.4.5. With little damping the system oscillates badly, whereas a large damping value reduces the response time since the time to reach the final steady state output is delayed. The step response may be misleading in this case because the perfect step rarely occurs naturally.

A better indicator of system performance is the response to a terminated ramp input as shown in Figure 3.4.6. The response of the system is (16)

$$\frac{q_o}{K} = \frac{t}{T} - \frac{2\zeta}{\omega_n T} + \frac{1}{\omega_n T \sqrt{1-\zeta^2}}\, e^{-\zeta\omega_n t} \sin\left(\sqrt{1-\zeta^2}\ \omega_n t + \phi\right) \qquad 0 \leq t \leq T$$

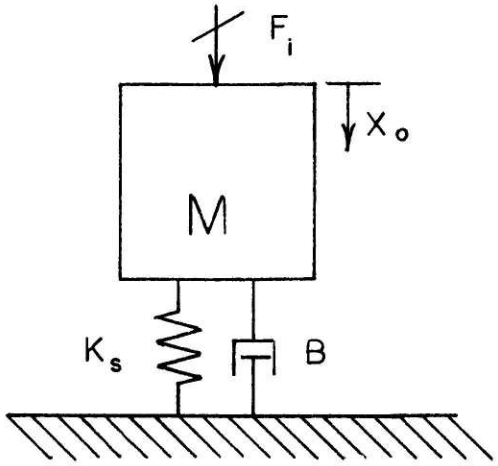

Figure 3.4.4 A second order system.

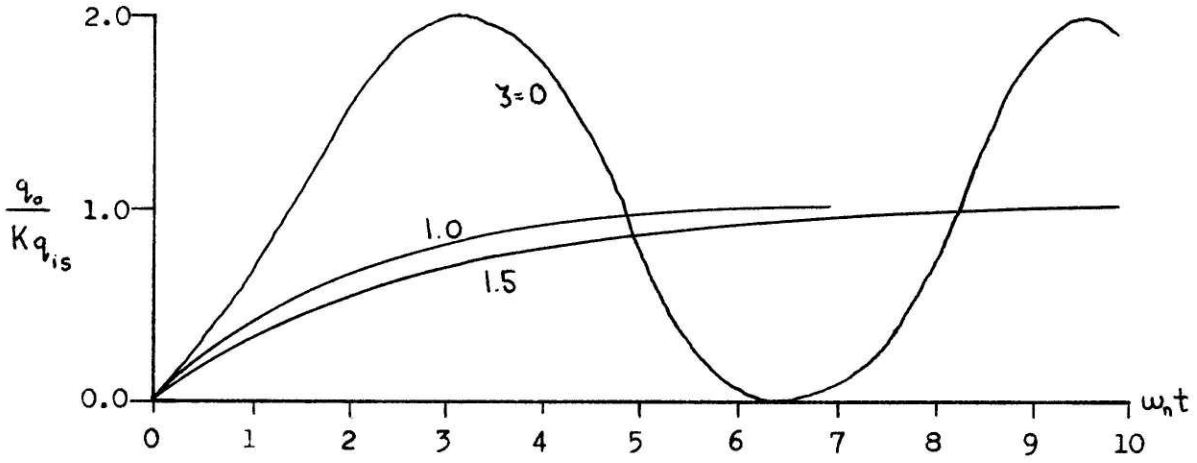

Figure 3.4.5 The second order system response to a step input for different amounts of damping.

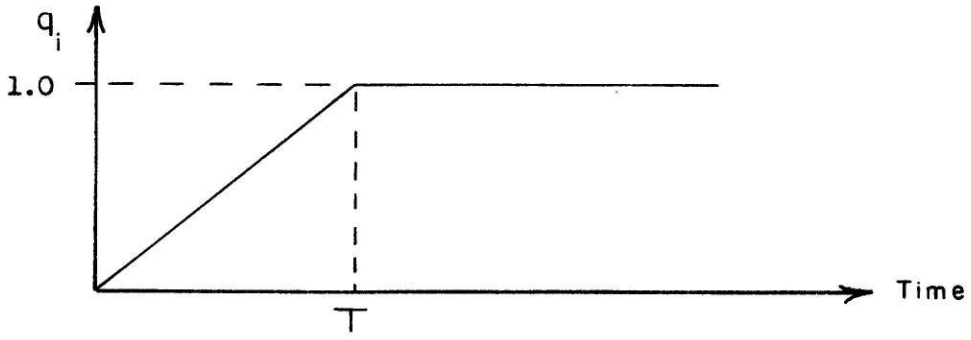

Figure 3.4.6 A terminated ramp.

$$\frac{q_o}{K} = \left[\frac{t}{T} - \frac{2\zeta}{\omega_n T} + \frac{1}{\omega_n T\sqrt{1-\zeta^2}}\, e^{-\zeta\omega_n t}\, \sin(\sqrt{1-\zeta^2}\,\omega_n t + \phi)\right] - \left[\frac{t}{T} - 1 - \frac{2\zeta}{\omega_n T}\right.$$

$$\left. + \frac{1}{\omega_n T\sqrt{1-\zeta^2}}\, e^{-\zeta\omega_n (t-T)}\, \sin(\sqrt{1-\zeta^2}\,\omega_n (t-T) + \phi)\right] \qquad T < t < \infty \,.$$

$$\phi = 2\tan^{-1}\frac{\sqrt{1-\zeta^2}}{\zeta}$$

All of which can be summarized by two statements:

1 - The steady state error is $\frac{2\zeta}{\omega_n T}$

2 - The transient error is smaller than $\frac{1}{\omega_n T\sqrt{1-\zeta^2}}$

Thus if there is no damping, i.e. $\zeta = 0$, there is no steady state error and the transient error can be made small if ω_n is large with $\frac{1}{T}$. Figure 3.4.7 shows the response of a second order system with $\zeta = 0$ to a terminated ramp forcing function using 2 different values of ω_n; $\omega_n = \frac{3.3}{T}$, $\omega_n = \frac{1}{5T}$ (from Biggs (4)). As a result, the higher the natural frequency of the force plate system and the smaller the damping, the better the response. Ramey (51) recommends a system natural frequency about 10 times the "equivalent frequency of the fastest rising part of the applied force".

The stiffness of a force plate assembly is difficult to calculate analytically because of the lack of knowledge of the rigidity of the plate it-

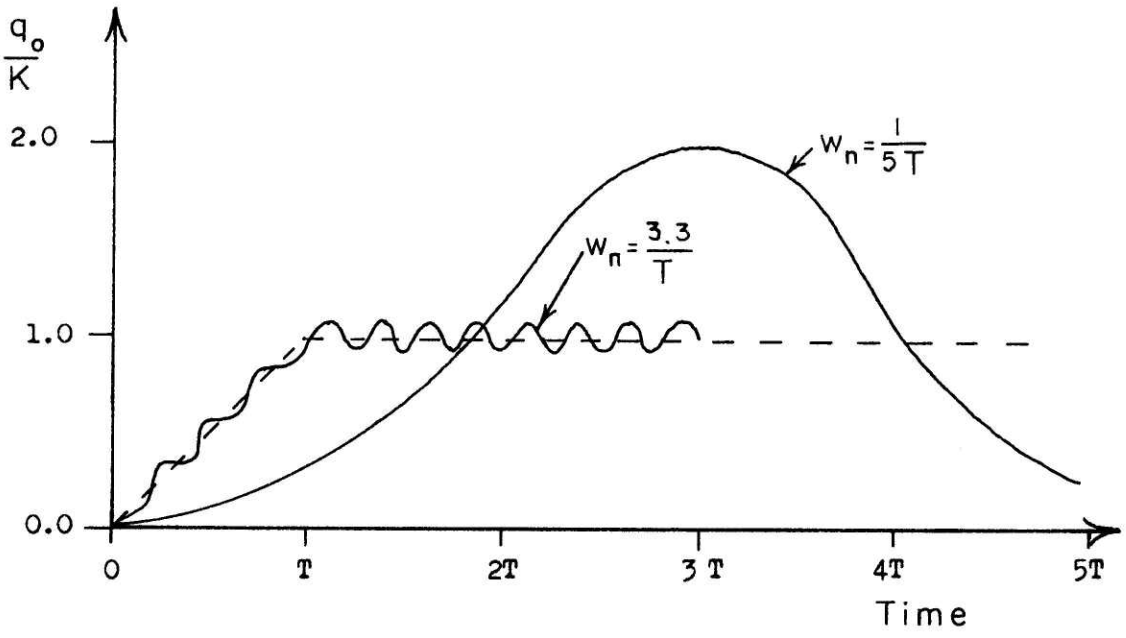

Figure 3.4.7 The responses of two second order systems with different natural frequencies and no damping to the terminated ramp.

self, the transducing elements and the connection of the two. Studies have been done on the natural frequency of vibration of triangular plates. Leissa (37) investigated the vibrations for several edge conditions, unfortunately the simply supported corners case was not among them. For the case of three simply supported edges using an equilateral triangular plate, the equation for natural frequency is (37)

$$f_n = \frac{40.0}{a^2}\sqrt{\frac{D}{\rho}}\ \frac{1}{2\pi}$$

where ρ = mass density/unit area

D = equivalent stiffness = $\frac{Et^3}{12(1-\nu^2)}$

E = Young's Modulus ν = Poisson's ratio

t = plate thickness a = triangle height

Thus using aluminum the value of f_n for a plate 17.6 cm high, 2.5 mm thick was calculated to be 800 hz and 1600 hz for a plate 5 mm thick. These estimates are expected to be lower than the actual values because of the reinforcing incorporated.

Using the simple models from Harris and Crede (25) and Fertis (21) illustrated in Figure 3.4.8 the natural frequency of the transducing elements was calculated. Various methods were considered for obtaining the forces as is described further on in this thesis.

One transducer type analyzed consisted of a stack of three PZT-8, 25.4 mm diameter, 2.54 mm thick piezoelectric ceramic crystals separated by 3 mm thick 29 mm diameter glass optical flats. Since the glass and the ceramic had almost the same material properties, this stack was approximated by 5 crystal pieces. The PZT-8 material had a modulus of elasticity of

TYPE OF SYSTEM	NATURAL FREQUENCY	STIFFNESS
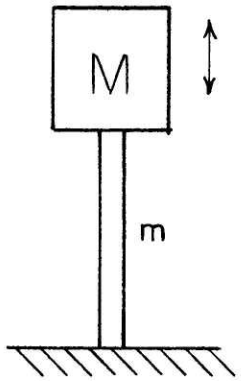 Elastic column with a mass attached	$\omega_n = \sqrt{\frac{K}{M + \frac{m}{3}}}$	$K = \frac{SE}{l}$ S - cross sectional area E - Young's modulus l - column length
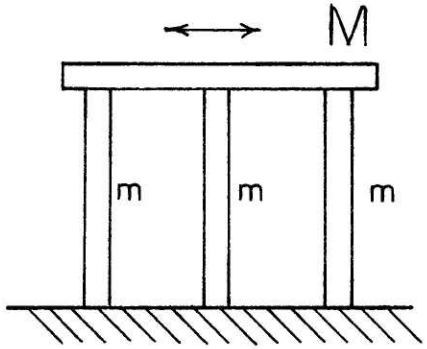 A girder supported on columns	$\omega_n = \sqrt{\frac{K}{M + .023\,m}}$	$K = \sum_{i=1}^{3} k_i$ $k_i = \frac{12EI}{l^3}$ I - moment of inertia

Figure 3.4.8 Models and equations used to analyze the transducer dynamics.

1.17×10^{11} N/m^2. The mass of the plate was calculated to be .224 kg and that of the column .05 kg. Thus the natural frequency in the vertical mode is

$$f_n = \frac{1}{2\pi}\sqrt{\frac{\frac{\pi}{4}(25.4 \times 10^{-3})^2 \text{ m}^2 \; 1.17 \times 10^{11} \text{ N/m}^2}{\frac{(13.62 \times 10^{-3})\text{m}}{(.224 + \cdot\frac{05}{3})\text{ kg}}}} = 21{,}400 \text{ hz}$$

Another consideration for transducer was a strain gauged column 5 mm square and 15 mm high, made of aluminum ($E = 6.89 \times 10^{10}$ N/m^2). For this structure, the natural frequency is 3,600 hz vertically.

In the horizontal mode the natural frequencies were 17,800 hz for the piezoelectric stack and 600 hz for the aluminum column.

The above calculations are for the case of rigidly connected columns and plates. However, with the actual hardware and mounting technique, the natural frequency of the system would probably be lower than the estimates given by these calculations. The value of the natural frequency of the system is difficult to estimate. Perhaps the only feasible method would be a finite element analysis. Since the first approximations described above are so high, the system natural frequency does not seem to be a major problem; therefore no finite element analysis was done.

3.4.4 Mounting the Plate

At the time of conception of the triangle-pathway idea, the piezoelectric crystals seemed most suited for the force transducers. As a result most of the design calculations involved this force-sensing element. Chapter 4 deals with piezoelectric crystals in more detail.

The original plan had the crystals stacked three high, using a crystal

for each of: normal, lateral and fore-aft shear forces. In the first configuration, the crystals would be separated by printed circuit board which, covered with copper on both sides, etched to provide connections with the required amplifiers. The revised design still had three crystals in a column, however each crystal would be sandwiched between glass optical flats epoxied to the crystal surface with the lead wires soldered to the silver electrodes of the crystals as in Figure 3.4.9. This change was made because the optical flats are stiffer than the printed circuit board, thus giving a higher natural frequency. Also the optical flats provide a flat surface that the load is applied to, reducing the amount of non-normal loading and therefore cross talk.

In order for the shear forces to be transmitted, the triangular plate must preload the columns, with a mechanism that is flexible enough to allow the transmission of shear forces. Such a system is illustrated in Figure 3.4.9. The wire in tension should be flexible enough with respect to the column, to allow the horizontal forces to be exerted on the shear mode crystals. Using the initial design of copper clad printed circuit board for connection, the frictional force required to resist a fore-aft shear force of 622 Newtons was calculated from

$$F_{frictional} = \mu F_{normal}$$

where μ - coefficient of static friction

= .76 for copper to copper.

Using this equation, the normal force required was 818 N. Assuming at least 400 Newtons of force would be exerted normal to the plate at the time of maximum shear force, a conservative estimate since the maximum shear as

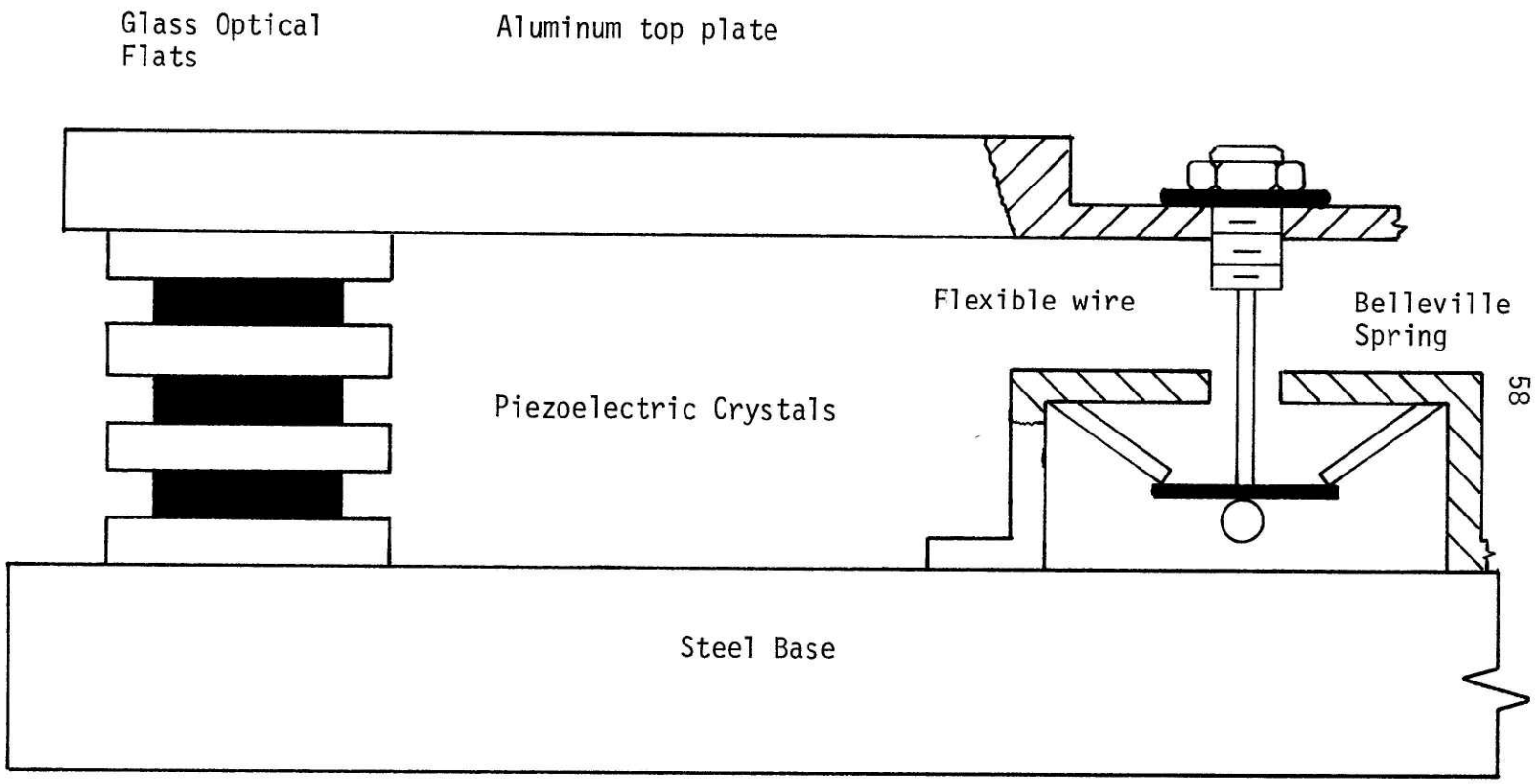

Figure 3.4.9 A sketch of the mounting system.

measured by previous researchers (5) occurs at the heel strike which is the time of maximum normal force i.e. 2224 Newtons, then a preload of 418 N was necessary.

This load would be applied by tightening the nut on the preload bolt (keyed to prevent applying torque to the wire) attached to the wire as indicated in Figure 3.4.9. With the epoxy scheme, the horizontal forces would be transmitted by the epoxy, thus preload is reduced requiring just enough preload to prevent movement between the plate and columns. The baseplate would be made of steel and cemented to a concrete floor, thus ensuring a rigid connection.

3.5 The Optical Attempt

A possible method of obtaining pressure distribution data easily and inexpensively was considered. This would consist of a two layered force plate system. The upper level would consist of a rubber mat flat on the top side and with hemispherical solids on the lower side. This mat would sit on a plexiglass sheet 6.4 mm thick, with edge lighting along one side. In a fashion similar to Arcan and Brull's (1) the rubber solids would deform, but in this case would change the amount of refracted and reflected light from the plexiglass sheet downward as shown in Figure 3.5.1. This light would be sensed by photosensitive diodes, one per solid, and the amount of light received would give an indication of the force exerted on the area of the mat above the solid.

The lower layer would be the force plate as described in the previous sections producing data on the total forces and moments for all 3 axes and the center of application of the force.

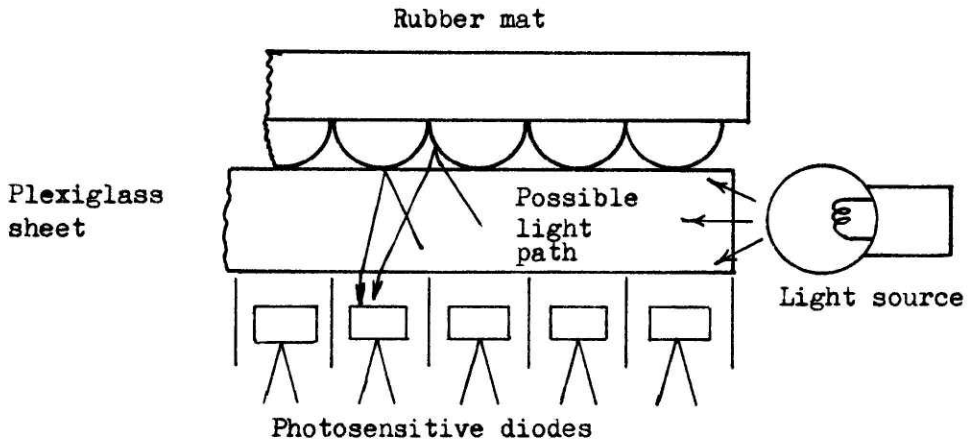

Figure 3.5.1 A sketch of the optical system.

Experimental difficulties were encountered with this scheme. The measurable amount of light at the photosensitive diodes in the middle of the plate, represented only a 15 mV change from the background level of 10 mV when the solid was considerably depressed. The nonlinear compression characteristics of the rubber with force was also a major dissuading factor against using this idea as was the complexity of processing the photodiode outputs. As a result, this method was abandoned and the work continued with the force plate system alone.

3.6 Signal Processing

The goal of this project is to obtain data on the interaction between humans and the floor during movement. This interaction is characterized by the three orthogonal forces: F_z, F_x, F_y, the three moments about the axes: M_z, M_x, M_y and the point of application of the force for each plate. The analyses resulting in these parameters can be accomplished using analog circuitry.

A diagram of one plate with a force on it together with the circuitry for obtaining the total vertical force and its coordinates are shown in Figures 3.6.1 and 3.6.2. A midline between the triangles, spaces included, was used as the x-axis and the bisection line of the triangle's apex as the y-axis. The distance from these datum lines to each transducer were taken as X, Y_1, Y_2 as shown. The total forces in x, y, z are the algebraic sum of the forces from the transducers in each direction

$$F_z = F_{1z} + F_{2z} + F_{3z}$$
$$F_x = F_{1x} + F_{2x} + F_{3x}$$
$$F_y = F_{1y} + F_{2y} + F_{3y}.$$

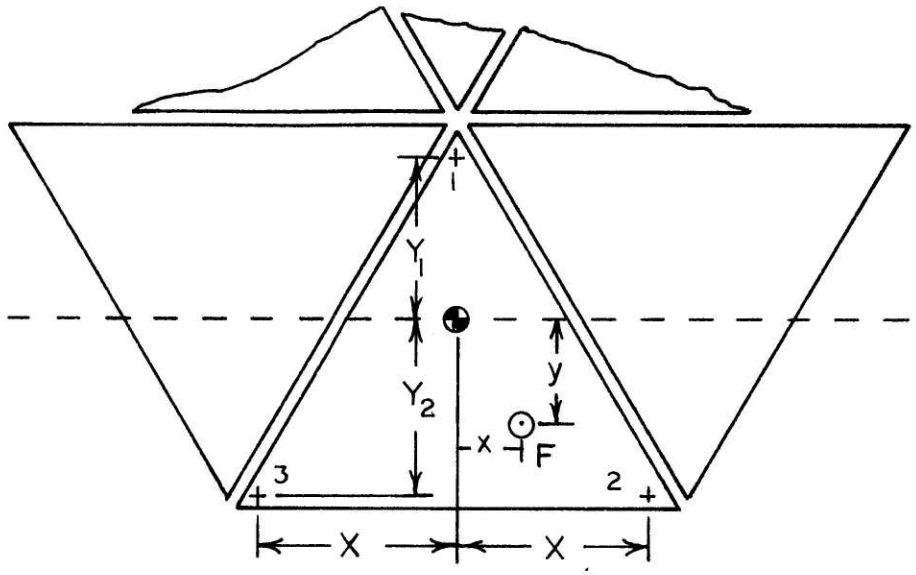

Figure 3.6.1 A force applied on a plate.

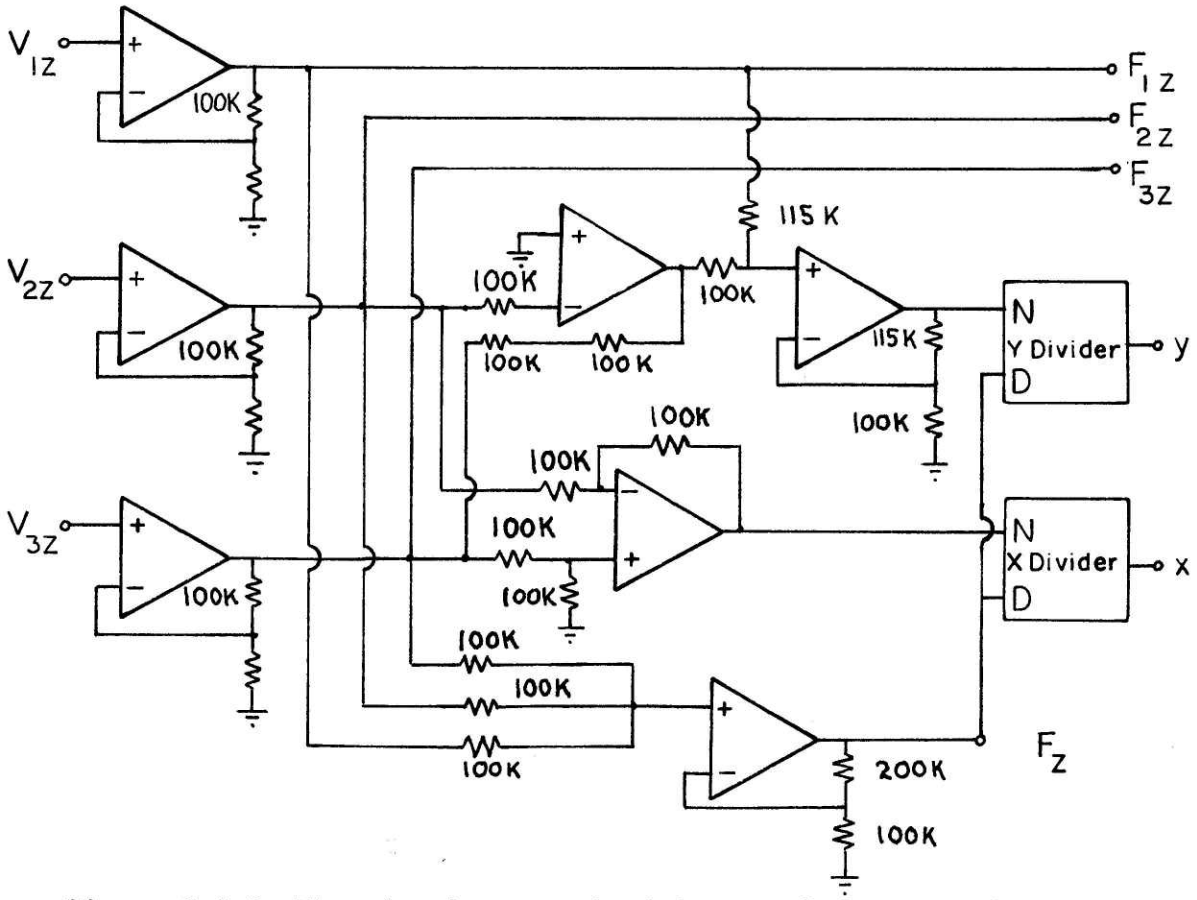

Figure 3.6.2 The circuitry required for total forces and x & y values.

Taking moments about these central axes yield the values for x and y

$$x = \frac{(F_{2z} - F_{3z})X}{F_z}$$

$$y = \frac{(F_{2z} + F_{3z})Y_2 - F_{1z}Y_1}{F_z}$$

The forces, moments and point of application of each plate are calculated separately and then using either more analog circuitry, or more likely digital processing with either a minicomputer or a microprocessor, the total forces associated with a subject's step are determined. In addition the point of application and its travel as the weight is transferred from heel to toe would be calculated. Appendix B reviews the necessary detailed calculations for the determination of total forces, moments and point of application for each plate.

3.7 The Force Transducer

As has been mentioned previously, several transduction methods were considered. The three investigated more thoroughly were; piezoelectric crystals, strain gauged columns and linear variable differential transformers (LVDTs) measuring the deflection of beams.

After preliminary calculations, it was decided that the piezoelectric crystals were the most promising. As a result, crystals were purchased, a prototype plate was machined and an assembly was made. However as is reported in Chapter 4, in the calibration of the crystals for use in the plate, some nonlinearities were observed. Most of the work on the project then was aimed at defining these nonlinearities and eliminating them.

Chapter 4 deals with the three transducing methods considered. Sections 4.2 and 4.3 describe the preliminary calculations made for strain gauges and LVDTs respectively. Section 4.1 discusses the piezoelectric crystals and Appendix A is associated with this section.

CHAPTER 4 FORCE TRANSDUCERS--A VARIETY OF ALTERNATIVES

4.1 The Piezoelectric Crystal

4.1.1 The Piezoelectric Effect

Piezoelectricity was best defined by W.G. Cady (6) in his classical book on piezoelectricity as "Electric polarization produced by mechanical strain in crystals belonging to certain classes, the polarization being proportional to the strain and changing sign with it". Piezoelectricity is also a reversible process which makes it different from other transductions. That is, an electric field may be applied to a piezoelectric crystal and a corresponding proportional strain will be produced. The piezoelectric effect was first discovered by the Curie brothers in 1880. Two years later they observed the reverse piezoelectric effect.

In crystallography there are 32 classes of crystals based on structure. Of these 32 classes, 20 can show piezoelectricity to some extent. A necessary condition for any piezoelectric crystal is that it lacks a center of symmetry, thus when stressed a net dipole is created within the crystal and charges develop on the crystal surfaces. Figure 4.1.1 shows a simplified model of a quartz crystal in stressed and unstressed condition.

A further classification of piezoelectric crystals includes those crystal classes that have a permanent dipole axis. These crystals are called pyroelectric. Ten of the 20 piezoelectric crystals are pyroelectric. The term pyroelectric was coined because when these crystals are heated uniformly, a net charge occurs on the crystal face

Figure 4.1.1 A simplified quartz crystal.

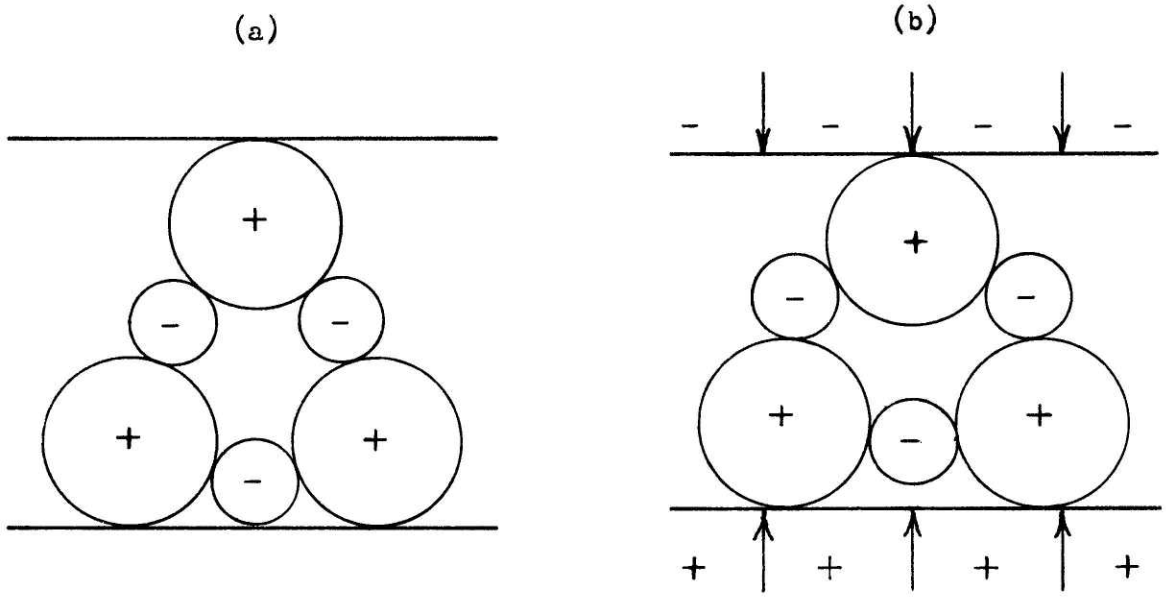

Figure 4.1.2 Schematic structure of a simplified crystal.

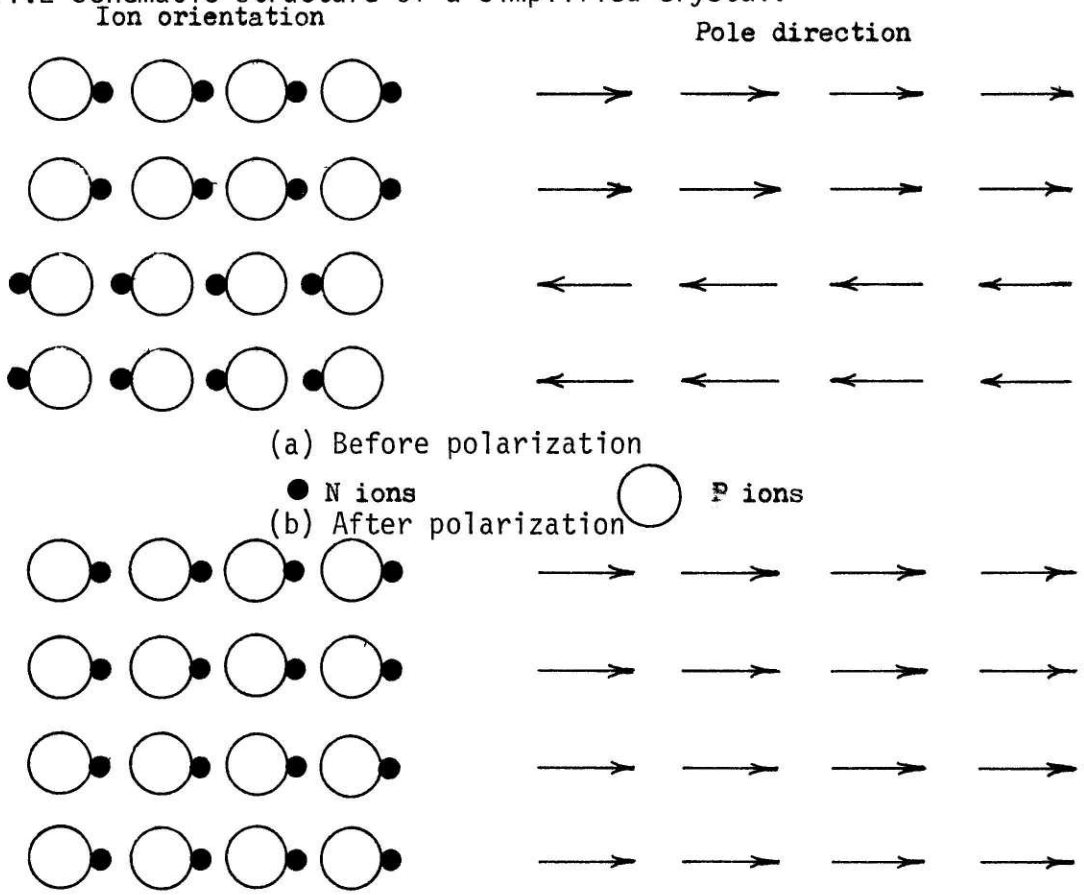

as a result of increasing the separation between poles of the crystal. Note also that when stressed uniformly a charge will develop in the same way as that caused by thermal expansion. This is called the hydrostatic effect and is useful in some applications such as sonar and ultrasonic cleaners.

Piezoelectricity must not be confused with a phenomenom known as electrostriction which occurs in all dielectrics. This is the straining of a material under the influence of an electric field. This results because the electric field moves electrons and nucleii to induce polar moments or alter existing ones and thereby changing the crystal dimensions. Electrostriction is not however, reversible, that is material which will strain under an electric field will not necessarily create charge under strain caused by stress. Thus with materials with a center of symmetry, when stressed, the particles move not according to their charge but according to their mass and therefore no dipole is produced. Also in electrostriction, the strain is proportional to the square of the field applied, whereas with piezoelectricity, the strain is proportional to the field.

One other subdivision of piezoelectric crystals is the classification according to the effect of ferroelectricity. This is the reversal of the dipole direction present in a piezoelectric crystal by the application of an electric field. Since this inherently requires an existing permanent dipole, the effect is seen only in pyroelectric crystals. Ferroelectrics are classified according to the degree to which the polar axes can be reversed.

Because of this ferroelectric phenomenon, ceramic crystals can be permanently polarized. To illustrate, consider the simple planar two ion crystal structure as shown in Figure 4.1.2. This crystal consists of N negative ions located at the lattice points of a net structure and P ions, the positive ions, the floating ions. Upon formation of the crystal, the P ions can lie on either side of the N ions along a horizontal line as shown in part (a). Note that the upper region of the crystal has a spontaneous polarization where the P ions are on the right of the N ions and the lower region has the reverse situation. This illustrates another characteristic of the crystals, regions where the polarization is uniformly in one direction, called domains. When a large electric field is applied the P ions receive energy and can jump to the other side of the N ion following the polarity of the applied field. Thus it is possible to polarize an originally unpolarized crystal. Figure 4.1.2 (b) represents the condition of the crystal after polarization.

This is a very simplified illustration of the polarization of a crystal but the idea can be extended to the three dimensional case. Figure 4.1.3 gives a side view of a crystal before and after polarization. Originally, the crystal structure is random in nature, with domains oriented in various directions as in case (a) below. Once the electric field has been applied and removed, the domains lie with poles in roughly the same direction and there is some reduction of the domain structure resulting in fewer domains. Hence the ceramic now resembles a single pyroelectric crystal with a net dipole moment.

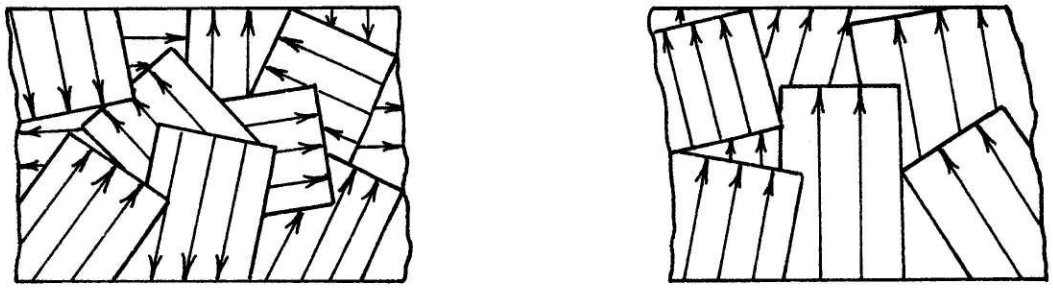

(a) (b)

Figure 4.1.3 A side view of a ceramic before and after polarization. (a) Before (b) After The arrows indicate the direction of spontaneous polarization.

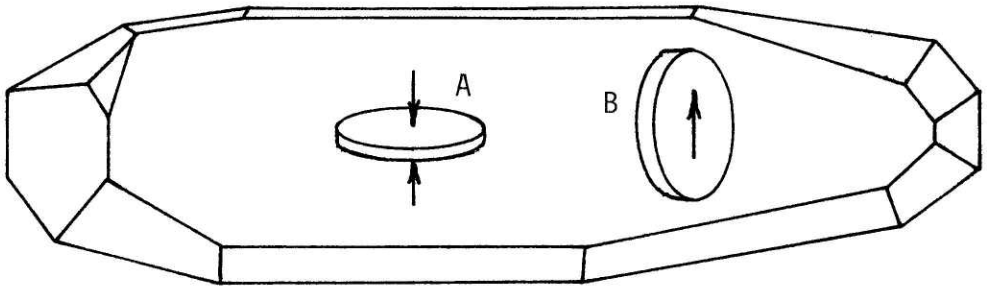

Figure 4.1.4 A quartz crystal and alignment of two discs. A - Normal force sensitive, B - Shear force sensitive

This ceramic will respond linearly to stress as long as the field produced by this stress is below that needed to switch the poles of the domain regions.

This ferroelectric effect can also occur as a result of heating. Upon heating, the P ions of the fictitious crystal mentioned will gain energy and if sufficient energy is received, they may "jump" to the other side of the N ion. Thus it is possible to depolarize a crystal by heating it. The temperature at which the "jumps" occur is called the Curie point. Above the Curie point the crystal is non-polar and below it, it is polar.

Piezoelectric materials can occur naturally or can be manufactured as ceramics, as mentioned above. An example of a natural piezoelectric material is quartz, and that of a manufactured one is lead zirconate-titanate.

Natural piezoelectric crystals are actually artificially grown so that the purity can be assured. Once a large crystal is grown, smaller transducer-size crystals are cut perpendicular to a particular axis depending on the application of the crystal i.e. sensitive to normal forces or to shear forces. Figure 4.1.4 is a sketch of a quartz crystal and the orientation of two discs, one sensitive to normal forces A and one sensitive to shear B.

A ceramic is a conglomeration of small crystals. It is normally formed at high temperature and upon cooling through the Curie point the crystals form spontaneous dipoles and arrange themselves in the domains described above. This ceramic is not

initially piezoelectric because of the random orientation of the domains causing cancelling effects between individual crystals. However, as described above the ceramic can be poled by the application of a strong electric field.

4.1.2 The Piezoelectric Coefficients

When a stress is applied to a crystal, the state of the stress can be described using a second rank stress tensor T composed of axial stress (σ) and shear stresses (τ) employing the axes notation in Figure 4.1.5.

$$T = \begin{bmatrix} \sigma_x & \tau_{xy} & \tau_{xz} \\ \tau_{yx} & \sigma_y & \tau_{yz} \\ \tau_{zx} & \tau_{zy} & \sigma_z \end{bmatrix} .$$

T is a symmetrical matrix, thus $\tau_{xy} = \tau_{yx}$, $\tau_{xz} = \tau_{zx}$, $\tau_{yz} = \tau_{zy}$. The state of strain can be similarly expressed in a tensor S

$$S = \begin{bmatrix} \varepsilon_{xx} & \varepsilon_{xy} & \varepsilon_{xz} \\ \varepsilon_{yx} & \varepsilon_{yy} & \varepsilon_{yz} \\ \varepsilon_{zx} & \varepsilon_{zy} & \varepsilon_{zz} \end{bmatrix} .$$

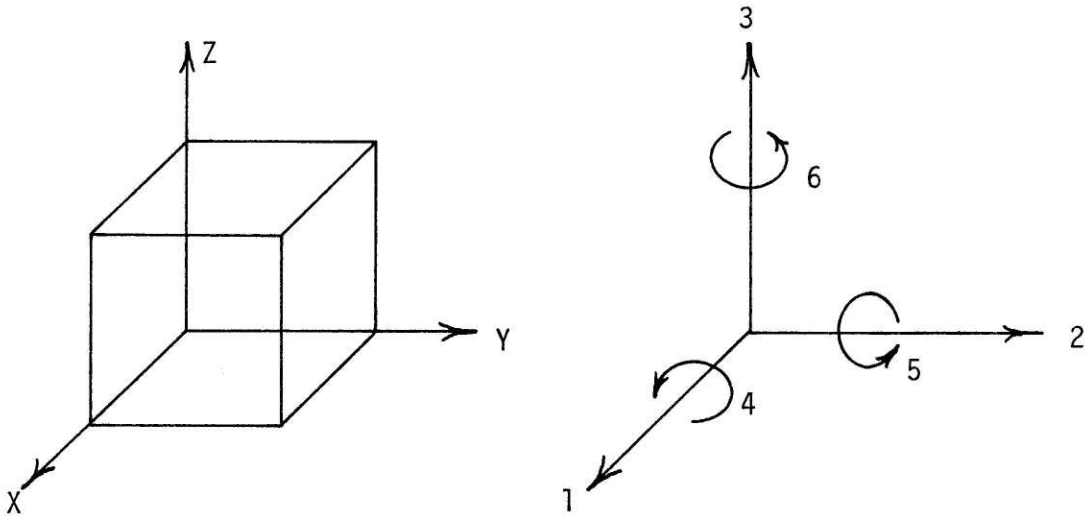

Figure 4.1.5 Axes notation used in the equations.

Using Hooke's law the strain is related to the stress linearly expressed by six equations

$$\varepsilon_{xx} = s_{11}\sigma_x + s_{12}\sigma_y + s_{13}\sigma_z + s_{14}\tau_{xy} + s_{15}\tau_{yz} + s_{16}\tau_{zx}$$
$$\varepsilon_{yy} = s_{21}\sigma_x + s_{22}\sigma_y + s_{23}\sigma_z + s_{24}\tau_{xy} + s_{25}\tau_{yz} + s_{26}\tau_{zx}$$
$$\varepsilon_{zz} = s_{31}\sigma_x + s_{32}\sigma_y + s_{33}\sigma_z + s_{34}\tau_{xy} + s_{35}\tau_{yz} + s_{36}\tau_{zx}$$
$$\varepsilon_{xy} = s_{41}\sigma_x + s_{42}\sigma_y + s_{43}\sigma_z + s_{44}\tau_{xy} + s_{45}\tau_{yz} + s_{46}\tau_{zx}$$
$$\varepsilon_{yz} = s_{51}\sigma_x + s_{52}\sigma_y + s_{53}\sigma_z + s_{54}\tau_{xy} + s_{55}\tau_{yz} + s_{56}\tau_{zx}$$
$$\varepsilon_{zx} = s_{61}\sigma_x + s_{62}\sigma_y + s_{63}\sigma_z + s_{64}\tau_{xy} + s_{65}\tau_{yz} + s_{66}\tau_{zx}.$$

In much the same fashion the piezoelectric polarization is related to the stress in three equations

$$P_{xx} = d_{11}\sigma_x + d_{12}\sigma_y + d_{13}\sigma_z + d_{14}\tau_{xy} + d_{15}\tau_{yz} + d_{16}\tau_{zx}$$
$$P_{yy} = d_{21}\sigma_x + d_{22}\sigma_y + d_{23}\sigma_z + d_{24}\tau_{xy} + d_{25}\tau_{yz} + d_{26}\tau_{zx}$$
$$P_{zz} = d_{31}\sigma_x + d_{32}\sigma_y + d_{33}\sigma_z + d_{34}\tau_{xy} + d_{35}\tau_{yz} + d_{36}\tau_{zx}.$$

The constants d_{mn} are the electromechanical coupling coefficients called the piezoelectric coefficients. The coefficient d matrix is symmetrical thus only 15 of the 18 elements are independent ($d_{12} = d_{21}$, $d_{13} = d_{31}$, $d_{23} = d_{32}$). This matrix physically represents the sensitivity of the crystal to a certain stress. The units of d are

$$d_{mn} = \frac{\text{Coulumb}}{\text{Newton}}.$$

The d coefficients can be converted to another coefficient called the g coefficient by dividing the d matrix by the dielectric constant of the material. The units of g are

$$g_{mn} = \frac{\text{Volts/meter}}{\text{Newton/meter}^2}.$$

The g matrix relates the stress acting on the crystal to the open circuit voltage developed.

For the piezoelectric ceramics the g matrix is greatly simplified due to symmetry in the crystal. There are only three active g coefficients according to

$$g_{mn} = \begin{bmatrix} 0 & 0 & 0 & 0 & g_{15} & 0 \\ 0 & 0 & 0 & g_{15} & 0 & 0 \\ g_{31} & g_{31} & g_{33} & 0 & 0 & 0 \end{bmatrix}.$$

Thus given a stress on the crystal a voltage is produced proportional to this stress.

Another important parameter of piezoelectric crystals is the coupling factor, k. This is a measure of the strength of the piezoelectric effect. It is calculated according to the formula

$$k^2 = \frac{\text{mechanical energy converted to electric energy}}{\text{input mechanical energy}}.$$

The value of k^2 must always be less than 1, thus the value of k is always less than 1. Typical values of k are 0.10 for quartz, 0.9 for Rochelle salt and 0.5 - 0.7 for lead zirconate-titanate.

4.1.3 The Manufacture of Piezoelectric Ceramics

Piezoelectric ceramics are manufactured from oxides of high purity, normally over 99% and often higher than 99.5% pure. Such high purities are required to achieve high reactivity and proper dielectric and conductive properties thus affecting ultimately the piezoelectric properities of the ceramic. These oxides are mixed in a ball mill or heavy muller roll to a homogeneous mixture. Homogeneity is also necessary for proper chemical reactions to occur. The mix is then calcined to a powder form by the application of heat to remove any volatile impurities in the material. After calcining, the powder is ground into a fine dust of between 1 and 10 micrometer size, also done in a ball mill. Finally, the mixture is formed into sheets, rods or cylinders using conventional forming techniques for ceramics such as dust pressing, casting centrifugal casting and extrusion. The shape is held by binding agents that are later burned out in the firing process.

Firing occurs at 1200° - 1300°C for lead zirconate-titanate in an electric furnace. It is important to get the proper grain size so that polarization is possible. If the grains are too small, the spontaneous ferroelectric polarization is locked in and can't be realigned by an electric field. Ideally the material should be 95%

dense, i.e. with pores and cavities occupying only 5% of the volume so that absorption of water is minimized and maximum strength, dielectric and piezoelectric properties are obtained.

The sheets are cut into shapes and ground to the designed size using normal grinding techniques and abrasives such as Al_2O_3, SiC and diamond. Conductive electrodes are a necessary part of any piezoelectric crystal and are applied next. The most common technique for making the electrodes is to apply silver in a liquid or paste form to the surface of the crystal and then to sinter the crystal in order to bond the silver to the surface. Sometimes a small amount of glass is mixed in with the silver in order to obtain a better bond with the ceramic. The degree of bonding of the electrode surface to the actual crystal material is critical since an air gap lowers the capacitance of the crystal. If a field is applied then most of the voltage drop will occur across the gap, thus the poling process could be impaired, and subsequently disrupts performance afterward.

The final step in the manufacture process is to actually pole the crystal. This is done by applying a large D.C. voltage on the electrodes. The magnitude of the field strength is in the tens of kilovolts per cm and the poling time varies from several minutes up to an hour.

4.1.4 Commercially Available Piezoelectric Load Cells

Presently quartz piezoelectric force transducers are manufactured by the Kistler Corporation (32). The most suitable for the purposes of force plate construction are the 3-component transducers Type 9251. Table 4.1.1 gives the specifications from Kistler (33) on this piezoelectric transducer and Figure 4.1.6 is a sketch of the transducer can.

TABLE 4.1.1
Specifications of the Kistler Type 9251 force transducer

Measuring Range: Normal force, F_z	$\pm$ 5000 N
Shear force, F_x, F_y	$\pm$ 2500 N
Resolution:	.01 N
Overload	20%
Sensitivity: Normal mode, F_z	-4.1 pC/N
Shear mode, F_x, F_y	-7.5 pC/N
Rigidity: z-direction	1000 N/um
x,y-direction	300 N/um
Resonant frequency in z direction loaded with 400 g	8 Khz
Linearity	$\leq \pm$ 1%
Cross influence of the components	< 5%
Insulation resistance	$> 5 \times 10^{13}$
Capacity: Each mode	30 pF
Temperature coefficient	.02%/C
Working temperature range	-60 to +150C
Weight	32 g
Cost	$1090.00

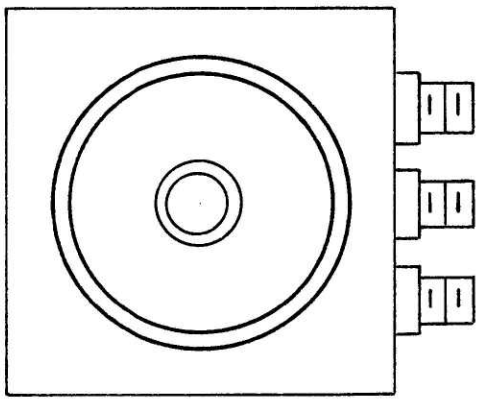

(a)

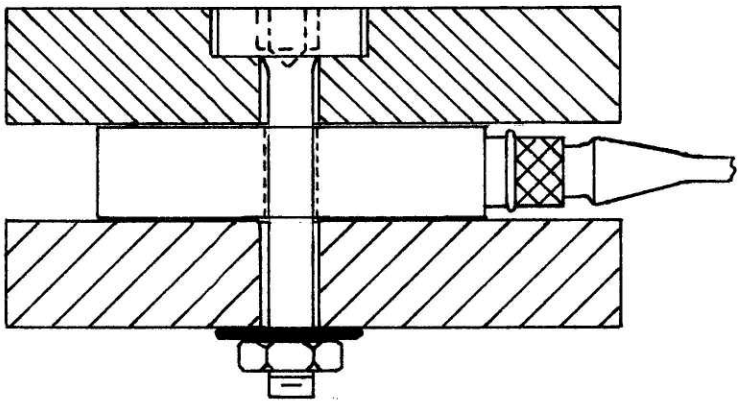

(b)

Figure 4.1.6 A sketch of the Kistler type 9251 3-component force transducer.
(a) Top view (b) Typical pre-load method

These load cells are designed for dynamic and quasistatic force transduction and require the use of a charge amplifier (Kistler type 5001 is specifically designed for this purpose) for each of the 3 channels. The transducer must also be preloaded with a compressive load of 25 kN in order to permit the shear forces to be transmitted to the crystals. The method of applying a preload must be very elastic with respect to the stiffness of the transducer in order to minimize the load carried by the preloading device, especially in the shear directions. Kistler recommends the use of an expansion bolt. In addition, they recommend the mounting surfaces be ground, flat and parallel.

4.1.5 The "In-house" Development of an Amplifier

Due to the high cost of each 3-component Kistler transducer as well as the requirement of a high preload and flat surfaces, it was thought that the piezoelectric transducer idea could be implemented using piezoelectric ceramic discs and an amplifier built in the lab.

The discs purchased are manufactured by the Clevite Corporation (9). Table 4.1.2 gives the pertinent technical data for the two types of material used, PZT-5 and PZT-8 which are lead zirconate-titanate crystals. Originally, the idea was to use a charge amplifier to obtain the voltage developed by the crystal, as in the Kistler transducers. For this purpose square crystals were purchased 6.35 mm to the side and 2.54 mm thick. A schematic of the amplifier is shown in Appendix A, Figure A-1. However upon static calibration

tests as described in Appendix A using the apparatus in Figure A-2, it was found that the voltage developed by the amplifier was not linear with load. Figure A-3 is a reproduction of the calibration curve showing an 8% deviation from a straight line fit by eye to the data points. There was much concern about the accuracy of calibration using this technique, mostly with respect to the fricitional force at the hinge of the lever. As a result it was decided to test the crystals on the Material Testing System, abbreviated as MTS, (41) in the MIT Mechanical Engineering Department. The MTS is a computer controlled multipurpose testing machine used for compression and tension tests. A general description of the machine, its capacity and operation is given in Appendix A. The experimental set up is shown in Figure A-6.

TABLE 4.1.2

Some of the properties of PZT-5 & PZT-8

	PZT-5	PZT-8
Relative free dielectric constant	1500	1000
Mechanical-electrical coupling factor: k_{33} (Normal)	.705	.62
k_{15} (Shear)	.685	--
Piezoelectric constant: Normal g_{33}	24.8	24.5×10^{-3} V-m/N
Shear g_{15}	38.2	-- $\times 10^{-3}$ V-m/N
Elastic compliance at constant electric field: Normal s^E_{33}	18.8	13.9×10^{-12} m^2/N
Shear s^E_{15}	-7.22	-4.8×10^{-12} m^2/N
Curie point	365°C	300°C

Also at this time it was decided to use a high-impedance voltage follower amplifier, capable of following an imput voltage of up to 300 Volts rather than a charge amplifier. The voltage follower was adopted to reduce the effect of a change in the crystal capacitance on the amplifier output. As can be seen from Figure 4.1.7 the Thevinen equivalent of the piezoelectric crystal is a voltage source with a series capacitance. Using a charge amplifier the leakage and load capacitance (C_L) as shown in Figure 4.1.7 (a) is infinite and current is drawn from the crystal. Since in this case the voltage V, measured is

$$V = \frac{1}{C} \int i \, dt$$

or

$$V = \frac{1}{C} Q$$

where Q is the charge developed from the crystal, the voltage is dependent on the capacitance of the crystal. It was suspected and confirmed by the manufacturer that the capacitance of the crystal is not constant with stress or frequency, and differs between crystals. As a result the decision was made to use a voltage follower amplifier with a Thevinen equivalent circuit as in Figure 4.1.7 (b). Here the load and leakage capacitance is almost zero and no current flows. The voltage measured by this circuit can be said to be due to three sources. The first and largest is the piezoelectric voltage developed

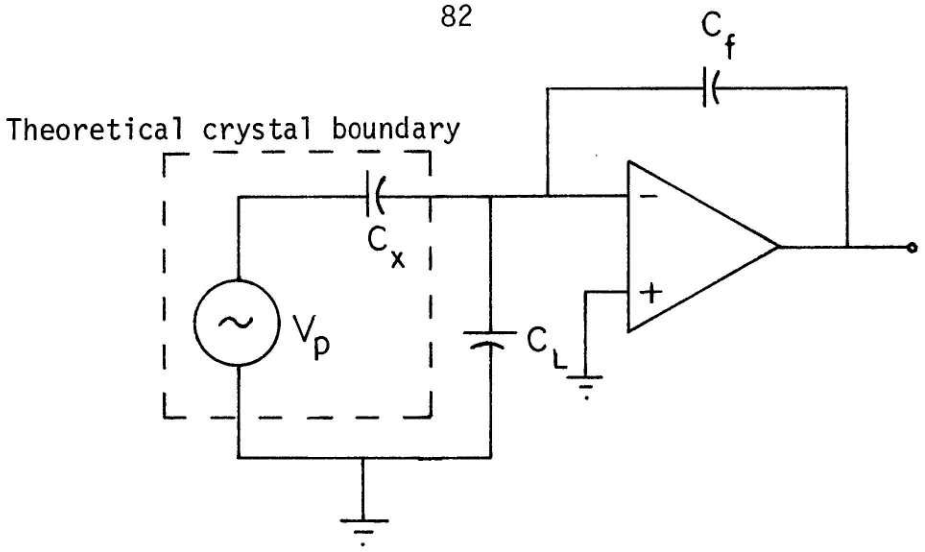

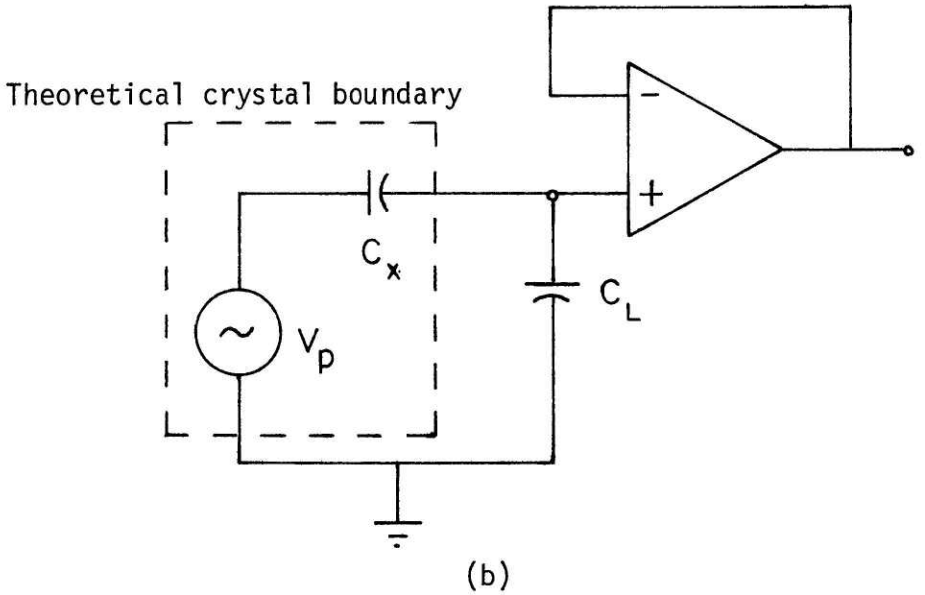

Figure 4.1.7 Thevinen equivalents. (a) Charge amplifier (b) Voltage follower

with stress. The second and much smaller contributor is due to an internal constant charge built up in the crystal due to preload and other effects. When and if the capacitance of the crystal changes, a voltage is developed according to

$$V = \frac{Q}{\Delta C}$$

Finally there is a capacitive voltage divider effect since the load and leakage capacitances are finite values. The measured voltage is a fraction of the piezoelectric voltage as

$$V_{out} = V_p \frac{C_x}{C_x + C_L} .$$

Since C_L is very small with respect to C_x (approximately 10^{-3} as large) this voltage divider effect is negligible. With the voltage follower the effect of crystal nonlinear capacitance has not been eliminated but it has been reduced to a second order effect.

The schematic of the voltage follower amplifier is shown in Figure 4.1.8. The amplifier essentially consists of a high impedance CA-3140 T op-amp (input impedance = 1.5 T Ω) at the input, which has its power supply bootstrapped to the input voltage. The op-amp is connected in a typical voltage follower configuration with the negative input tied to the output. The negative input, negative power supply and output are connected to a guard line which surrounds the op-amp capturing any leakage current. The output of the op-amp

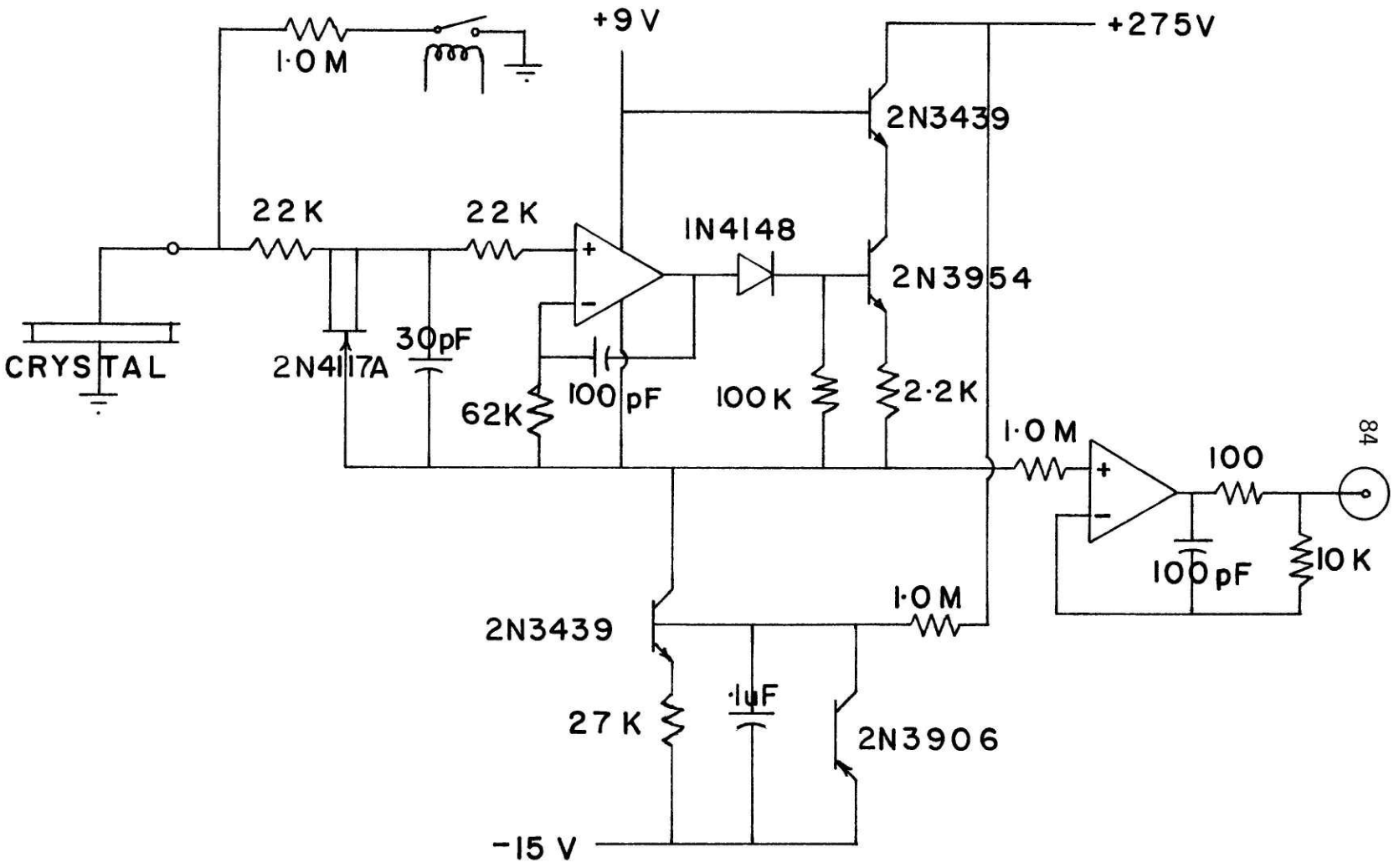

Figure 4.1.8 A schematic of the voltage follower amplifier.

controls a high voltage transistor follower which supplies the current forcing the guard to follow the positive input from -14.5 V to +275 V. A second op-amp attenuates this guard voltage to allow measurements with a chart recorder and interfacing with an analog to digital converter for computer use. A reset circuit is used to ground the input thus eliminating any voltage that builds up on the crystal due to preload and zeroes the amplifier at the particular preload. In the design of this circuit, attention was paid to reducing the leakage current, thus the choice of the CA-3140 T op-amp which has a leakage current less than 1 pA and the use of an FET as a diode to keep the positive input .5 volts above the guard voltage.

The amplifier was checked for linearity with the set-up shown in Figure A-4 using a high voltage signal applied to the amplifier through the crystal. Linearity as measured as the difference between input and output was found to be approximately .03% of full voltage with a slow triangular input varying from -5V to +275V and .29% of full voltage with inputs of a 500 Hz -5V to +275V triangular wave and a 1 Khz sine wave of the same amplitude. Figure A-5 is a photograph of the oscilloscope trace showing the input signal and the corresponding error.

For use with the voltage follower, larger crystals were needed, since the original smaller, square crystals developed an unmanageable peak voltage of approximately 3900 Volts according to

$$V = g_{33} t \, F/A$$

where g_{33} = voltage sensitivity to axial stress = $24.8 \times 10^{-3} \frac{V/m}{N/m^2}$

t = thickness of the crystal = 2.54×10^{-3} m

F = applied force = 2500 Newtons

A = crystal area = 39.94×10^{-6} m^2.

Thus new 25.4 mm diameter and 2.54 mm thick discs were purchased. These developed a theoretical voltage of only 276 Volts for a load of 2500 Newtons.

Figure A-7 is a sketch of the crystal in place to be loaded by the MTS machine hydraulic ram. The ball bearing-plate assembly was used to apply the load as normal to the crystal's surface as possible, thus reducing the shear load on the crystal. The load was applied using the force feedback mode of operation of the MTS machine. Normally a triangular shaped load versus time curve was used in which the load was applied gradually up to a peak load and then removed at the same rate as it was applied. Various rates of load application (N/sec) were used. A strain gauge load cell manufactured by Lebow Industries (36) was in series with the hydraulic ram and using this signal a reference load versus time curve was obtained. For any particular load application two runs were performed. On the first run the load cell voltage was plotted versus time on the X-Y recorder of the MTS machine. This curve was converted to a load versus time graph using the calibration curve of the load cell. The subsequent run, using the same load pattern, plotted on the same piece of paper the crystal voltage versus time. Using the load cell as a standard, calibration of the crystal was possible.

The first method of making an electrical connection with the crystal shown in Figure A-7 (a), used printed circuit board material. This is a composite of an epoxy resin impregnating a glass cloth with a bonded layer of copper. The particular type used was number G-11 which is a .794 mm thick glass-epoxy board covered with a layer of .038 mm thick copper. The compressive strength of the composite is approximately 345,000 N/m^2. The copper layer was etched to provide an electrical guard for the amplifier. An area of copper cladding encircling the positive electrode of the crystal was connected to the guard. Thus any surface leakage current from the crystal would be picked up by the guard. Testing in the configuration of Fig. A-7 (a) led to apprehension about the rigidity of the printed circuit board material and the possibility that the board was carrying some of, and therefore dividing, the load. This was suggested by the circuit board bending over the edges of the crystal because the loading rams were larger in diameter than the crystal.

To circumvent this problem the configuration used was as shown in sketch (c) of Figure A-7. This technique used glass optical flats which were smaller in diameter (22 mm) than the crystal (25.4 mm) to electrically insulate the crystal from the loading ram. The crystal was then connected to the amplifier by soldering leads directly to the silver electrodes on the crystal. This method was used for the plots shown in Figure 4.1.9.

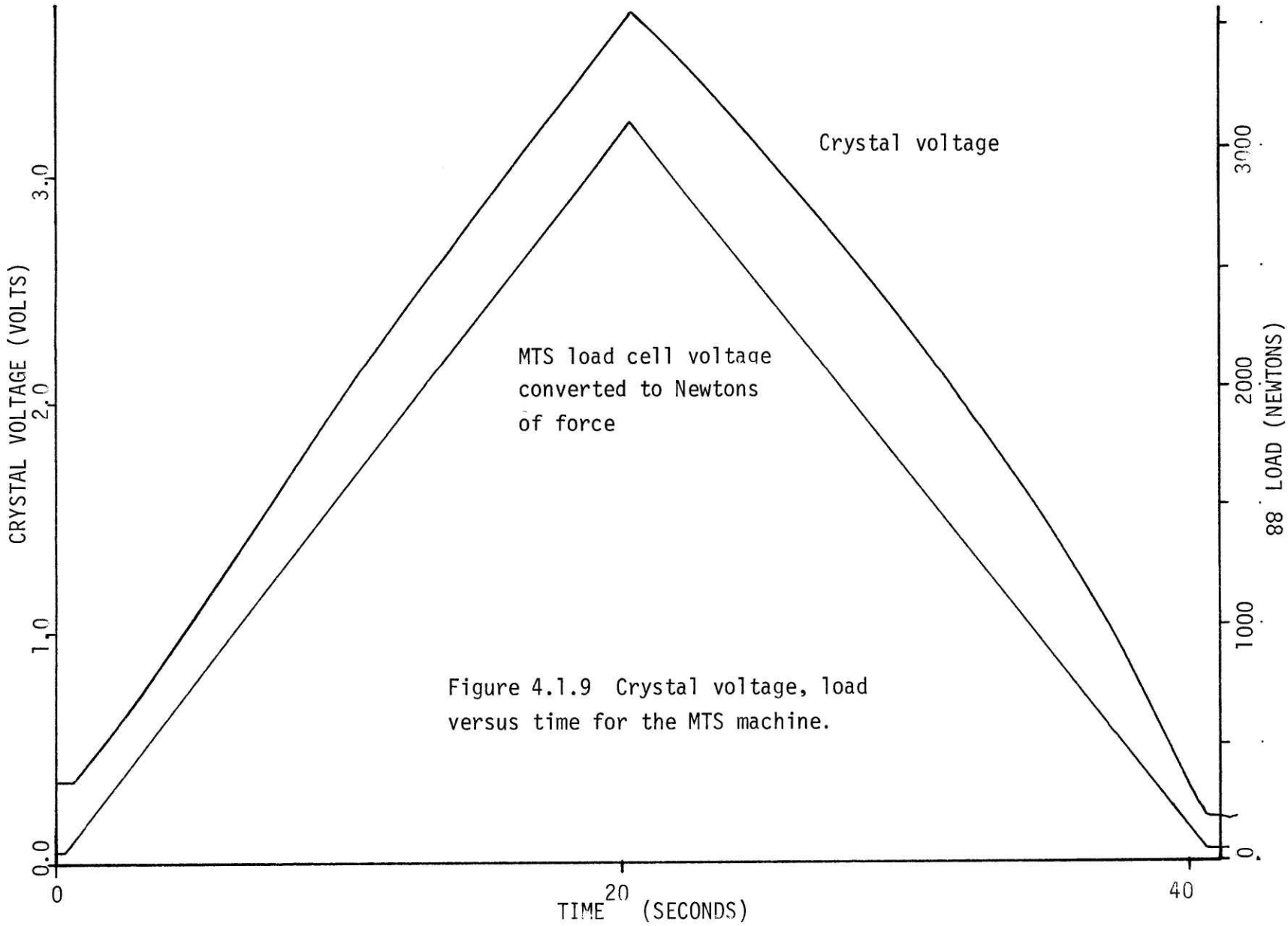

Figure 4.1.9 Crystal voltage, load versus time for the MTS machine.

A reproduction of a typical output voltage versus time curve from the crystal compared with the corresponding curve from the MTS load cell is shown in Figure 4.1.9. Note the bowed out deviation from a straight line in the crystal curve as the load was applied and removed, especially as it was removed. These results will be compared with later developments to be discussed further on in this section.

Due to the high cost of renting the MTS machine and its more than adequate load capabilities (up to 490,500 N load capacity) it was decided to use the hip simulator machine of the MIT Hip Prosthesis Research Project, forthwith called the HSM, for further calibration. This machine was designed and built by David Palmer and Paul Rushfeldt. The primary purpose of the HSM is to study pressure distributions in the human hip socket using an instrumented hip prosthesis with 14 pressure transducers in the prosthesis. The HSM, as shown in photographs on Figures 4.1.10 and 4.1.11, was built along the same lines as the MTS machine with the modification that the yoke assembly holding the hydraulic ram can rotate about a horizontal axis so that loads may be applied at any angle from the vertical ranging from -90 to +90 degrees, a useful feature in the study of the hip (54,55). A strain gauge load cell is also included in this machine, in series with the hydraulic ram. It consists of 4 columns, each column having a strain gauge on it as in Figure A-8. The HSM is controlled either manually or by a computer, a Digital Equipment (15) PDP-11/40. The maximum load capability of the HSM is 4448 Newtons (1000 pounds); the load cell is calibrated for pounds force rather than Newtons.

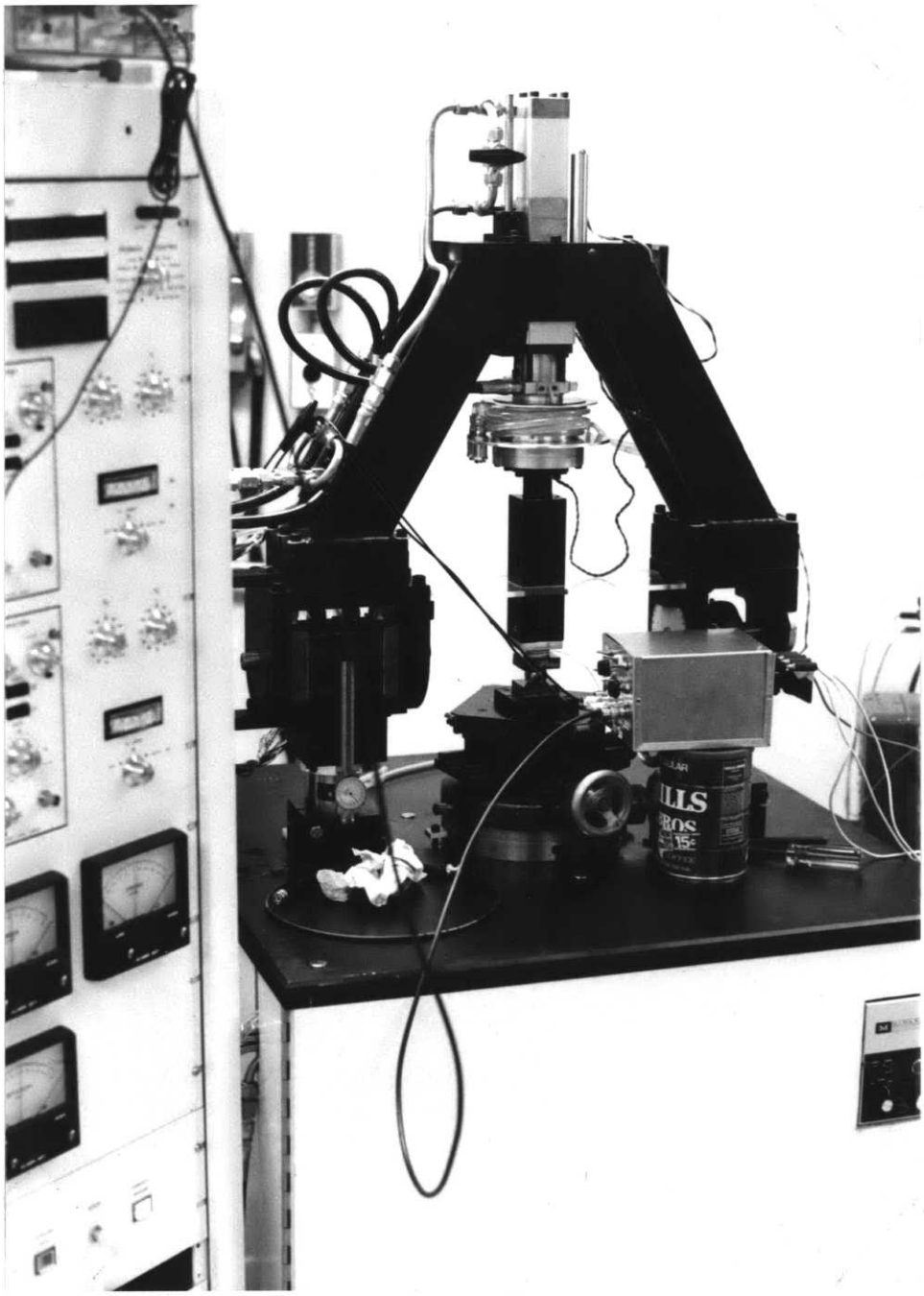

Figure 4.1.10 The HSM showing table and yoke.

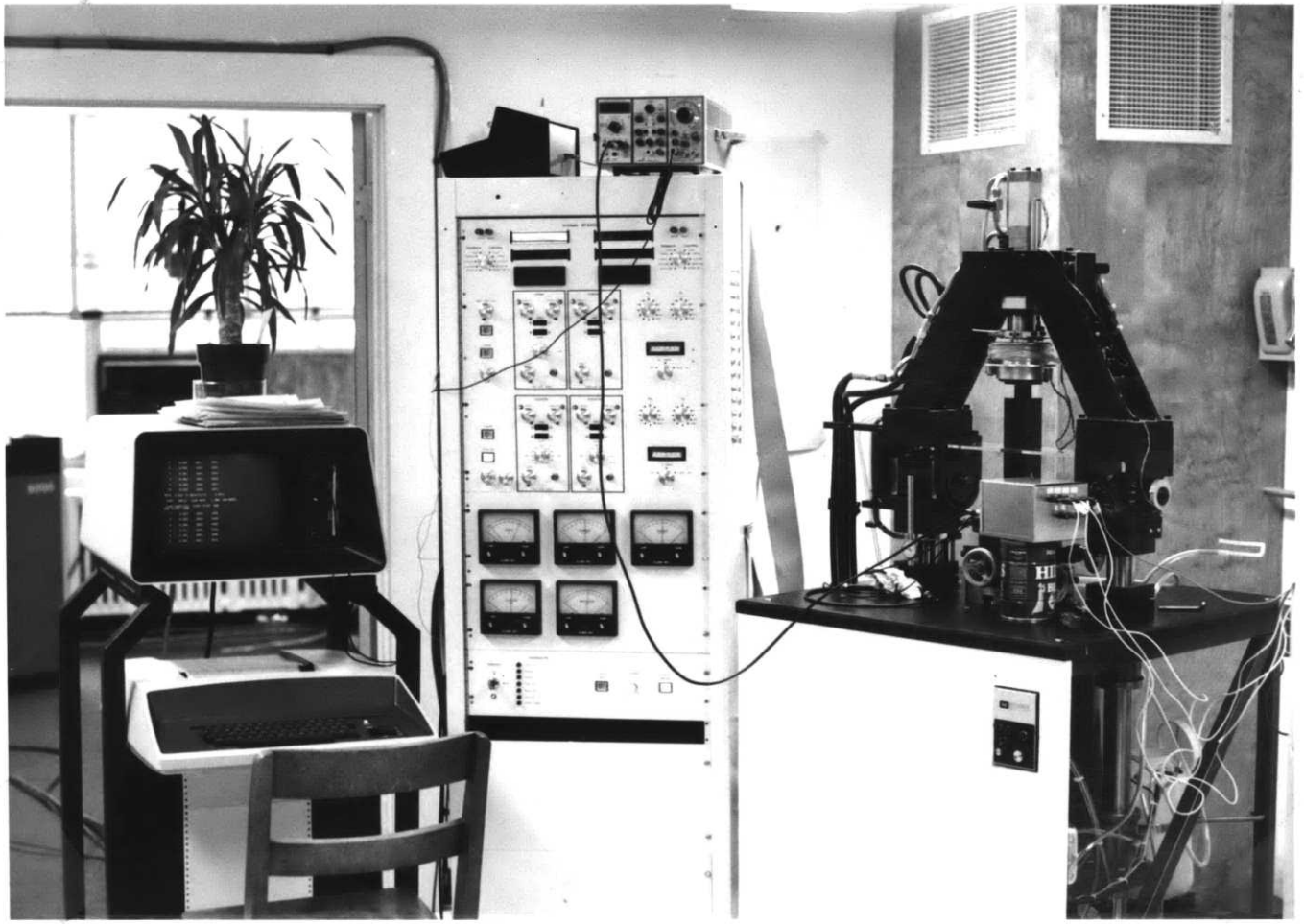

Figure 4.1.11 The HSM with controller and computer.

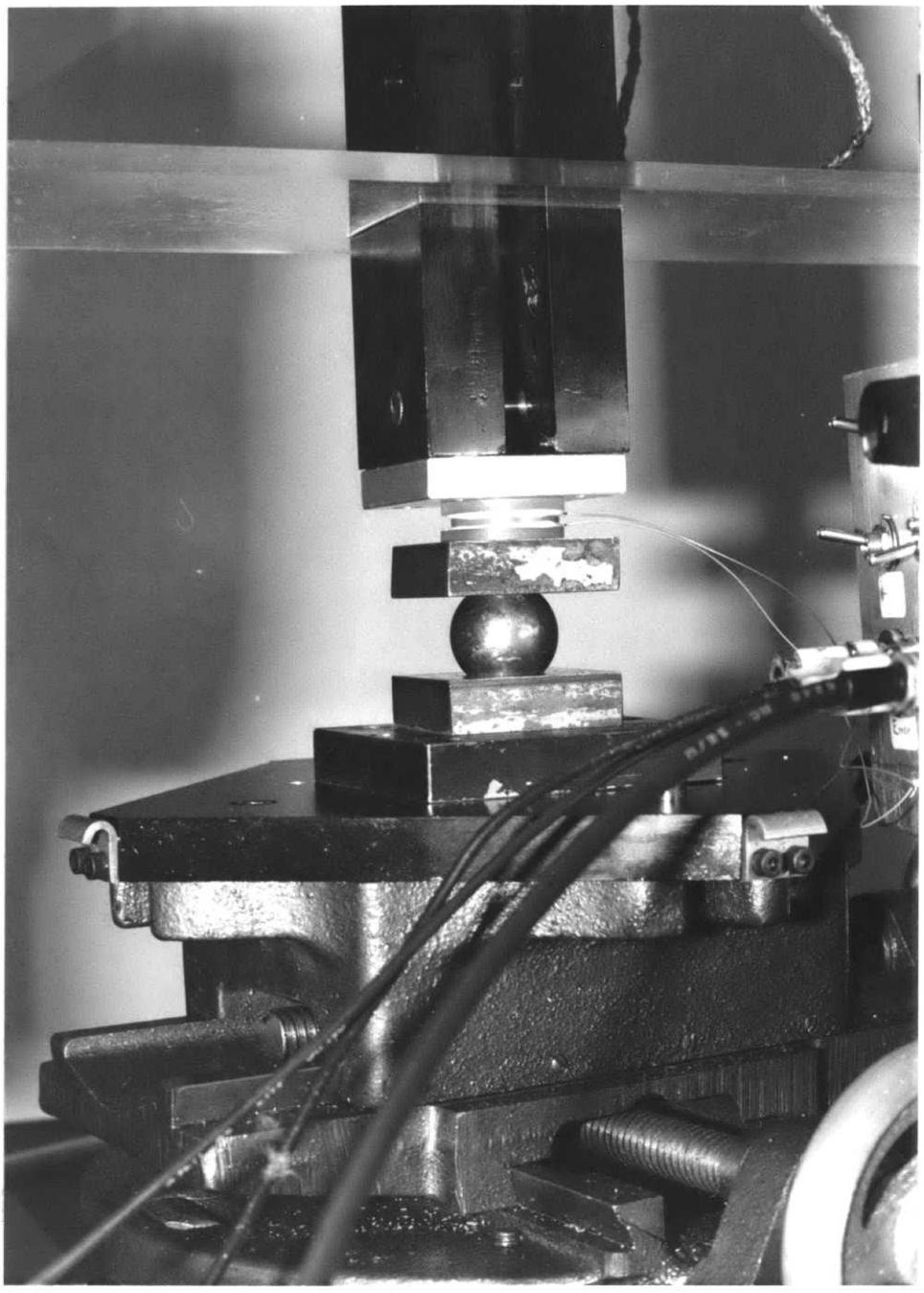

Figure 4.1.12 The loading system used with the HSM.

across the entire surface. Furthermore, because the lead-in wires form a leakage capacitance to ground, the length of the connections were reduced to a minimum by situating the amplifier directly beside the crystal. The amplifier capacity was measured to be less than 1 pF. The amplifier circuit was constructed on printed circuit board with the guard surrounding the inputs of the op-amp to capture any possible leakage current at this point. The reset switch that re-zeroes the amplifier was replaced by an electromechanical relay to enable the amplifier to be reset by a command from the computer. This relay used glass bead pivots thereby providing a high impedance to ground. Initially the HSM load cell voltage, crystal voltage and the difference of the two as measured by a differential amplifier were recorded with a strip chart recorder, Brush Clevite model 2400. The differential amplifier used an op-amp in a summing configuration since the HSM load cell signal polarity was opposite to that of the crystal. Variable gain available on the load cell signal allowed a scale factor adjustment and nulling of the "error" signal. The HSM was controlled manually and the data was analyzed from the strip chart recordings. Figures A-9 and A-10 are typical recordings for a step input and a slow rise input.

Time consumption and interpretation difficulties in analyzing the results from the recordings, led to the use of the analog to digital converter (abbreviated A/D) of the PDP-11/40 and with the computer sampling the signal and performing the necessary calculations. This eliminated the need for the analog error signal, as the

computer used the digital signals and applied the necessary scale factors. The sampling rate chosen for the A/D converter was 500 Hz. This allowed accurate reconstruction of signals with frequency component of up to 250 Hz, which was considered above the expected upper limit of the frequency content of any present or future experiments.

The digital signal from the HSM load cell was calibrated by first removing the load from the cell and sampling the signal, then the HSM was set manually to a load of 2224 Newtons (500 pounds) using the panel digital voltmeter. The signal sent to the computer was then sampled and a linear fit for the calibration curve was calculated using the zero signal, the loaded signal and the known load. Problems were encountered with 60 Hz noise appearing on the inputs to the A/D converter, due to ground loops occuring between the HSM load cell, controller and computer because of slightly different ground potentials. Thus sampling was done for .25 seconds (15 periods of a 60 cycle signal) with arithmetical averaging of the sampled values to obtain a true value.

Static calibration was done in the following manner. A diagram of load versus time used for the calibration "runs" is shown on Figure 4.1.13. First, a zero point was established by setting the HSM to a load of 133 N (30 lbs) preloading the crystal. The amplifier was reset by the computer and sampling started. The zero point was sampled for .50 seconds (again an integral number of periods (30) of the 60 Hz noise signal, thus nullifying the effect of noise) and

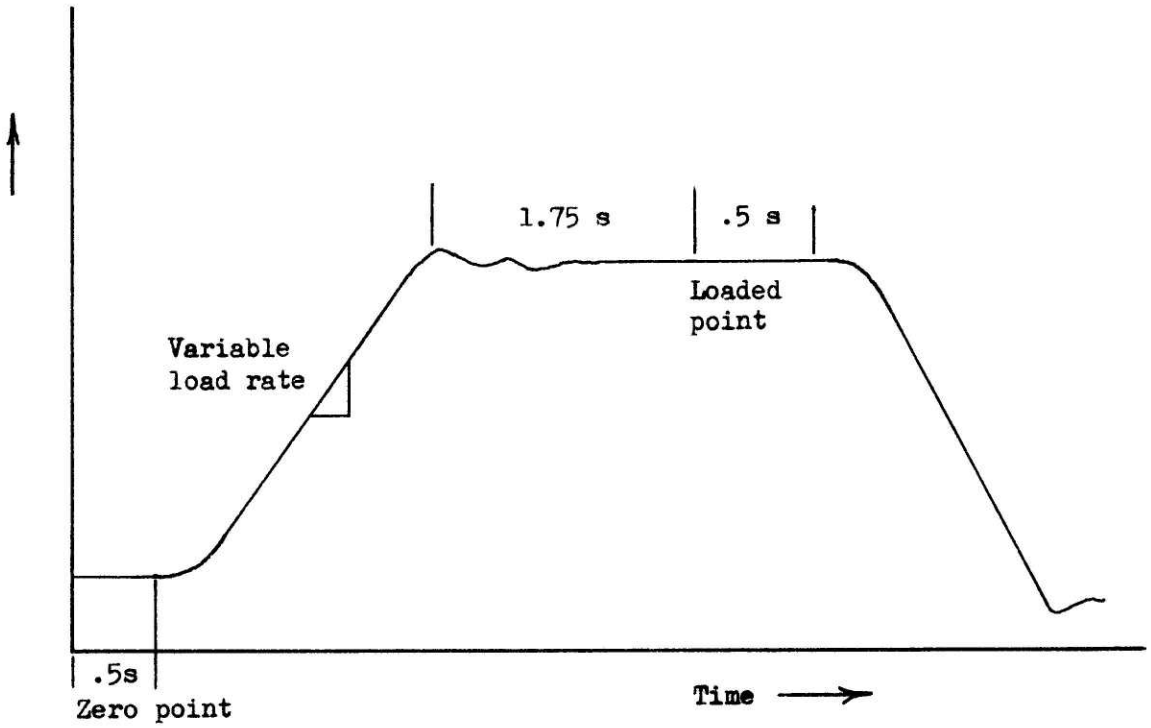

Figure 4.1.13 The loading pattern used for a calibration run.

then the load was applied. The rate of loading was varied from a step load which was limited by the hydraulics to approximately 89 N/msec (20 lbs/msec), to a slow rate of 2.22 N/msec (.5 lbs/msec), using five rates in all. The full load level was also varied from 222 N (50 lbs) to 2224 N (500 lbs) above the preload level. Sampling continued throughout the loading but only .5 seconds worth of data at the full load was used for the calibration. As shown a small 1.75 second settling time was used to allow for transients in the hydraulics to die. At each combination of rate and load level, 10 runs were made, so that in all 500 data points were used. These 500 pairs of values (load cell voltage, crystal voltage) were used to fit a curve of load as a function of crystal voltage. The results of a typical calibration run for a crystal made of PZT-8 and 25.4 mm in diameter, 2.54 mm thick are shown on Figures 4.1.14 and 4.1.15, with the values tabulated in Table 4.1.3.

Figure 4.1.14 is a plot of the crystal voltage versus the load applied. Each cross represents 50 data points (5 rates at the particular load level and 10 loadings per combination of load and rate). The line is the best fit calculated using a least squares linear regression. Figure A-11 is a plot of the same values with a quadratic curve used to fit the data. Figure 4.1.15 is a graph of the sensitivity in mV/N versus load again plotted at the 10 different load levels. The bars associated with each point represent one standard deviation above and below the value. Table A-1 lists the values of voltage and sensitivity for the 50 combinations of rate

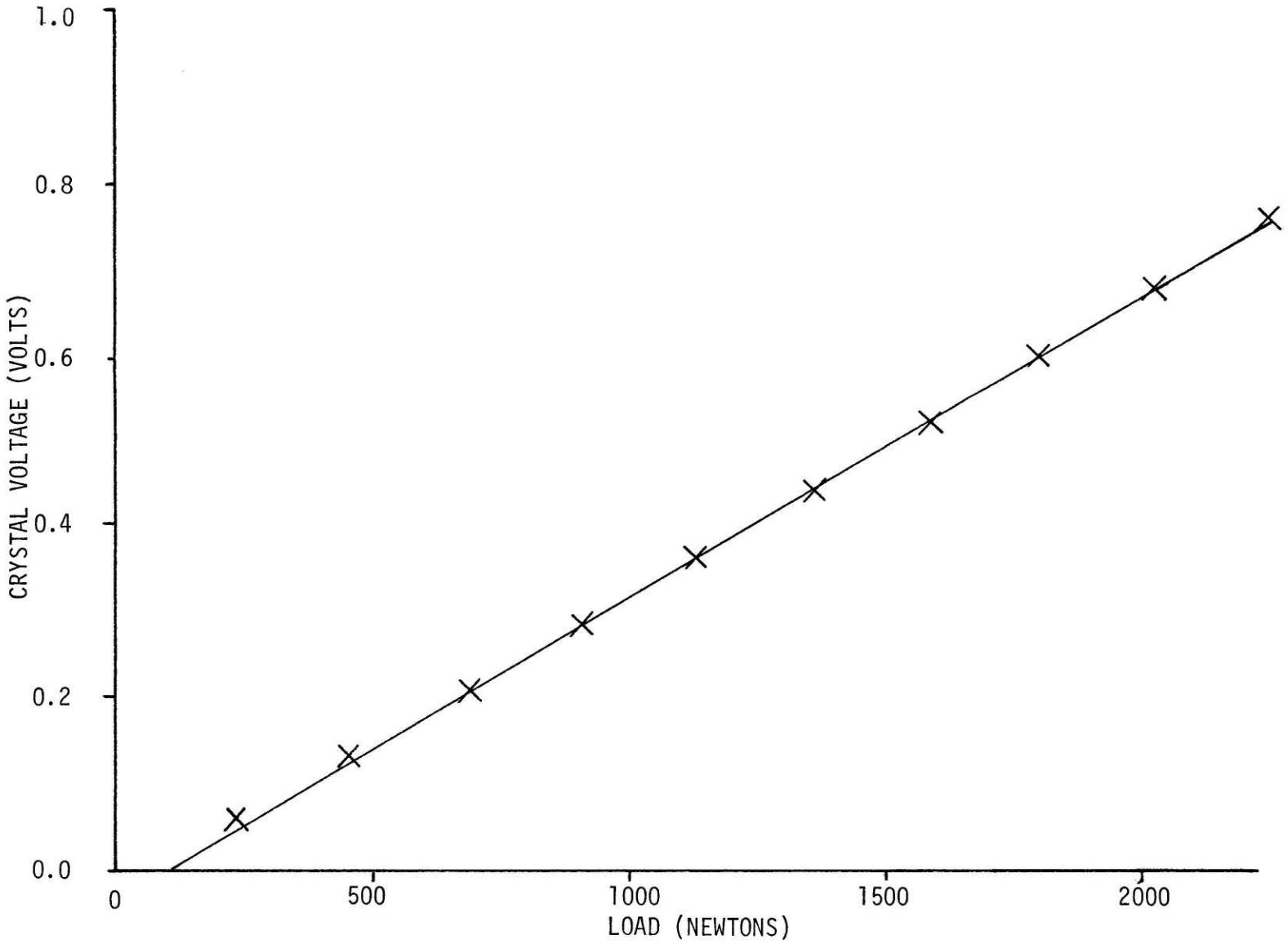

Figure 4.1.14 Crystal voltage versus load, data points and fitted line.

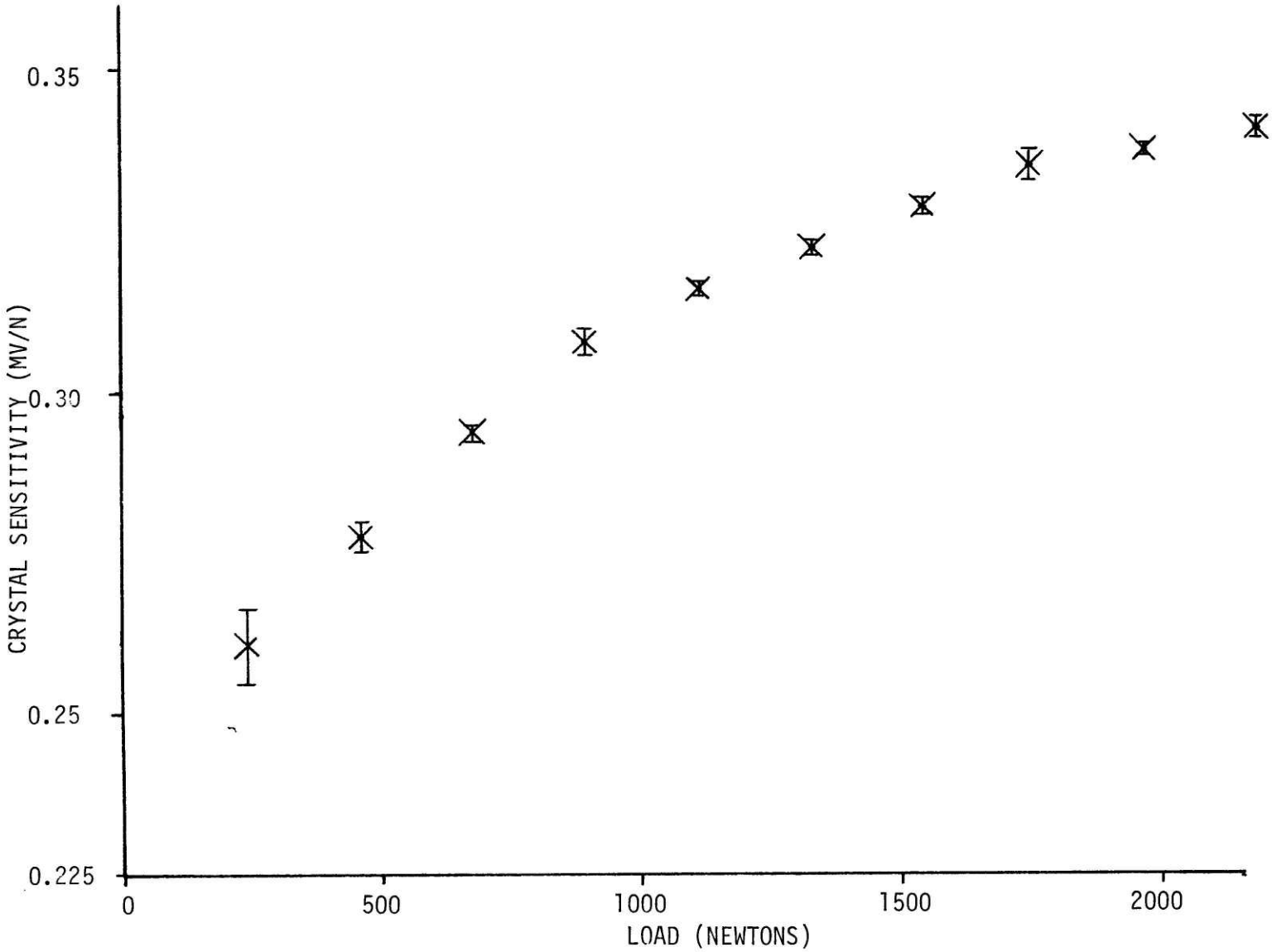

Figure 4.1.15 Crystal sensitivity versus load.

TABLE 4.1.3

Crystal Voltage Values and Load Values for Calibration Run 12 (Figure 4.1.14)

Load (Newtons)	Crystal Voltage (Volts)
224	.062
445	.131
667	.204
889	.281
1112	.359
1334	.438
1557	.519
1779	.600
2002	.661
2224	.764

Crystal Sensitivity Values and Load Values for Calibration Run 12 (Figure 4.1.15)

Load (Newtons)	Crystal Sensitivity (mV/N)	Standard Deviation ($mV/N \times 10^{-3}$)
224	.256	5.62
445	.281	3.82
667	.297	2.69
889	.309	2.225
1112	.317	2.02
1334	.323	2.02
1557	.327	1.57
1779	.335	2.70
2002	.337	2.47
2224	.340	1.79

and load level. Figures A-12 and A-13 plot the crystal voltage and crystal sensitivity versus the loading rate. As can be seen from these plots, both voltage and sensitivity are invariant with the speed of application of the load. Once a curve was fit to the data, the expected values of load at each point were calculated using the crystal voltage and the curve coefficients previously arrived at and compared with the actual load as measured from the load cell. The error is the absolute value of the difference. Table 4.1.4 is a typical output from the computer for the results of a calibration run. As can be seen, the crystal static nonlinearity with respect to the HSM load cell is .70% of full scale on the average.

To check the method of calibration and the linearity of the HSM load cell itself, exactly the same procedure was done using a Statham load cell (62). This is a cantilevered beam style load cell where the deflection is measured by a strain wire transducer. The results shown in Figures A-14 and A-15 and tabulated in Tables A-2 and A-3 show the Statham load cell to be more linear with respect to the HSM load cell than the crystal, 0.24% of full scale average error versus 0.70%. Also, looking at the table of error values histogram of the two (Table 4.1.2 and Table A-2 at the bottom), the Statham shows less dispersion from a line thus better repeatibility.

Dynamic tests were performed with either a step or sinusoidal load as the input. Figures 4.1.16 to 4.1.19 are typical results from a step input and Figures 4.1.20 to 4.1.23 are from sinusoidal load inputs. The step input was obtained by sending a step function

TABLE 4.1.4

CALIBRATION RUN NUMBER 12 PZT-8 25.4 MM DIA 2.54 MM THK

THE LARGEST LOAD WAS 508.3 POUNDS

THE FOLLOWING ARE THE COEFFICIENTS
FIT TO A POLYNOMIAL OF ORDER 1
GIVING LOAD IN POUNDS IN TERMS OF CRYSTAL VOLTAGE IN VOLTS

THE INTERCEPT = 21.80
THE COEFFICIENT OF X ** 1 = 637.91

THE STANDARD DEVIATION OF THE ABOVE CURVE FIT IS 4.4002
THIS CURVE FIT IS BASED ON 500 DATA POINTS

ANALYSIS OF LOAD CURVE COEFFICIENTS

THE FOLLOWING RESULTS WERE CALCULATED
TO CHECK THE EXPECTED VALUES AGAINST ACTUAL VALUES
USING THE DATA FROM THE CALIBRATION RUN AS INPUT

AVERAGE ERROR:	3.58	POUNDS(ABSOLUTE VALUE)
	0.70	PERCENT OF FULL SCALE
	2.35	PERCENT OF READING
RMS ERROR:	4.39	POUNDS
	0.86	PERCENT OF FULL SCALE
	4.45	PERCENT OF READING
LARGEST POSITIVE ERROR:	23.58	POUNDS
	4.64	PERCENT OF FULL SCALE
	17.87	PERCENT OF READING
LARGEST NEGATIVE ERROR:	-6.90	POUNDS
	-1.36	PERCENT OF FULL SCALE
	-10.70	PERCENT OF READING

ERROR VALUES HISTOGRAM

154	POINTS	IN THE RANGE	0	LBS TO	2	LBS
151	POINTS	IN THE RANGE	2	LBS TO	4	LBS
126	POINTS	IN THE RANGE	4	LBS TO	6	LBS
43	POINTS	IN THE RANGE	6	LBS TO	8	LBS
20	POINTS	IN THE RANGE	8	LBS TO	10	LBS
2	POINTS	IN THE RANGE	10	LBS TO	12	LBS
2	POINTS	IN THE RANGE	12	LBS TO	14	LBS
1	POINTS	IN THE RANGE	14	LBS TO	16	LBS
0	POINTS	IN THE RANGE	16	LBS TO	18	LBS
0	POINTS	IN THE RANGE	18	LBS TO	20	LBS
0	POINTS	IN THE RANGE	20	LBS TO	22	LBS
1	POINTS	IN THE RANGE	22	LBS TO	24	LBS

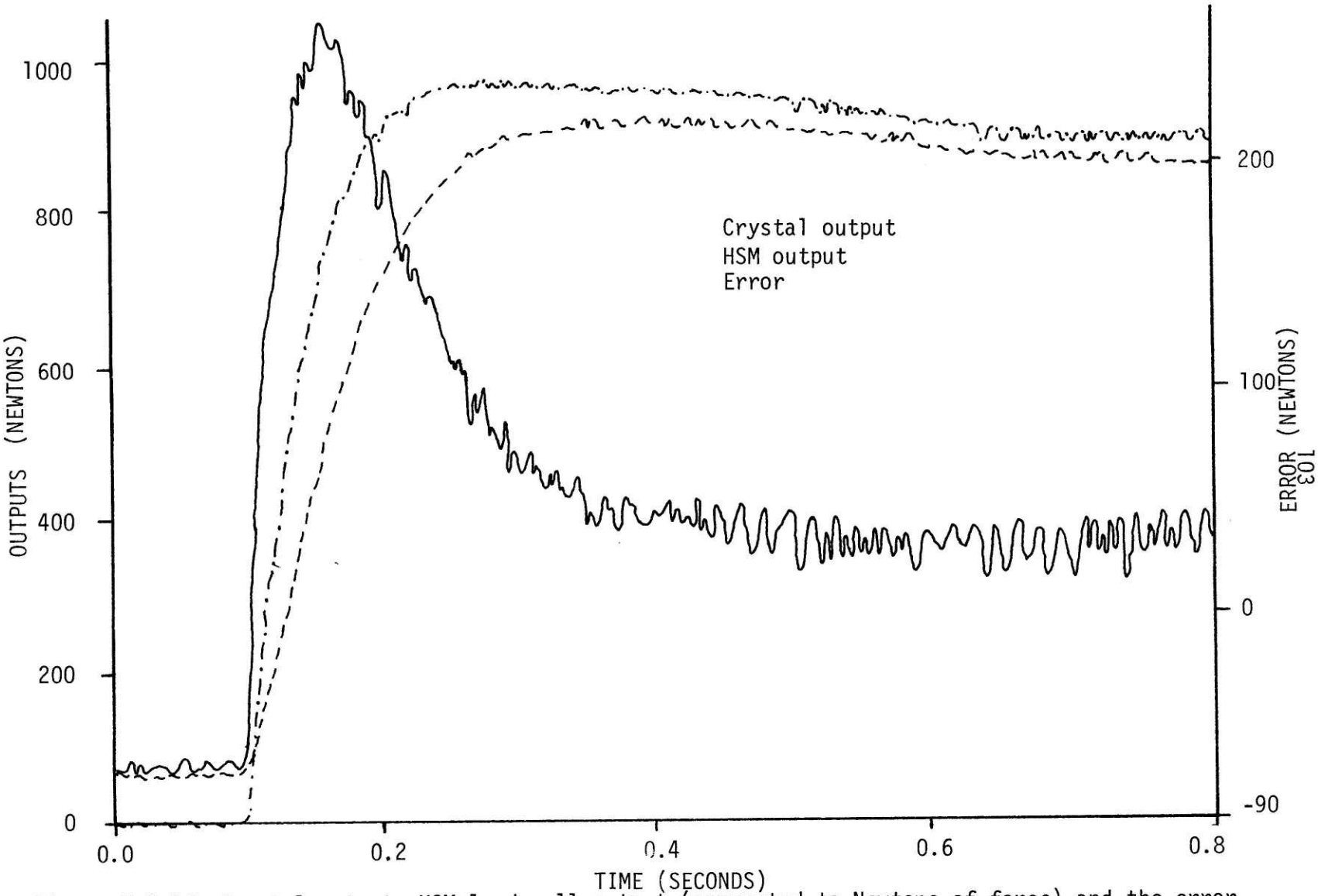

Figure 4.1.16 Crystal output, HSM load cell output (converted to Newtons of force) and the error versus time for a step load, outputs unfiltered.

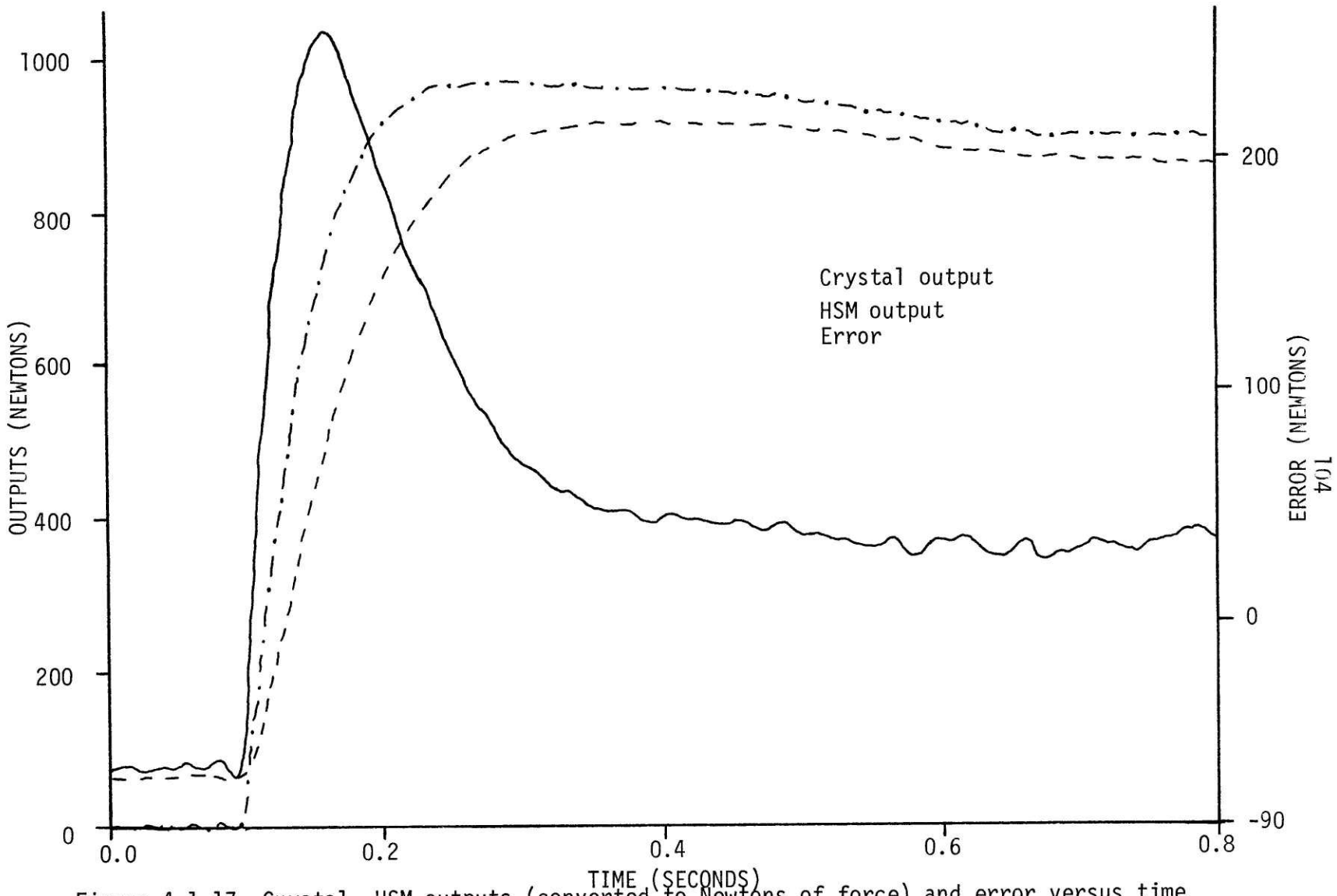

Figure 4.1.17 Crystal, HSM outputs (converted to Newtons of force) and error versus time for a step load, both outputs filtered.

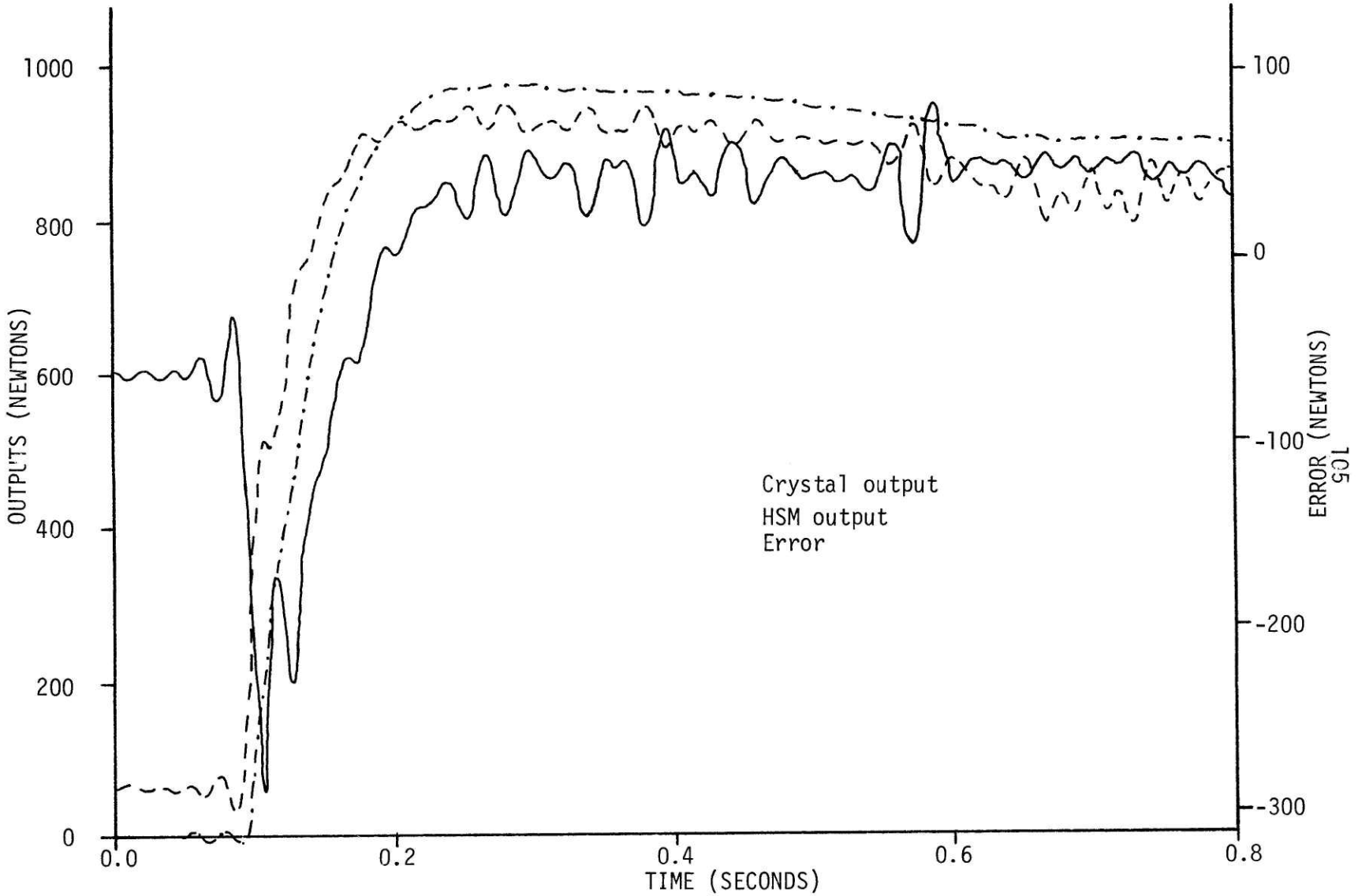

Figure 4.1.18 Crystal, HSM outputs (converted to Newtons of force) and error versus time for a step load, both outputs filtered. A first order lead applied to the crystal output with a 50 ms time constant.

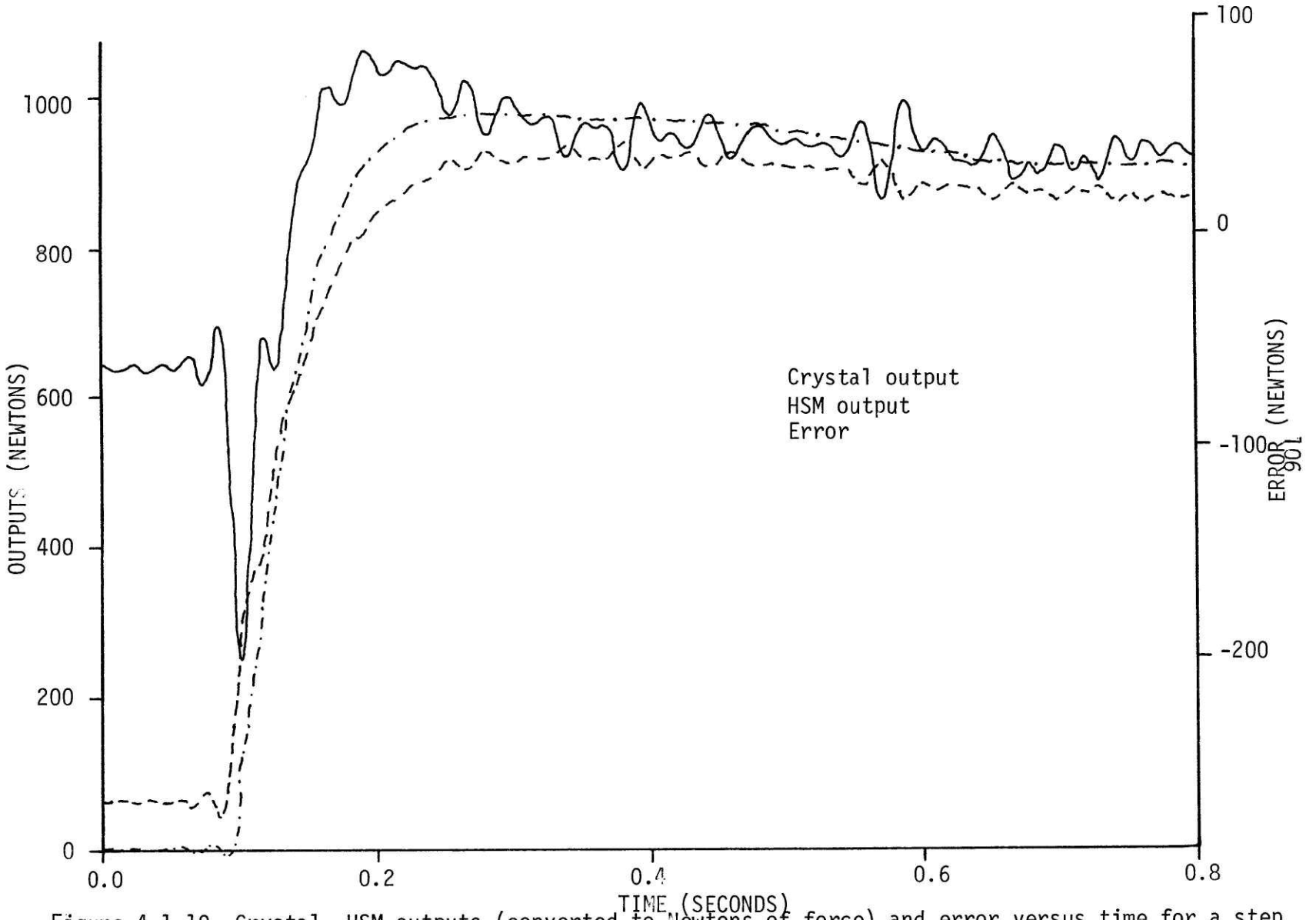

Figure 4.1.19 Crystal, HSM outputs (converted to Newtons of force) and error versus time for a step load, both outputs filtered. A first order lead applied to the crystal output with a 30 ms time constant.

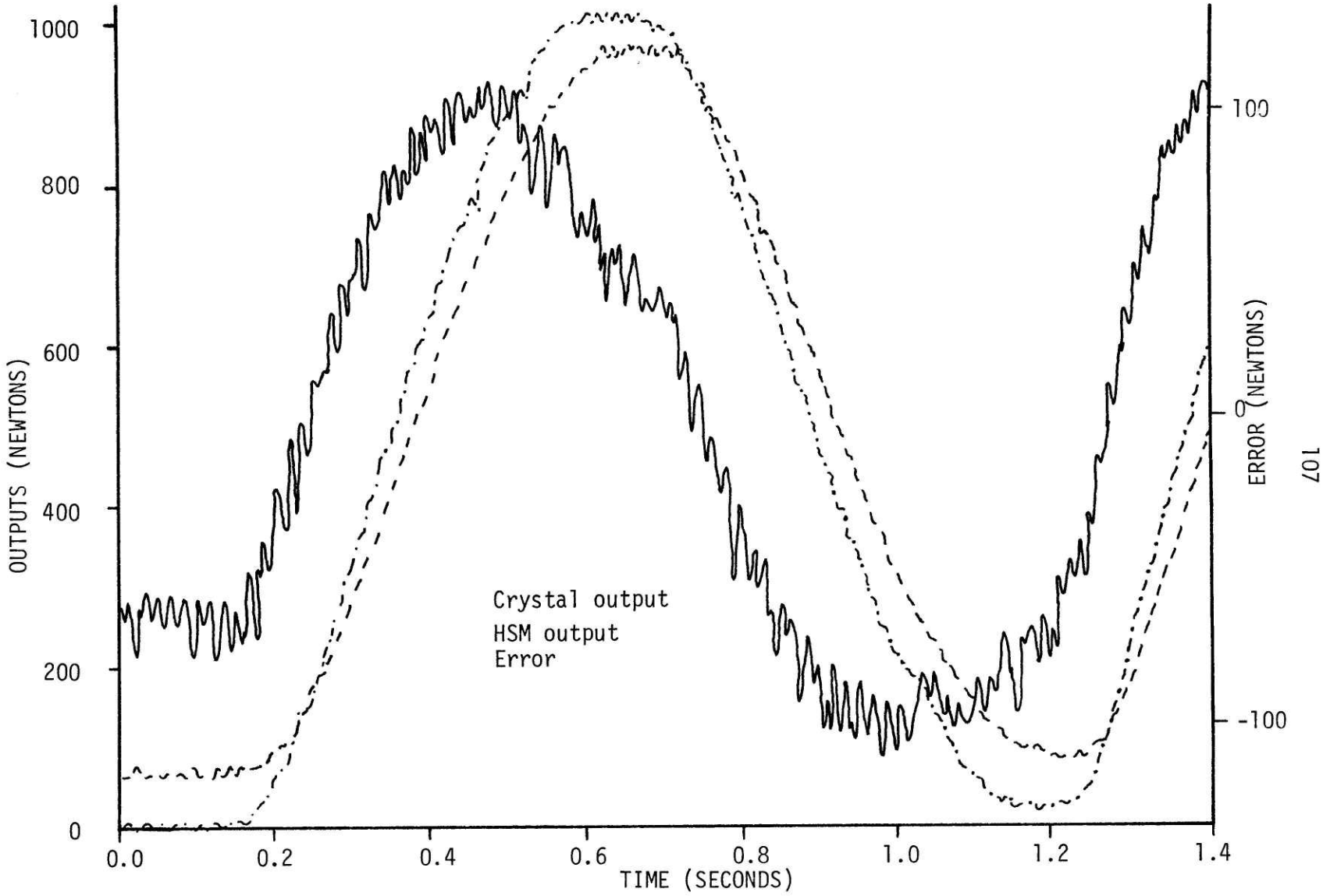

Figure 4.1.20 Crystal, HSM outputs (converted to Newtons force) and error versus time for a sinusoidal load, both outputs unfiltered.

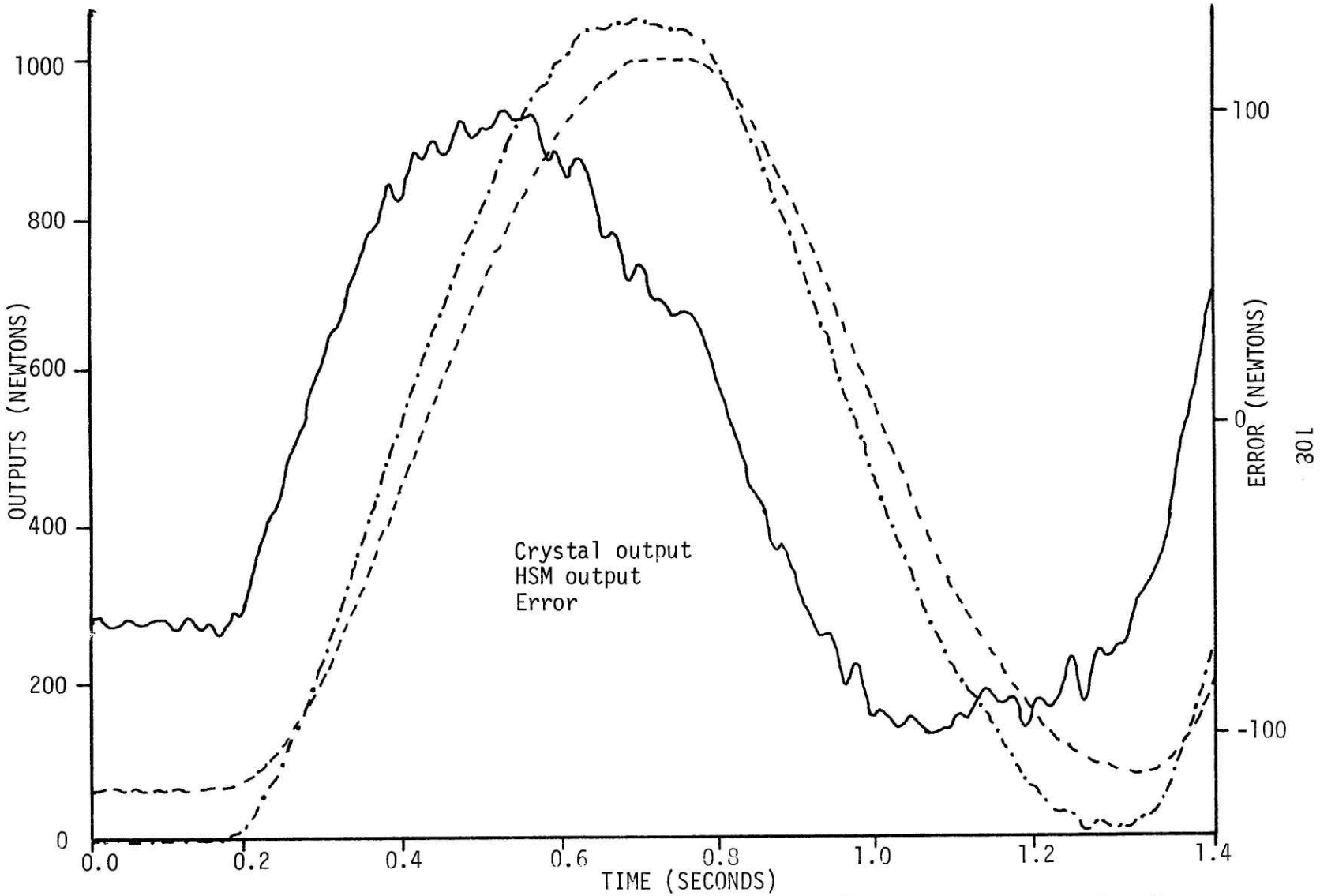

Figure 4.1.21 Crystal, HSM outputs (converted to Newtons force) and error versus time for a sinusoidal load, both outputs filtered.

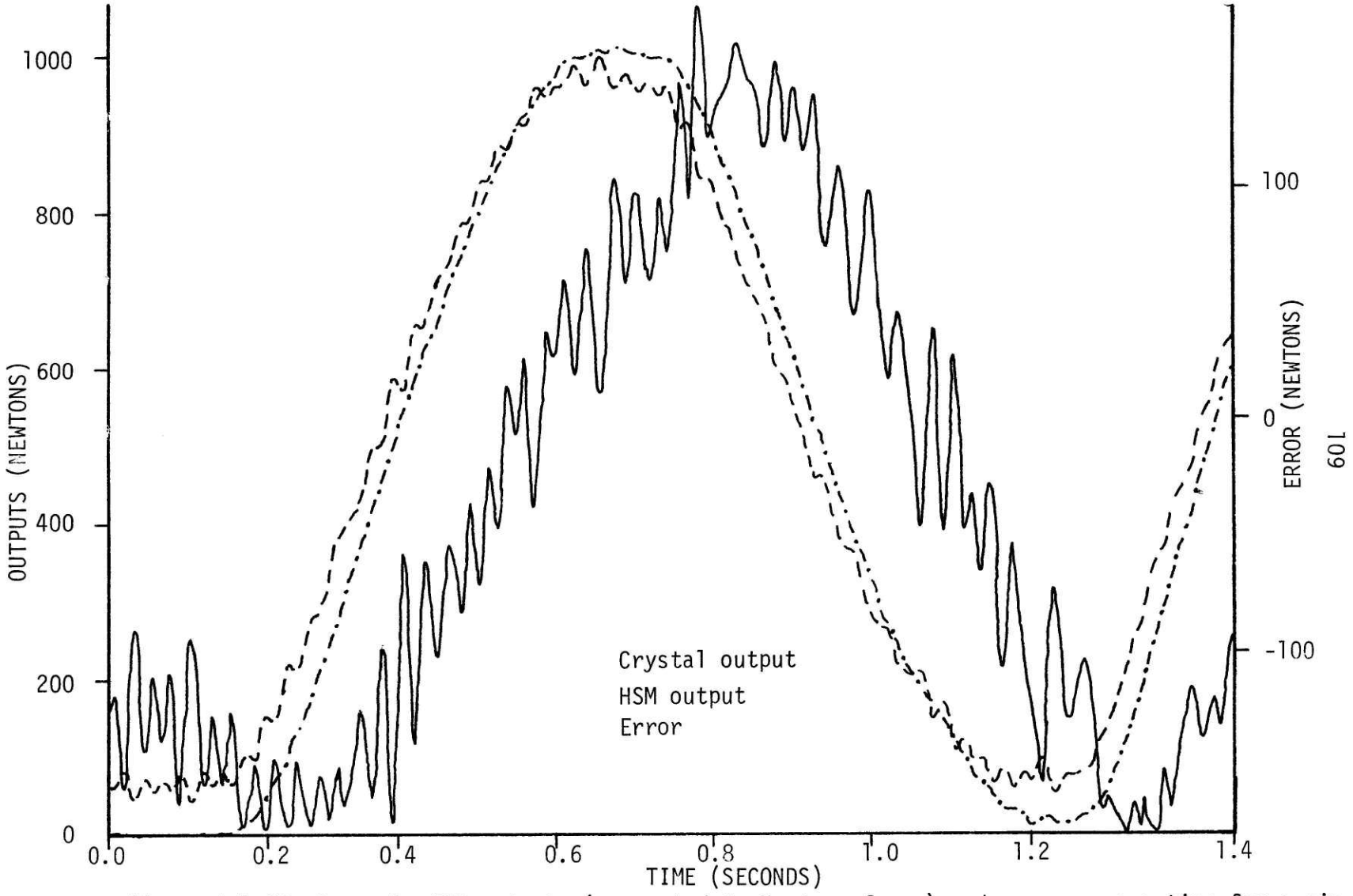

Figure 4.1.22 Crystal, HSM outputs (converted to Newtons force) and error versus time for a sinusoidal load, both outputs filtered. A first order lead applied to the crystal with a 50 ms time constant.

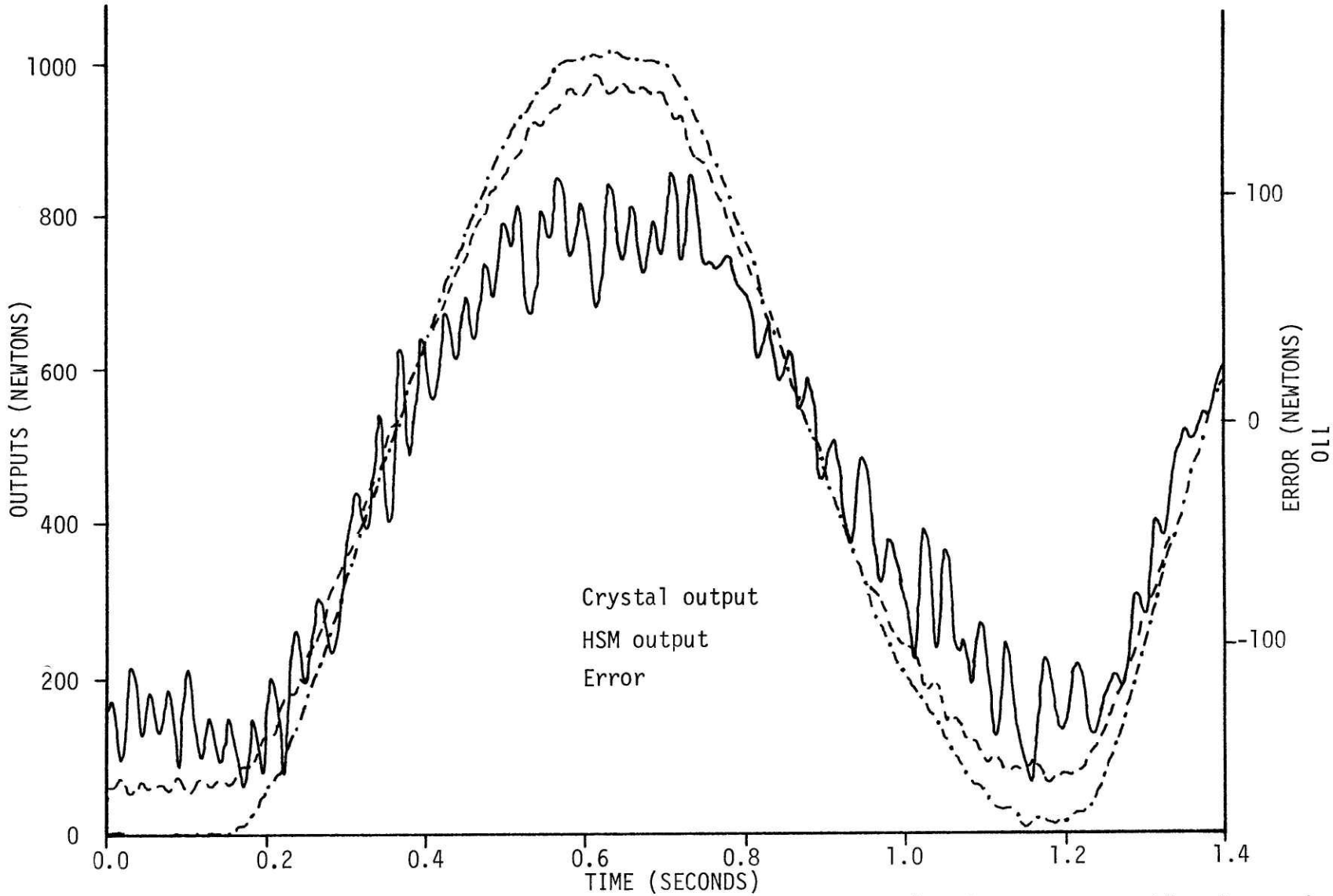

Figure 4.1.23 Crystal, HSM output (converted to Newtons force) and error versus time for a sinusoidal load, both outputs filtered. A first order lead applied to the crystal with a 30 ms time constant.

from the computer to the HSM controller. Again the A/D converter sampled both the HSM load cell and the crystal amplifier output at 500 Hz. Just prior to the application of the loading function the crystal amplifier was rezeroed. The graphs show the load cell readings minus the preload; thus the load starts and ends at 0 Newtons force. The crystal voltages were translated into load by use of the coefficients calculated from the calibration run for that particular crystal. Because of the problem of 60 Hz noise, a digital filter was used on the data. The particular filter used was a 10th order low pass Butterworth filter with a breakpoint at 46.7 hertz and gain down 20db at 59.8 hertz. Note the difference between the curves in Figures 4.1.16 and 4.1.17. This error curve was generated by subtracting the crystal values from the HSM load cell values, the scale for the error curve being on the right hand vertical axis.

From Figures 4.1.16 and 4.1.17, one can see a similarity between the response of the crystal and the response of a system with a first order lag, as shown in Figure 4.1.24, both to a step input.

Note that the input to the crystal is not a perfect step, thus the calculation of T the time constant in the equation

$$\frac{G(s)}{F(s)} = \frac{1}{Ts + 1}$$

where G(s) = Laplace transform of the system output

F(s) = Laplace transform of the system input

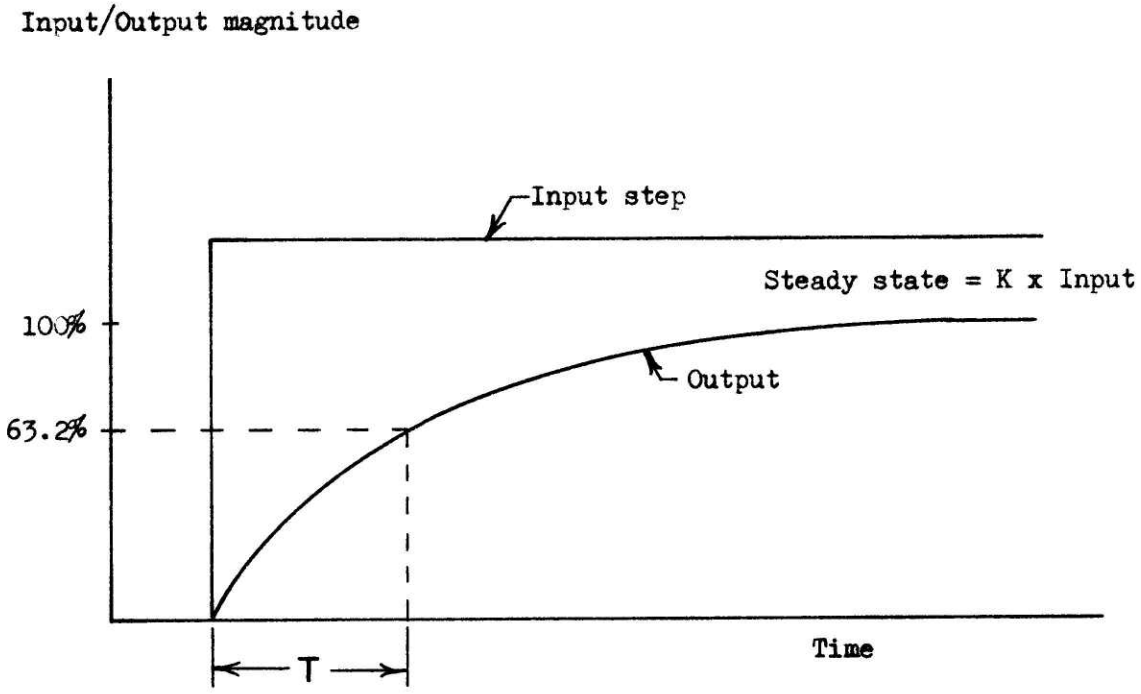

Figure 4.1.24 The step response of a system with a first order lag.

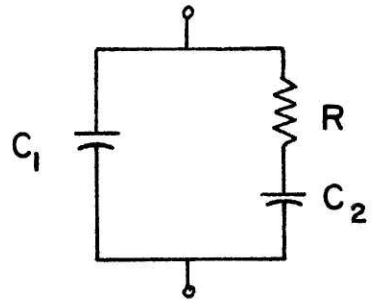

Figure 4.1.25 A first order model of a capacitor.

describing the system response of a first order lag, cannot be calculated directly as the time for the output to reach 63.2% of the steady state value. One can, however, get a rough approximation of the value of T. For Figure 4.1.17 the value was calculated to be .065 seconds. Since the input was slower than ideal, this value of T was expected to be larger than the real value. This indeed seemed to be the case. Using the filtered data the crystal values were put through a phase lead according to

$$G'(s) = F(s)(Ts + 1).$$

The Ts term being just a differentiation of the input signal; thus the digital equivalent using first order differentiation is

$$G(n) = T \frac{(F(n) - F(n-1))}{P} + F(n)$$

where G(n) = output at point in time n

F(n) = input at point in time n

F(n-1) = input at point in time n-1

P = sampling period = .002 seconds

T = time constant in seconds.

The results using different values of T are shown in Figures 4.1.18 (T=0.05) and 4.1.19 (T=0.03). Note from these figures the crystal output phase lag was changed, in the case of Figure 4.1.18 the lag actually became a lead. In the case of T=0.03 (Figure 4.1.19) the crystal curve almost coincides with the HSM load cell.

Figures 4.1.20 to 4.1.23 show the same calculations as used for the step input applied to a sinusoidal input. Again the value of the time constant of 0.03 seconds provided the best results.

To prove that this lag was not introduced in the A/D converter or the digital processing, the same step input was applied to the Statham load cell. Figure A-15 shows the Statham and HSM load cell filtered plots from this run. As can be seen, there is no lag in the Statham load curve similar to that seen in the crystal.

Despite much investigation no one correct explanation for this phase lag was discovered. Three theories are presented; probably a combination of the three result in the overall effect.

The first theory hypothesizes that the lag is due to the effect of dielectric absorption. To a first order approximation a real capacitor can be modelled as in Figure 4.1.25 with a series capacitor-resistor (C_2 and R) in parallel with a capacitor (C_1). If a voltage builds up on the capacitor plates to a certain level and is then discharged by shorting the electrodes a monitoring of the voltage across the capacitor will show a gradual restoration of the initial voltage over time. This effect is due to the storage of the initial charge not only on C_1 but also on C_2. When the short circuit occurs only C_1 is fully discharged. Capacitor C_2 slowly discharges through the resistor R accounting for the voltage appearing.

For the piezoelectric crystal capacitor C_2 may be the piezoelectric charge generator, which when stressed generates a charge. This charge flows through the series resistor collecting on C_1 which represents the actual capacitance of the crystal. The voltage produced is the output voltage generated at the node of the Thevinen equivalent. By this mechanism then, the crystal becomes in effect an integrator and this could cause the observed phase lag.

The second idea, proposed by Mr. Mell Kullen of Vernitron, the manufacturer of the crystals used, deals with the ferroelectric effect. His thoery is that the domains of the crystals may actually be moving and reorienting themselves when a stress is applied. This reorientation would tend to reduce the piezoelectric effect by the cancellation of piezoelectric charges with polar moments. However, once the steady state is reached the full charge due to the piezoelectric effect is developed. The time for the domains to actually stop moving may be compatible with the observed lag.

The third explanation (not personally accepted by the author) is the possible effect of force cross coupling. Since the crystals were restrained from moving radially at each surface (by virtue of being epoxied to the glass) it is possible that shear forces were set up internally in the crystal as the crystal was compressed and tried to expand radially due to the Poisson effect. This would affect the shear mode piezoelectric component developing charges from this effect. The total charge developed would be a combination of the two in some heretofore unknown fashion. This explanation can

be partially rebutted by comparing the situation when the MTS machine was used, where the crystals were not clamped, to that of the HSM testing in which they were. The same phase lag effect occured in both cases.

Unfortunately, no clear physical explanation of the observed phase lag effect was discovered. The electronics associated with the crystals and the digital processing after the amplifier were exonerated by tests made using different signals. In both cases the lag was eliminated. The problem appears to be inherent in the crystals and remains there. If these crystals are to be used as the transducer for the plates, the phase lag will have to be compensated for by either analog or digital processing. Each crystal then would be calibrated for sensitivity as well as the phase lag time constant.

4.2 Strain Gauges

4.2.1 The Strain Gauge

Strain gauges, in contrast to piezoelectric transducers, are passive devices. That is to say that they require an external electric excitation in order to measure the input variable, strain.

Strain gauges function on the principle of a change in resistance of a wire when its cross-sectional area and length changes. The initial resistance of a wire is

$$R = \frac{\rho L}{A}$$

where ρ = material resistivity

L = conductor length

A = conductor cross-sectional area.

When the wire is stretched or compressed the change in resistance is given by

$$dR = \frac{\rho dL(1 + 2\nu)}{A} + \frac{Ld\rho}{A}$$

where ν = Poisson's ratio for the material.

The gauge factor F, the fractional change in resistance with the fractional change in length, is defined by

$$F = \frac{dR/R}{dL/L} = 1 + 2 + \frac{d\rho/\rho}{dL/L} .$$

The last term is often expressed as $\pi_l E$ where π_l is the longitudinal piezoresistance coefficient and E the modulus of elasticity. Knowing the gauge factor, one can calculate the strain dL/L of the wire according to

$$\frac{dL}{L} = F \frac{dR}{R} .$$

For most strain gauge materials the gauge factor is between 2.0 and 4.0. A summary of the most common alloys used is given in Table 4.2.1. (Taken from (45))

TABLE 4.2.1

Properties of some strain gauge materials

ALLOY	COMPOSITION	GAUGE FACTOR	RESISTIVITY Ω m	THERMAL COEFF-ICIENT OF RES-ISTANCE %/C	ULTIMATE STRENGTH MN/m^2
Constantan		2.1	.48		
Ferry	45% Ni, 55% Cu	2.2	.45	.002	460
Advance		2.1	.45		
Karma	75% Ni, 20% Cu, etc.	2.1	1.25	.002	1000
Iso-elastic	36% Ni, 8% Cr, .5% Mo	3.6	1.05	.0175	1250
Nichrome V	80% Ni, 20% Cr	2.5	1.0	.01	800
Alloy No. 479	92% Pl, 8% Tg	4.7	.62	.024	2000
Nickel		-12	.065	.68	400
Platinum		4.8	.10	.40	200

In the late 1950s a different type of strain gauge was developed, the semiconductor gauge. These gauges are made of P or N doped silicon filaments. They have a high gauge factor commonly in the range of 120 to 130. This is due to a much larger longitudinal piezoresistive coefficient π_1 and most of the resistance change comes from this piezoresistance effect. Unfortunately, semiconductor gauges are distinctly non-linear and very much affected by temperature. For lightly doped silicon, the fractional resistance with moderate stress levels is (45)

$$\frac{\Delta R}{R} = 175\ \varepsilon\ + 72625\ \varepsilon^2.$$

where ε = the strain in the gauge.

Figure 4.2.1 shows the variation in both the gauge factor and resistance with temperature.

For metal gauges, the gauge may be in the form of a wire bent into a grid shape or a foil, etched into a grid pattern. Figure 4.2.2 shows a gauge made of wire and one of foil. Note that the foil gauges are thinner than the wire gauges due to both the wire size and thicker backing material. The minimum wire size is approximately 25.4 μ m in diameter whereas foil can be as thin as 3.8 μ m; the paper backing is 75 μ m thick as opposed to 25 μ m for the plastic used in the foil gauges.

4.2.2 Applications of Strain Gauges

Strain gauges are normally cemented to an elastic member. The force exerted on the member is inferred by the strain using the equation

$$F = a\ \varepsilon\ E$$

where a = the cross-sectional area

ε = the strain

E = Young's Modulus for the material

for loads aligned with the strain.

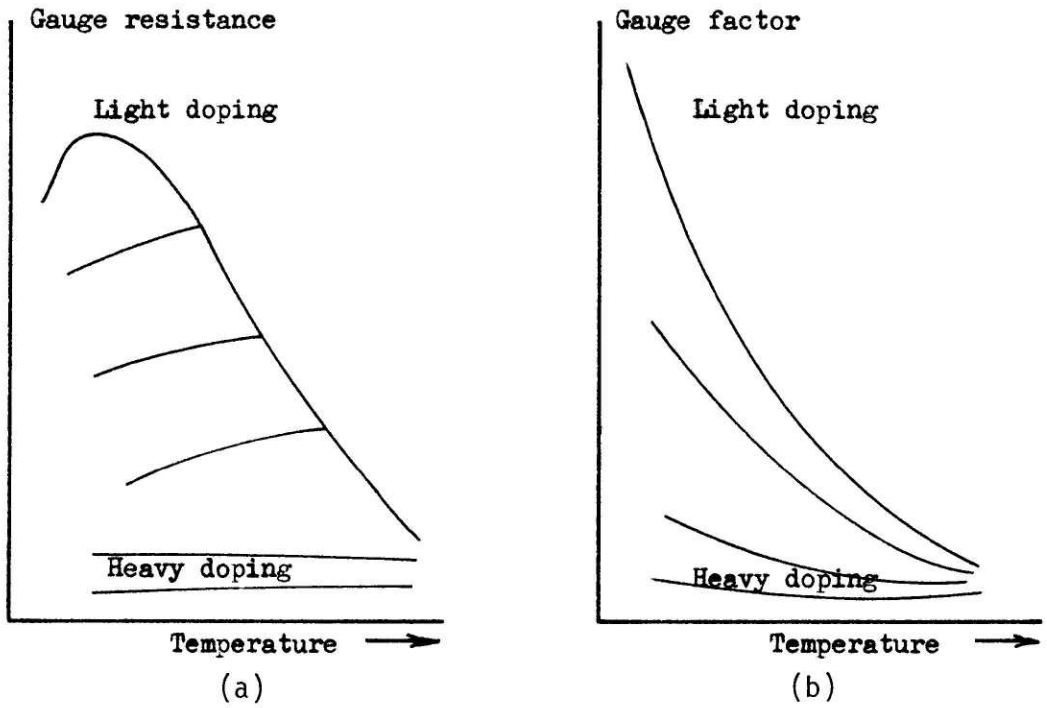

Figure 4.2.1 Variation of gauge resistance (a) and gauge factor (b) with temperature in silicon gauges.

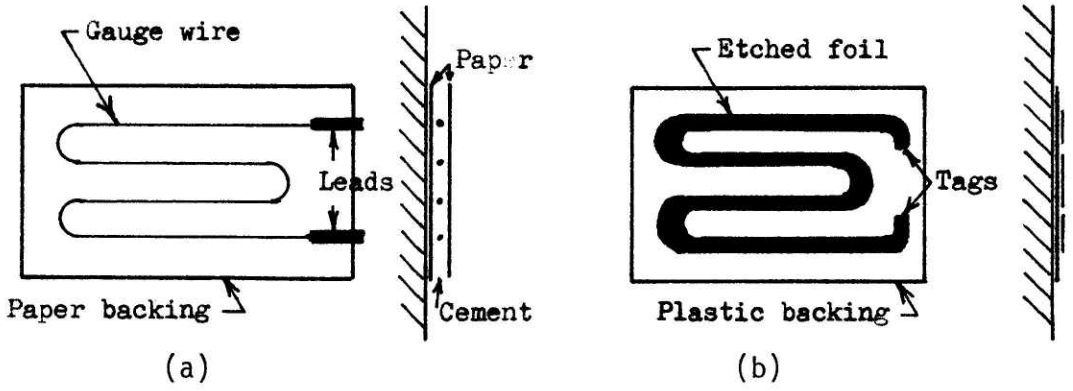

Figure 4.2.2 Typical construction of metal strain gauges.
(a) Wire (b) Foil

The bonding of the gauge to the element in which the strain is to be measured is an important factor in the performance of the gauge. Various cements are used ranging from a cellulose based cement for glueing paper backed gauges to epoxies used with the plastic backed foil gauges. Once bonded to the material, the gauge is effectively a part of the surface which it is adhered to and undergoes the same strain as the material.

Using high quality electronics, strains down to 10^{-7} mm/mm can be sensed. This lower limit is due to a thermal voltage (called Johnson noise (45)) generated due to electron motion in the gauge. The thermal voltage is calculated according to

$$V_{tn}, \text{ RMS} = \sqrt{4KTRB}$$

where K = constant = 1.38×10^{-23} $\frac{\text{Joule}}{°K}$

T = temperature in °K

R = resistance in ohms

B = bandwidth of measuring device, Hz

This thermal voltage is a white noise on the order of .5 μ V in magnitude using an oscilloscope with a 10 Mhz bandwidth to measure it which can be as large as the signal voltage at low signal levels. Note that sensitivity can be traded for bandwidth of the measuring device, for example with a 10 Khz bandwidth the .5 μ V noise is reduced to .02 μ V. Gauges are sensitive to strains along their longitudinal axis. Because of the loops in the wire at the end of

each turn there is some transverse sensitivity, normally on the order of 1% of the longitudinal sensitivity. With foil gauges this cross coupling is reduced by increasing the area at the end of the turns.

Strain gauges are usually electrically connected in a bridge configuration such as the Wheatstone Bridge shown in Figure 4.2.3. Here, using a full bridge, the output voltage will be proportional to the strain in the beam shown according to

$$\frac{e_o}{E} = \frac{F\ R_1 R_2}{(R_1 + R_2)^2}\ (\varepsilon_2 - \varepsilon_1) + \frac{F\ R_3 R_4}{(R_3 + R_4)^2}\ (\varepsilon_4 - \varepsilon_3)$$

where F = gauge factor

ε_i = strain in gauge i

R_i = resistance of gauge i

This reduces to

$$e_o = F\ E\ \varepsilon$$

where ε = the strain at the neutral axis of the beam.

Strain gauges have excellent dynamic response from 0 Hz up to 50,000 Hz (16). Thus they can be readily used in dynamic force measurements. Since the gauges are bonded to an elastic material the force measuring system can be idealized as a second order system. Using this bridge circuit very accurate measurements can be made, .1% linearity over the full range of loads is not uncommon.

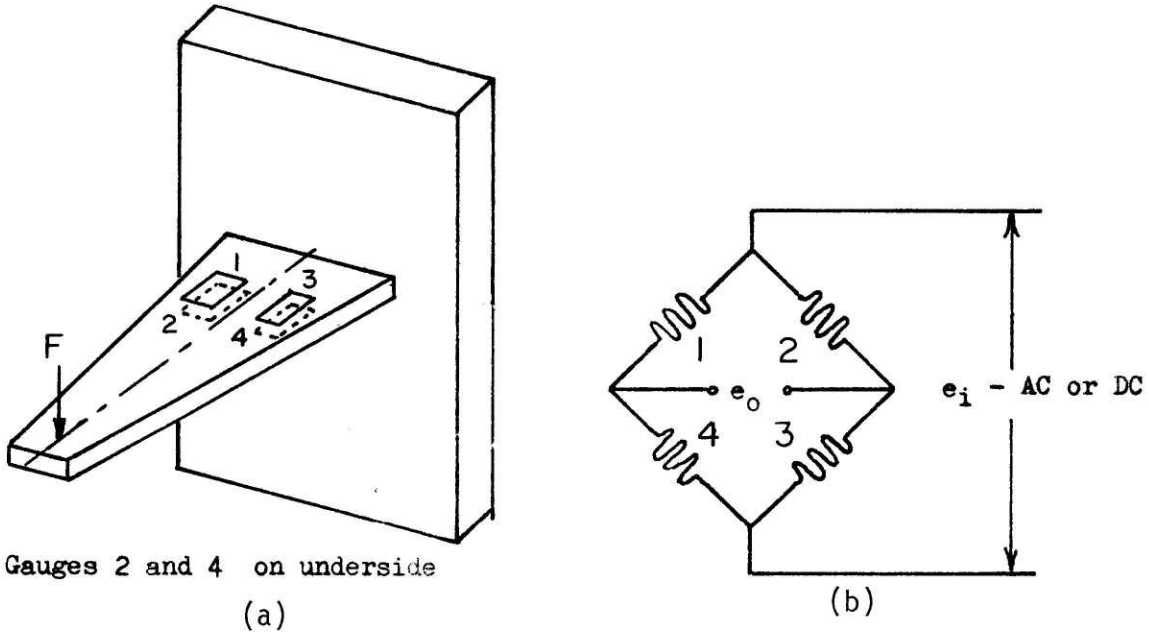

Figure 4.2.3 Four strain gauges connected in a Wheatstone bridge configuration. (a) Cantilever beam with gauges attached (b) Circuit diagram

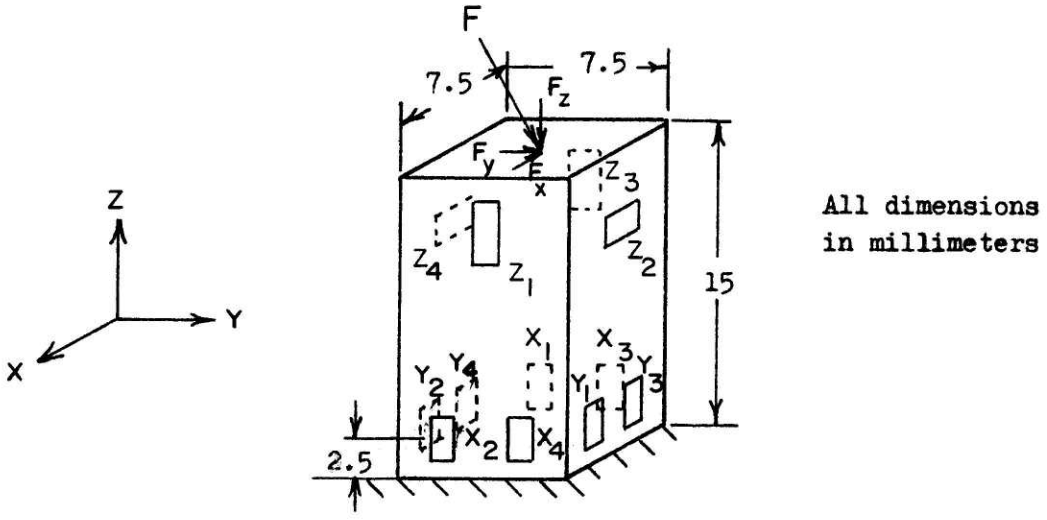

Figure 4.2.4 A strain gauged column for use in resolving the three orthogonal force vectors.

A typical configuration for a load cell to measure the three orthogonal force vectors is shown in Figure 4.2.4. This requires three separate bridge circuits to obtain the forces and the loading must be at the center of the beam cross section. Considering the use of such a column for the particular task of the force plate transducer, the strains required to calculate forces in each of the three orthogonal directions can be calculated. With an aluminum column 7.5 mm square and 15 mm high as shown in Figure 4.2.4, for a 77 kg person walking normally, with the forces evenly distributed on the plate, F_z = 322 N, F_x = 90 N and F_y = 48 N. The resulting strains are

$$\varepsilon_z = \frac{F}{AE} = \frac{322\ N}{(7.5 \times 10^{-3})^2\ m^2 \times 6.89 \times 10^{10}\ N/m^2} = 8.31 \times 10^{-5}\ \frac{mm}{mm}$$

and

$$\varepsilon_x = \frac{7.5}{2}\ \frac{FL^2}{2EI} = \frac{7.5}{2}\ \frac{(90N \times (2.5 \times 10^{-3})^2\ m^2)}{2(6.89 \times 10^{10} N/m^2\ (\frac{1}{12}(7.5)(7.5)^3 x 10^{-2} m^4))}$$

$$= 5.81 \times 10^{-5}\ \frac{mm}{mm}$$

$$\varepsilon_y = \frac{7.5}{2}\ \frac{FL^2}{2EI} = 3.10 \times 10^{-5}\ \frac{mm}{mm}.$$

For a change in load of 1 Newton, $\varepsilon_z = 2.58 \times 10^{-7}\ \frac{mm}{mm}$, ε_x, ε_y = $6.45 \times 10^{-7}\ \frac{mm}{mm}$. Thus the strains to be measured in this configuration are approaching the achievable limits.

4.3 Linear Variable Differential Transformers

4.3.1 LVDT Operation

Similar to strain gauges, LVDTs are also passive elements. They work however, by changing inductance rather than resistance. A typical LVDT is shown in section in Figure 4.3.1. Longitudinal movement of the magnetic core (without contacting the sides of the cylinder) varys the mutual inductance of each secondary coil to the primary. As a result the voltage induced in each secondary varies with the position of the core. An AC excitation is applied to the primary. If the core is centered the magnitude of the voltage induced in each secondary is the same but since the two voltages are 180 degrees out of phase the output voltage is zero. As the core moves one way or the other, the voltage induced in one secondary will be greater than the other and a difference voltage appears at the output. This voltage is linear with core position and resolution is essentially infinite and there is no hystersis.

The LVDTs may be excited by an AC voltage (1-5 Volts RMS, 50 Hz-25 Khz) or by a DC source ($\pm$ 15 Volts). When excited in the DC mode the output is also a DC voltage since all the DC-AC and AC-DC conversion electronics are incorporated into the housing, as shown in the block diagram of Figure 4.3.2. This figure also shows that DC-LVDTs are self-contained and simplify external electronics, unlike piezoelectric or strain gauge devices, which require extensive input and output processing.

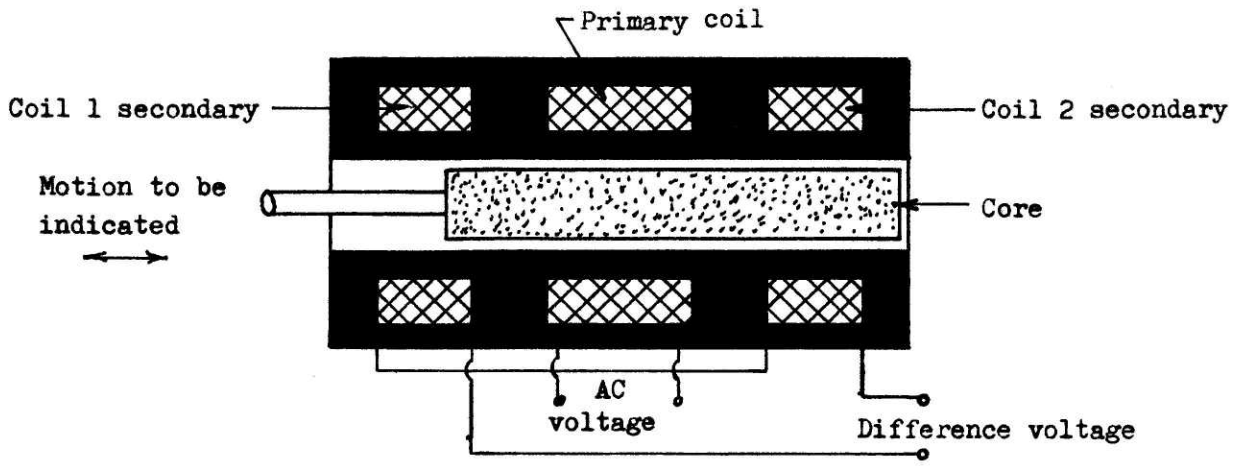

Figure 4.3.1 A cross-section of an LVDT.

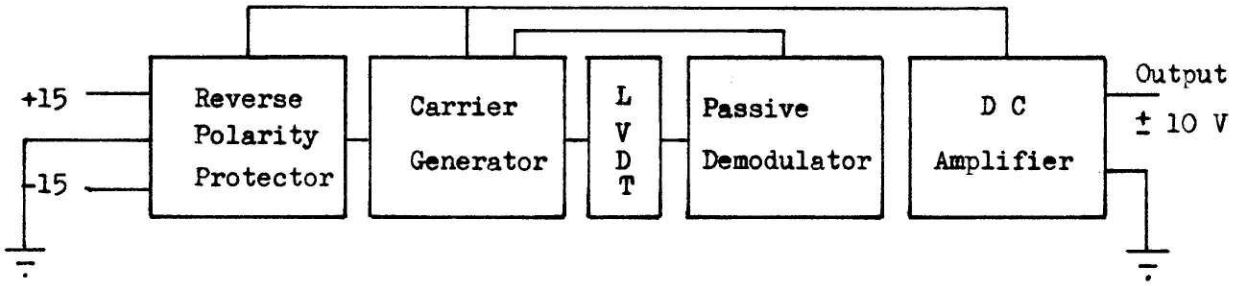

Figure 4.3.2 A block diagram of a DC-LVDT.

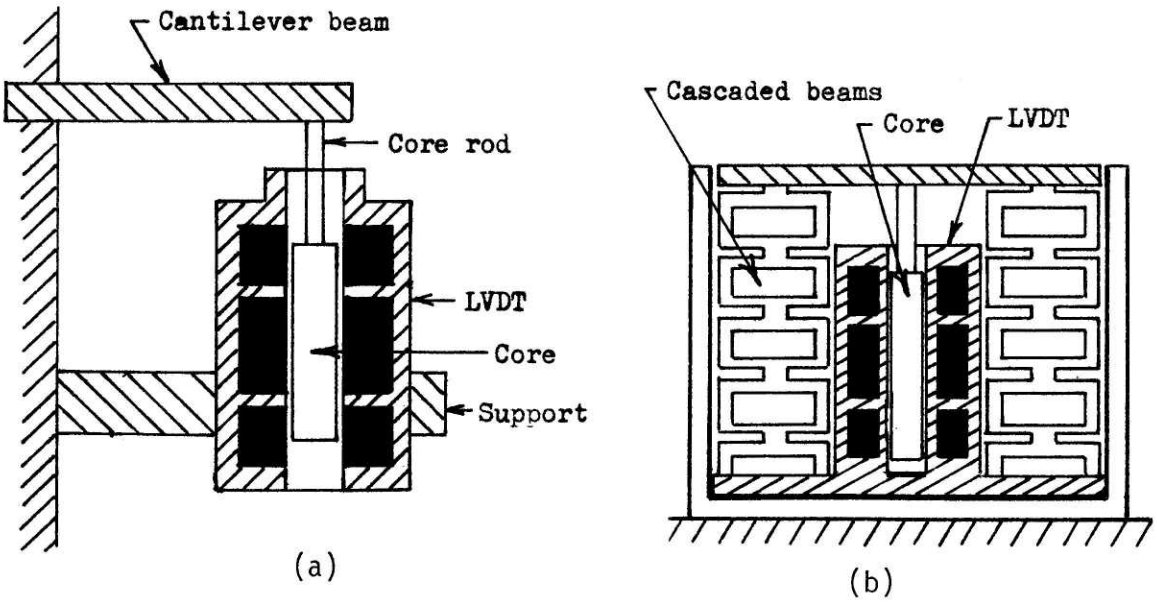

Figure 4.3.3 Two configurations for force measurment.
(a) Cantilever beam (b) Cascaded beams

The transformer of an LVDT consists of three symmetrically spaced coils wound onto an insulated bobbin. The windings are potted in an insulating compound and then the entire structure is shielded with a ferromagnetic material. The core is made of a uniformly dense cylinder of a nickel-iron alloy which is annealed carefully to homogenize its magnetic permeability. The core is threaded for connection to an external actuator. A non-magnetic core rod, such as stainless steel or plastics connects the movement source and core.

Because of the shielding, magnetic pickup from external sources is not a problem in using the LVDT. Temperature changes do have an effect on the performance due to two effects, a changing in primary resistance and thermal expansion (or contraction) of the components. As the temperature changes, the resistance of the primary windings changes and thus the impedance is altered, especially at low frequency excitations where the resistance is a sizeable fraction of the total impedance. As this impedance varies, the current in the primary changes, using a constant voltage source, and this results in a different voltage induced in the secondary. This problem is corrected to some extent by inserting thermistors in series with the primary, that have a negative temperature coefficient of resistance. The second effect is due to differential expansion or contraction of parts in the LVDT causing relative movement of the core with respect to the transformer yielding a false output. These temperature effects are much smaller in magnitude than the temperature effects on strain gauges.

The cross coupling effect is also smaller in LVDTs than in strain gauges because the core can move transversely to the longitudinal axis with no effect on the voltage induced in the secondary. The amount of allowable movement depends on the clearance between the core and transformer. For the LVDT the transverse sensitivity is roughly 0.1% of the longitudinal sensitivity as compared with 1% in strain gauges.

The frequency response limitations in an LVDT are the core inertia and the excitation frequency. For most applications the core mass is small enough to not affect the response when used in a force transducer. The excitation frequency must be at least 3 times, typically 10 times, the frequency of any dynamics to be measured. For the DC-LVDT the highest frequency component which can be measured is 500 Hz, because of low pass filtering in the output signal conditioning.

4.3.2 Applications of LVDTs

Figure 4.3.3 shows two LVDTs in possible configurations for measuring force. As with the strain gauge, force is calculated by measuring the deflection of an elastic member and inferring the force exerted from the strain measured. Part (a) of this figure shows a standard method of using a cantilever beam to amplify the strains, and thus the force, in a structure. Figure 4.3.3 (b) shows the LVDT used to measure tension and compression by the movement of cascaded H-cut spring beams. The connection of the load cell to the actuator can be made through gimballed core rods so that only the force along the axis of the LVDT will be measured.

To use LVDTs for the triangular shaped force plate would require six transducers in all. A sketch of the arrangement is shown in Figure 4.3.4. The shear mode transducers would use the cantilever beam principle to measure the force in one of three directions, the beam contact point being a groove in the triangular plate so that only forces in the direction of interest, along the longitudinal axis of the LVDT would be measured. A force in the vertical direction or transverse direction causes the plate to slide along the beam. To prevent shear forces from being transmitted to the vertical measuring load cell, the load can be exerted through a ball bearing as shown on the inset. The vertical force measuring load cells could be easily threaded into the base plate.

Commercially available load cells such as the one shown with the cascaded beams have excellent performance characteristics. For the Schaevitz Engineering (56) load cells, pertinent specifications are given in Table 4.3.1.

TABLE 4.3.1

Performance specifications of Schaevitz LVDT load cells

Linearity		.2% of full range
Resolution		.1% of full range
Repeatibility		.1% of full range
Operating Temperature		-3.9°C to 60°C
Temperature coefficient of sensitivity		.054%/°C
DC operation:	Excitation	±15 V @ 15 ma
	Min. Load Impedance	2K ohms
	Output Impedance	100 ohms
AC operation:	Excitation	1 - 5V RMS 400Hz - 10Khz
	Suggested Load Impedance	28 - 400 K ohms

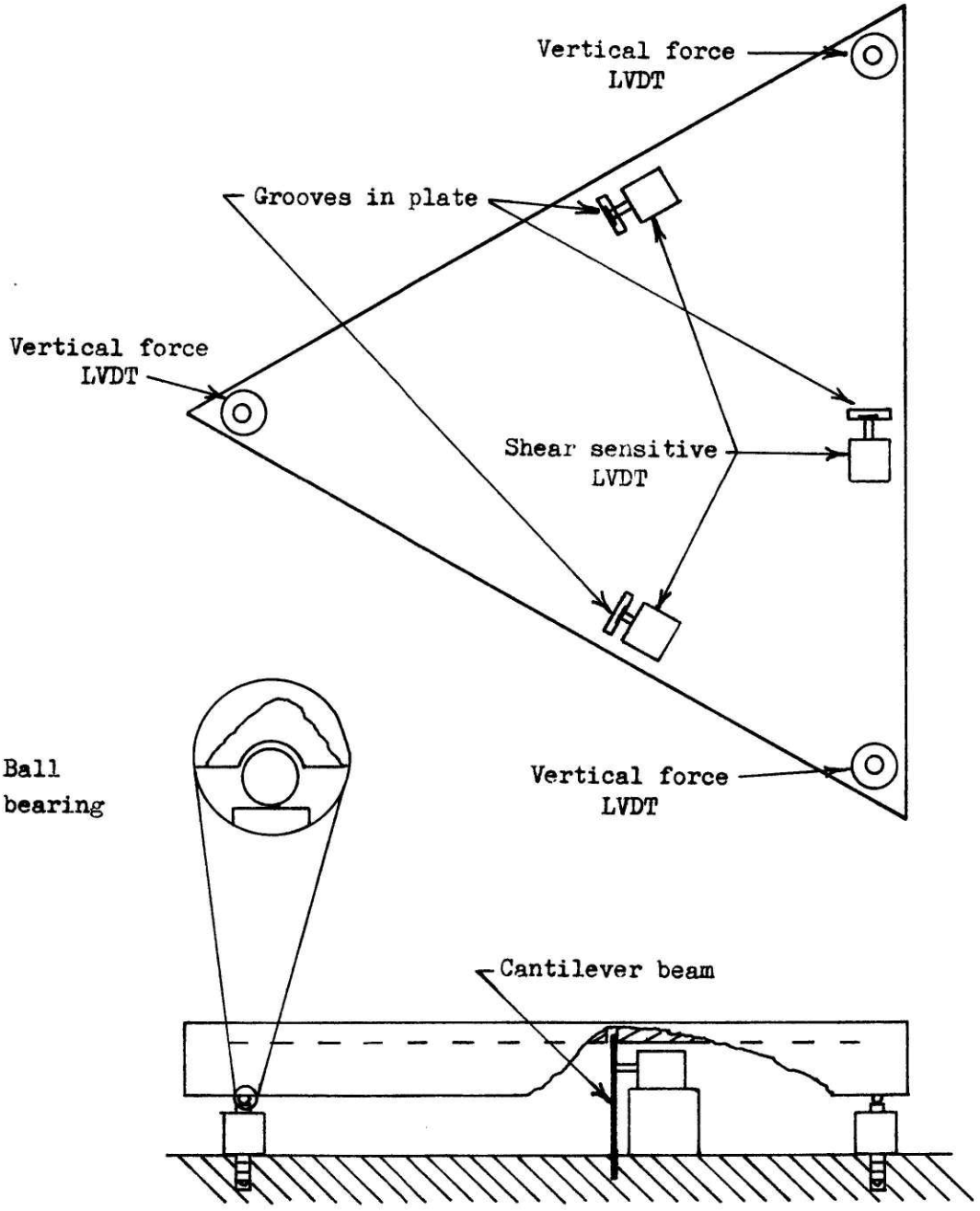

Figure 4.3.4 A possible configuration for using LVDTs to measure the forces exerted on the force plate.

4.4 Transducer Summary

4.4.1 A Comparison of Transducers

Table 4.4.1 summarizes the important performance specifications for the three types of force transduction considered for the triangular force plate concept. Linearity is defined as the maximum average deviation of calibration points from a straight line fit to the data points using a least squares routine. Resolution is the smallest load detected by the transducer. Cross talk is the ratio of the sensitivity of the transducer to forces in the transverse direction to the sensitivity to forces in the longitudinal direction, expressed as a percentage. Frequency response is the frequency range of dynamic loads the transducer can measure.

The prices quoted are without taxes and were obtained for each particular transducer as indicated by the notes. The cost of signal processing was estimated for those cases where the equipment could be made in-house.

As is shown by this table, the Kistler 3-component load cell is very expensive in relation to the other methods. The piezoelectric ceramic discs and the strain gauged columns are comparable in price and in difficulty of implementing. Ceramic piezoelectric transducers have an intrinsic phase lag as described in Section 4.1. Strain gauge techniques require the machining of accurate columns, with 12 gauges per column, and rigid attachment to base and force plate. As well signal processing in order to measure such small strains at the limit of resolution could be the source of much difficulty. The LVDT

TABLE 4.4.1

A summary of some of the specifications of the transducers considered.

	Piezoelectric		Strain Gauged	Linear Variable Differential
	Kistler 3 Component Load Cell	In-house Ceramic Transducer	Column	Transformer
Linearity	±1%	±1%	±.3%	±.2%
Frequency Response	0 - 8 Khz	0 - 1 Khz	0 - 50 Khz	0 - 2.5 Khz
Resolution	.01 N	.05 N	1 N	.9 N
Cross Talk	5%	3%	1%	.1%
Electrical Excitation Required	3 Charge Amplifiers per cell	1 Voltage follower per transducer	DC excitation in a bridge circuit	DC ± 15 V supply per transducer
Signal Processing Required	Each charge amplifier can be connected to an A/D converter	Each amplifier can be tied to an A/D converter Phase lag must be digitally eliminated	Each bridge output can be tied to an A/D converter	Each transducer output can be tied to an A/D converter
Number of Transducers Required per Plate	3	9	36	6
Unit cost of Transducer (Dollars)	1090[1]	20[2]	4.25[3]	90[4] & 410[5]
Signal Processing Cost	900[6]	10[7]	10[7]	1[7]
Cost of mounting Transducer	5[7]	.5[7]	.5[7]	1[7]
Total Cost per Plate($)	12555	320	315	1512

TABLE 4.4.1 (contd.)

Notes:
1. Kistler 3 component load cell type 9251
2. Vernitron Piezoelectric Ceramic 16050-8 PZT-8 25.4 mm dia., 2.54 mm thk.
3. Baldwin-Lima-Hamilton SR-4 series Constantan Foil gauge, polyimide backed 2.54 mm long, 1.27 mm wide
4. Schaevitz DC-LVDT Model 100-HR-DC for range of motion of 2.54 mm - used in shear force measurement
5. Schaevitz DC-LVDT Force Transducer FTD-1T-500 Load Cell capable of measuring 2224 N
6. Kistler charge amplifier Type 5003 (3 required)
7. Estimated values

approach also poses difficulties in the mounting of the transducers in a fashion suitable to obtain forces in all three orthogonal directions, especially given the large size of LVDTs, the 100-HR-DC model proposed for shear is 16.6 mm in diameter and the normal force load cell is 50 mm high. However, the LVDT method reduces signal processing to a minimum.

In the next chapter, the proposed triangle-transducer pathway concept is compared with a commercially available force plate manufactured by the Kistler corporation.

CHAPTER 5 CONCLUSION

5.1 The Kistler Piezoelectric Force Plate

Pertinent specifications of the biomechanical force platform manufactured by the Kistler Corporation (32) are summarized in Table 5.1.1. This system, illustrated in Figure 5.1.1, consists of a 400 by 600 mm magnesium alloy top plate mounted on four quartz piezoelectric transducers, of the three component design (type 9251) described in Section 4.1, under high prestress. The platform measures force in three orthogonal directions, the point of application of the force vector on the plate and the moment exerted on the platform about a vertical axis through the point of application. The external circuitry required to obtain these measurements are: 8 charge amplifiers, 2 summing amplifiers and an analog divider. The charge amplifier outputs, however, can be used as direct input to a computer, through an A/D converter, thereby eliminating the need for the analog circuitry. No major problems in the signal processing are anticipated. The platform is thin (60 mm) facilitating installation in a laboratory floor using a frame designed to be grouted into a concrete base. Each Kistler force plate ready to connect to an A/D converter for computer use, costs (as of February, 1978) $12,345. Additional costs would be encountered in fixing the plate(s) in the laboratory floor.

5.2 A Comparison of the Kistler Platform and Triangle Pathway Approach

The Kistler plate was chosen as an example of a commercial force plate because it is believed to be the best force sensing system for

TABLE 5.1.1

PERFORMANCE SPECIFICATIONS FOR THE KISTLER PLATFORM[1]

Load Range:	Vertical (F_z)	-10 to +20 kN
	Shear (F_x, F_y)	-10 to +10 kN
Overload:	Vertical (F_z)	-15 to +30 kN
	Shear (F_x, F_y)	-15 to +15 kN
Linearity		$\leq$.5% of FSO
Hysterisis		$\leq$.5% of FSO
Cross talk:	$F_x \rightleftharpoons F_y$, $F_z \rightleftharpoons F_{x,y}$	$\pm$ 1%
	$F_{x,y} \rightleftharpoons F_z$	$\pm$ 2%
Natural Frequency		1 kHz

1-Data for platform model number 9281A11

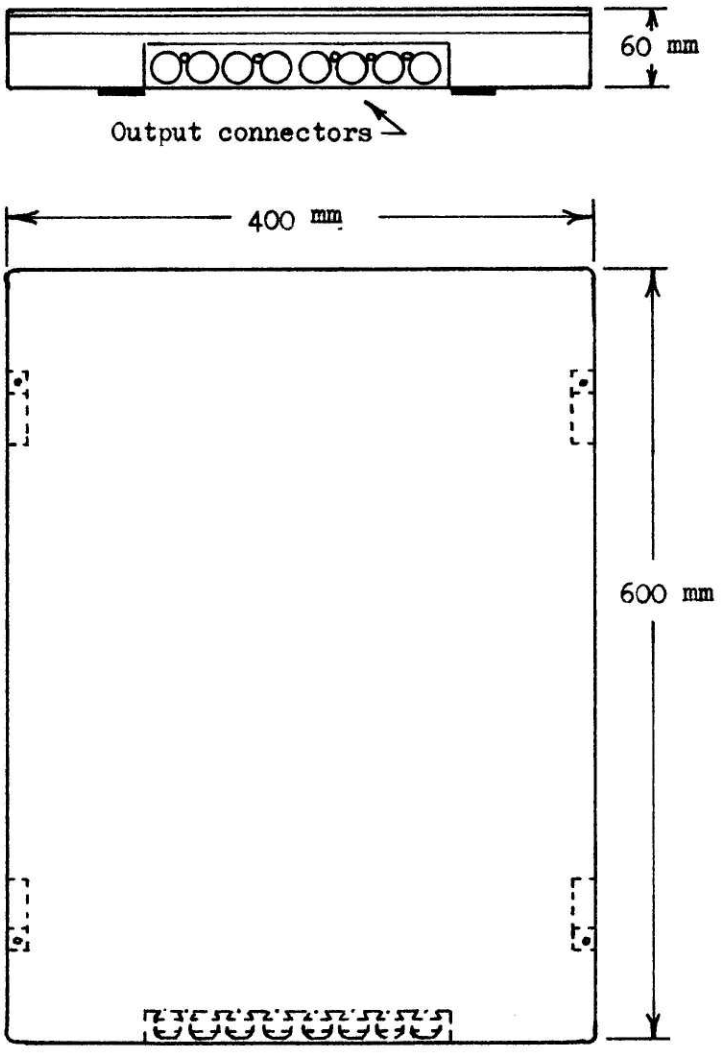

Figure 5.1.1 The Kistler force platform.

gait analysis available at this time. Numerous researchers and institutions are using the Kistler system now (Kistler reports 96 users), which is an indication of the quality of the system.

At this stage in the development of the pathway concept, data similar to the Kistler values listed above is not available. A combination of the ceramic transducer specifications given in Section 4.4 and the plate calculations of Chapter 3 project the performance of the system ultimately, disregarding any new unforseen difficulties arising during detailed design, fabrication and testing. In principle, the working characteristics of the two systems should be almost equal since they both use piezoelectric crystals in a similar manner. However, the considerable experience of the Kistler Corporation must be weighed. The triangle-pathway design can be implemented but it will take considerable more work to get the system operational for human mobility analysis.

5.3 Recommendations

The largest obstruction to the implementation of the triangle-pathway design is the lag problem with the transducer. This author believes that the piezoelectric ceramic crystals are the best choice for transducers, given the success of the Kistler Corporation and Hennacy (27), and that the problem of the apparent phase lag can be defined and eliminated.

Specifically, different mounting techniques should be tested, other than epoxying the optical flats to the crystal. An elastomer could be used in conjunction with the force feedback mode of the HSM to determine if the crystal is being held from straining radially. This can be done by using the elastomer instead of epoxy to affix the optical flats to the ceramic discs and use this sandwich in the same tests as before. The elastomer will allow the crystal to strain radially and still electrically insulate it. The force feedback made is required because the elastomer will compress considerably when a load is applied, with force feedback despite compression, a constant force will be exerted on the crystal. To electrically connect the electrodes to the amplifier, instead of soldering leads to the crystal, a thin aluminum plate between the crystal and the optical flat could be used. The sandwich of optical plate, aluminum plates and crystal would have to be held under a prestress to ensure electrical contact and to prevent horizontal movement of the components when shear forces are exerted on the stack.

Recent tests have indicated that the capacity of the crystal does not change greatly with stress. Further tests should be done to investigate this and quantify the amount of change of capacitance. If the variation of capacity is small then it may be worthwhile to implement the charge amplifier again and use it with the HSM testing procedure. The charge amplifier may be more linear (voltage to force) than the voltage follower and not have the same observed phase lag. Further, testing of the shear mode crystals must be done before any

construction of an actual plate occurs. A testing system must be constructed that applies a large force parallel to the crystal surface with a small exertion occuring normal to the surface. This perhaps can be accomplished with the HSM set at 90 degrees of flexion, exerting force parallel to the base of the machine. A measurement of the percentage of cross talk from normal to shear force and from shear to normal force must be made. This can of course be done by putting the shear sensitive crystals through the calibration run for a crystal poled for normal forces and vice versa. Finally a complete column must be assembled and tested in each calibration rig (shear and normal force testing) to ensure that the three orthogonal forces can indeed be measured accurately by this technique.

Upon completion of the transducer tests, a prototype plate must be assembled. The force plate should be mounted on a portable steel base in order that it be tested in the HSM with the amount of flexion ranging from -90° to +90° and the point of application being changed. These tests would determine if the plate actually can determine the total forces and point of application. Analog circuitry may be most appropriate to complete the force, moment and point of application calculations for each plate. Digital calculations will probably be needed for the overall system.

Microprocessor handling of the data from either the entire pathway or perhaps just a row or column must be investigated. Since it is expected that when using a large number of plates, many, in fact most, will not be loaded, a technique of sampling only those

plates on which a force is exerted, thus identifying them as "active", will be required. Two ideas already conceived are: 1) using an optical system to sense when a certain row has been passed, then turning the row "off" and 2) sampling a representative crystal from all plates (such as the normal force sensing crystal at the apex) when any one measurement exceeds a certain background level start sampling all the crystals at that plate and adjacent ones. It is clear that a reduction in the amount of data going to the main computer must occur, since if all 66 tiles, with 9 transducers per tile, are sampled at 500 Hz this would require storing 297,000 pieces of data per second.

5.4 Final Thoughts

Much work is still to be done to implement the triangle-pathway design. At least 9 months are estimated to achieve the minimum required (6) number of plates working to use as an actual laboratory tool, without microprocessor control, another 9 months are expected to implement the microprocessor system.

However, it is believed by the author that the system design as analyzed in this study is feasible and would be a significant advancement in force measuring techniques for human mobility analysis that it would justify the cost and effort of completing this work.

APPENDICES

APPENDIX A
TESTING THE CRYSTALS

A-1 A Description of the Figures

All of the figures, graphs and tables in this appendix relate to the material in Chapter 4, Section 4.1. Figure A-1 is a schematic of the charge amplifier first used as the amplifier for the piezoelectric crystals. The apparatus employed to calibrate the crystals using this charge amplifier is shown on the next figure, A-2. Using this setup the load was applied to the crystals via a second class lever. Placing weights on the pan exerted a horizontal force on the crystal. The crystal was compressed between two strips of printed circuit board, one on the lever arm and the other on the rigid base. This board provided the connections to the charge amplifier. The force exerted on the crystals was proportional to the load on the pan and was dependent on the location of the crystal. Four locations were used, giving four ratios of force exerted to mass on the pan:

Position:	$\frac{F_c}{F_p}$:
1	4.86
2	2.39
3	1.57
4	1.18

where F_c = force exerted on the crystal

F_p = weight of the mass on the pan.

By setting different masses on the pan, a calibration curve of output voltage versus force exerted on the crystal was obtained and is graphed in Figure A-3, with the data tabulated in Table A-1.

A straight line fit by eye to the data showed a nonlinearity believed to be due to a nonlinear change in capacitance with applied stress. As a result, as discussed in Chapter 4, a voltage follower amplifier was built (the schematic is shown on Figure 4-8). To test the amplifier as a voltage follower, independent of the crystal piezoelectric voltage, a setup was used as diagrammed in Figure A-4. A high voltage signal was input to the voltage follower through crystal. The input voltage was compared to the output voltage using a differential amplifier in a Tektronix Oscilloscope (model 503, input capacity = 10 pf, input resistance = 10 M ohms). Two typical oscilloscope traces are shown in the photographs of Figure A-5. The input in Figure A-5 (a) was a 170 Volt, 1 Khz sine wave (reduced in amplitude by a factor of approximately 46 for this picture). The difference signal was 700 mV peak to peak which represented a .29% "error". Similarly, for part (b), the error was also approximately .29% using a 170 V peak to peak 500 Hz triangular wave input.

The crystals were tested as force transducers on a Materials Testing Machine (MTS) with the layout of the components as in Figure A-6. Two different techniques were used to connect the crystal and the amplifier as shown in Figure A-7. Both employed the self-paralleling, ball bearing system sketched in part (c). The original method (sketch (a)) connected the transducer to the amplifier with etched printed circuit board. The layout of the board, showing the guard encircling the crystal is illustrated in part (b). The second procedure used glass optical flats to sandwich the crystal. The lead

wires were soldered to the silver surface of the crystal at a spot on the annulus of the crystal's surface unstressed because the crystal diameter was greater than that of the optical flats (c).

The next step taken was to use the Hip Simulator Machine (HSM) of the MIT Hip Project. Figure A-8 is a diagram of the load cell of this machine showing: the location of the strain gauges on the load cell column (a), a schematic of the bridge circuit used (b) and the general location of the load cell in the machine (c). The outputs of the load cell, the crystal voltage follower and the difference of the two were recorded by a strip chart recorder. Two typical recordings are shown on Figures A-9 and A-10. Figure A-9 is a graph of a step input of 980 Newtons (220 pounds). The load was applied in approximately 60 milliseconds, the force remained exerted on the crystal for 3.25 seconds and then removed in about 50 milliseconds. The top curve is from the HSM load cell, the curve below it from the crystal amplifier and the third graph is the difference, with scaling factors applied. The error signal was nulled at 980 N (220 pounds) which means that using the variable gain of the differencing circuit, the error was reduced to zero at this load giving in effect a scale factor between the two voltages. Using this scaling factor the step input was run. Note the 4% of full scale difference on loading and the 6% error on unloading. Figure A-10 used the same circuitry but with a slower rise time from zero load to full load, approximately 4.5 seconds. Here the error signal is 4.6% of full scale on loading and 5.1% while unloading.

The difficulty of interpreting data from these stripp chart records led to the use of the computer (a DEC(15) PDP-11/40) to analyze the data as described in Chapter 4. Table A-2 gives typical sensitivity values and voltage output values for a calibration run using the 10 load levels (222N (50 lbs) to 2224 N (500 lbs) in increments of 222 N (50 lbs)) and 5 rates (89 N/msec (20 lbs/msec) to 2.22 N/msec (.5 lbs/msec)). Figure A-11 is a graph of these data points and a second order polynomial fit to the points. Figures A-12 and A-13 plot the crystal amplifier voltage and sensitivity versus the loading rate. Both curves are essentially flat, indicating that the loading rate was not affecting the linearity of crystal voltage with load.

To be confident that the HSM load cell was accurate and was linear, a Statham (62) load cell was put through the same calibration run as a crystal. The results are shown in Tables A-3 and A-4 and the graphs of Figures A-14 to A-16. Table A-3 which can be compared with Table 4.1.4 shows that the average deviation from a straight line is .24% of full scale as opposed to .70% for the crystals. Also since the histogram of errors only ranges as high as an 8 pound (36 N) difference, compared with 24 pounds (107 N) for the crystal, the dispersion from a straight line is less with the Statham load cell. Table A-4 (similar to Table A-2) tabulates the voltage and sensitivity values for the Statham load cell, while Figures A-14 and A-15 plot voltage and sensitivity respectively versus load from this calibration run. Figure A-16, comparable to Figure 4.1.17, shows a reproduction of the data from a 980 N (220 lb) step input. This data was put

through the same low pass filter as the crystal data of Figure 4.1.17. As can be seen upon comparison of the curves, the Statham cell does not appear to lag the HSM load cell, whereas the crystal output voltage does.

A-2 The MTS Machine

The Materials Testing System (MTS) machine (41) is a custom built multipurpose device capable of applying loads in tension and compression. This machine uses a hydraulic ram moving with respect to a stationary crosshead to exert forces. Various jaws and grips can be threaded into the ram and crosshead platen to hold different specimens. This machine can be run manually, in a repetitive mode using a digital function generator or using a computer. In the case of the MTS machine owned by the Mechanical Engineering Department the computer is a PDP-11/08.

The MTS machine can exert forces up to 220,000 Newtons under one of: displacement feedback, force feedback, or strain feedback. Using displacement feedback, the ram is positioned with respect to the upper platen regardless of the force required to do this. In the force feedback mode, used for the experiments performed on the crystals, a constant force is exerted on the specimen mounted between the ram and crosshead. The force is sensed by a strain gauge load cell (manufactured by Lebow Industries (36)) in series with the mounting pylon in the crosshead and is compared with the command signal to give the error or control signal which opens or closes the

hydraulic valves. Strain feedback uses both displacement and force feedback to control the ram giving a constant strain rate.

The digital function generator can also be used to control the hydraulics. Various waveforms such as: sine, haversine, square and triangular are available at frequencies up to 20 Hz, which is the maximum speed of the machine. The number of cycles of repetitive operation can be selected as well as the amplitude of the function and therefore the force exerted. An X-Y plotter is also a component on this particular model. It has a frequency response of 0-5 Hz with 1% linearity. The plotter was used in these tests to plot the load cell voltage and crystal voltage versus time. The computer was not used to either control the hydraulic system or to take data.

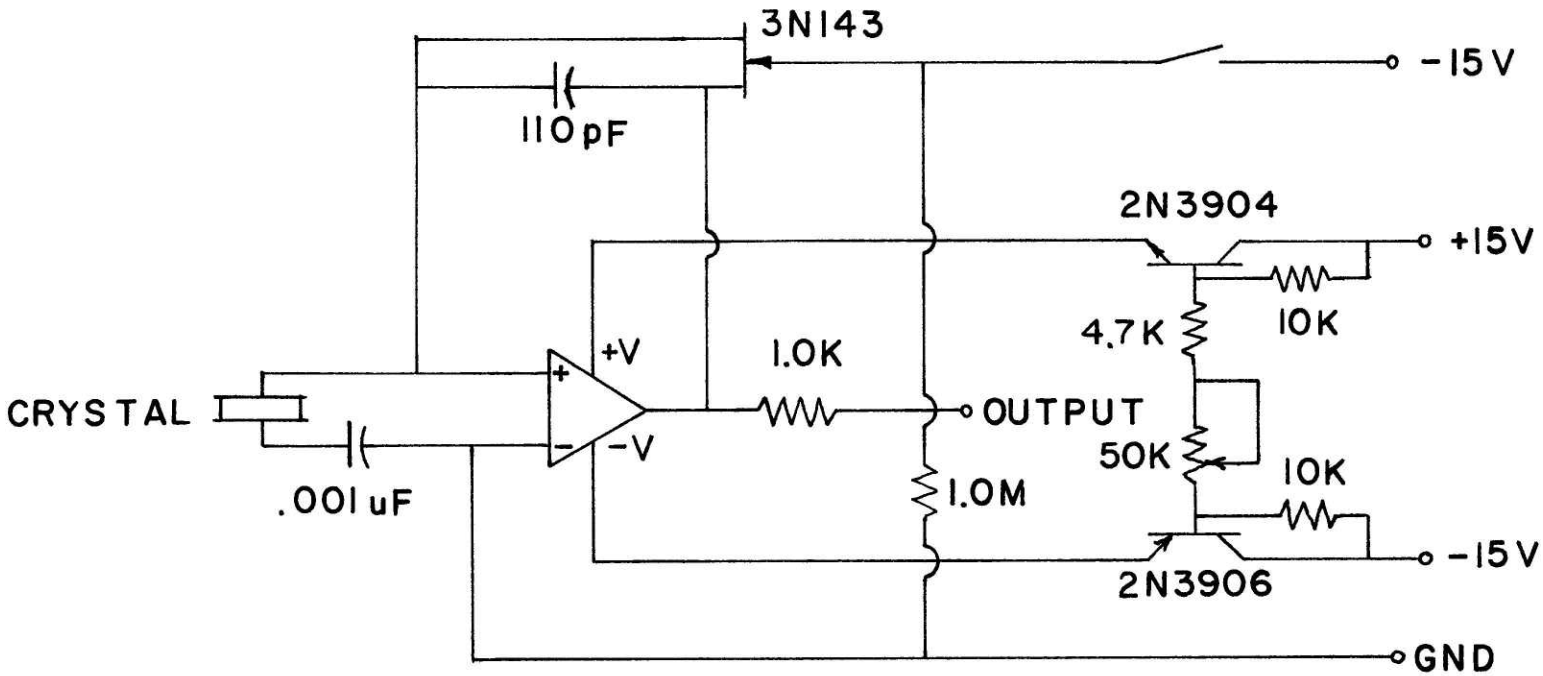

Figure A-1 Schematic of the charge amplifier.

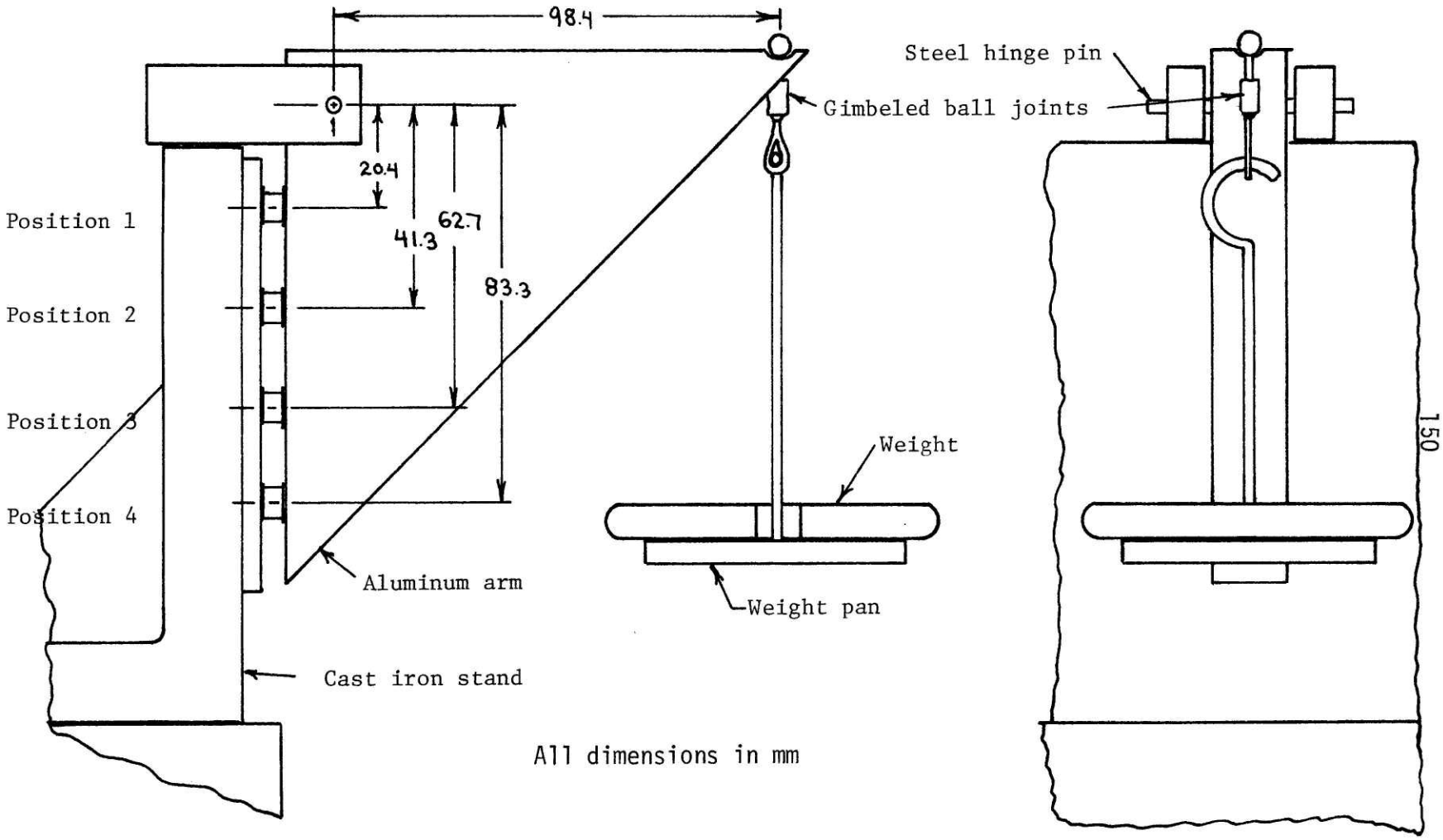

Figure A-2 Equipment used for calibration of the charge amplifier.

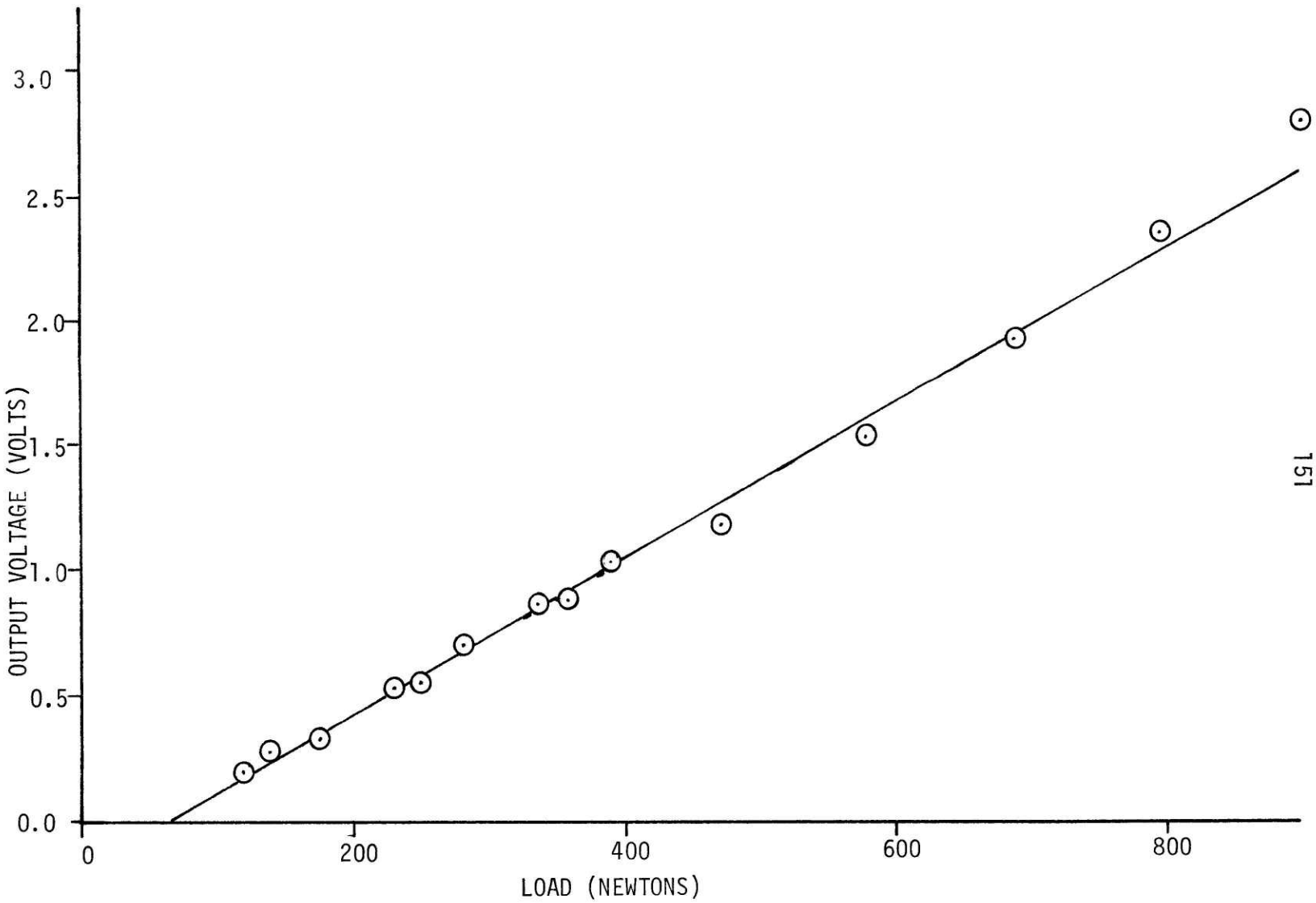

Figure A-3 Output voltage versus load for the charge amplifier.

TABLE A-1
Crystal voltage and load values for the charge amplifier and Figure A-3

Load (Newtons)	Crystal Voltage (Volts)
120	.20
140	.28
175	.33
225	.53
250	.55
280	.70
333	.86
355	.88
386	1.04
466	1.20
573	1.53
680	1.93
786	2.35
890	2.80

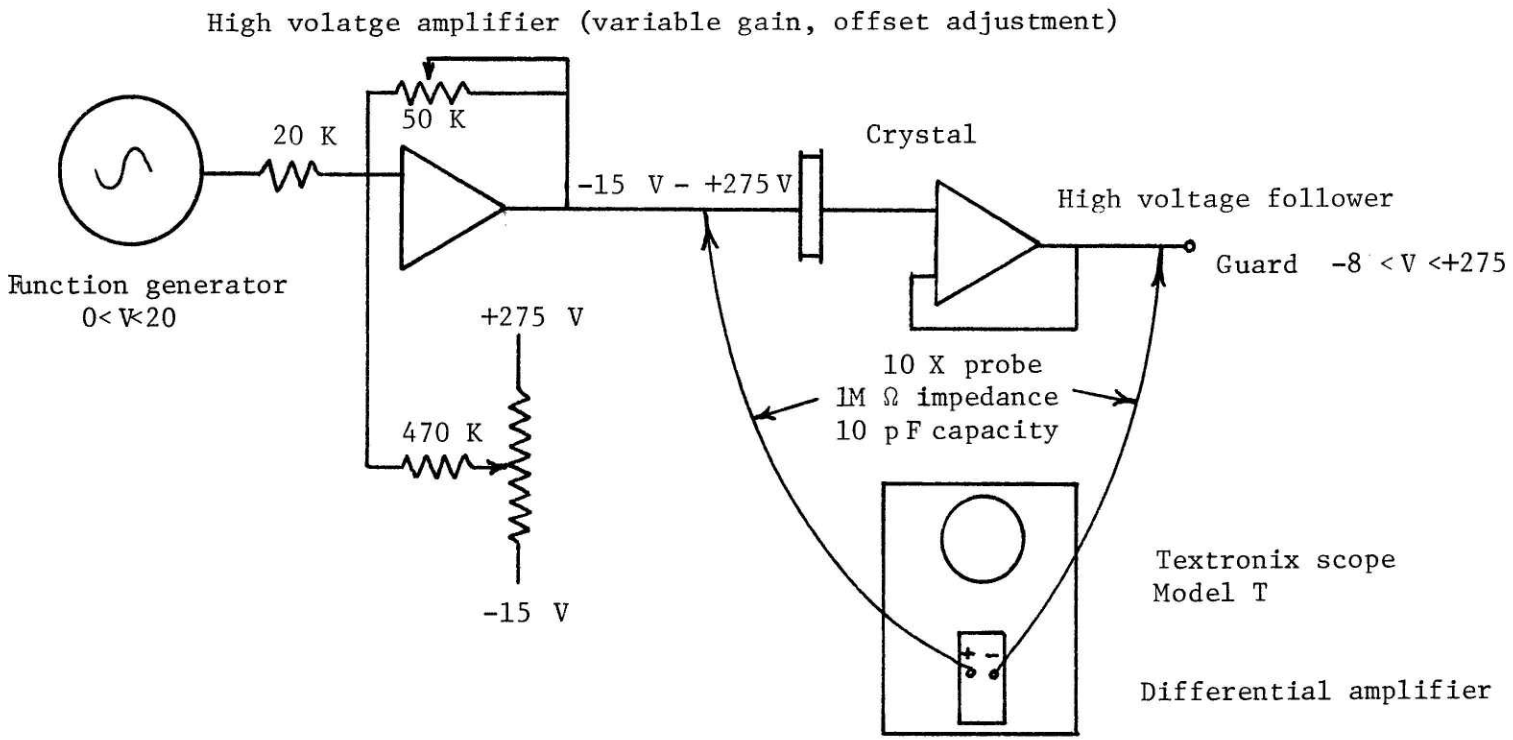

Figure A-4 Linearity test equipment for the voltage follower amplifier.

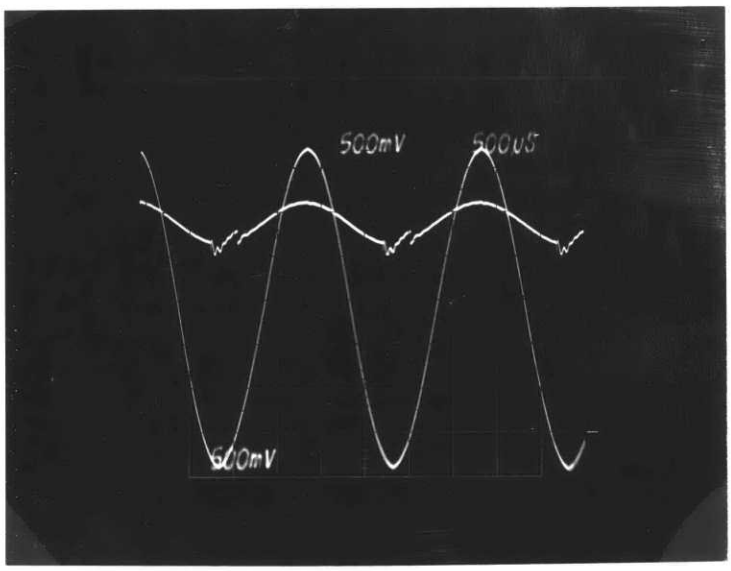

(a)

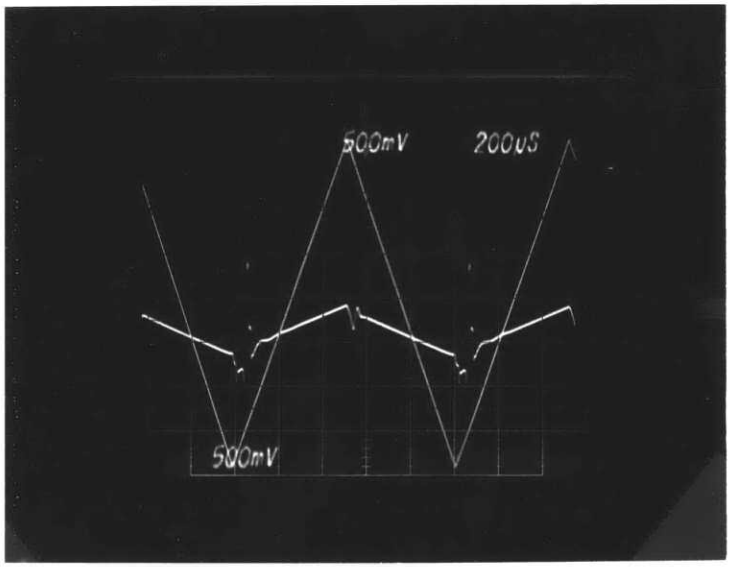

(b)

Figure A-5 Oscilloscope traces from the linearity test.
(a) 170 V_{pp} 1 Khz Sine Wave (b) 170 V_{pp} 500 Hz Triangular Wave

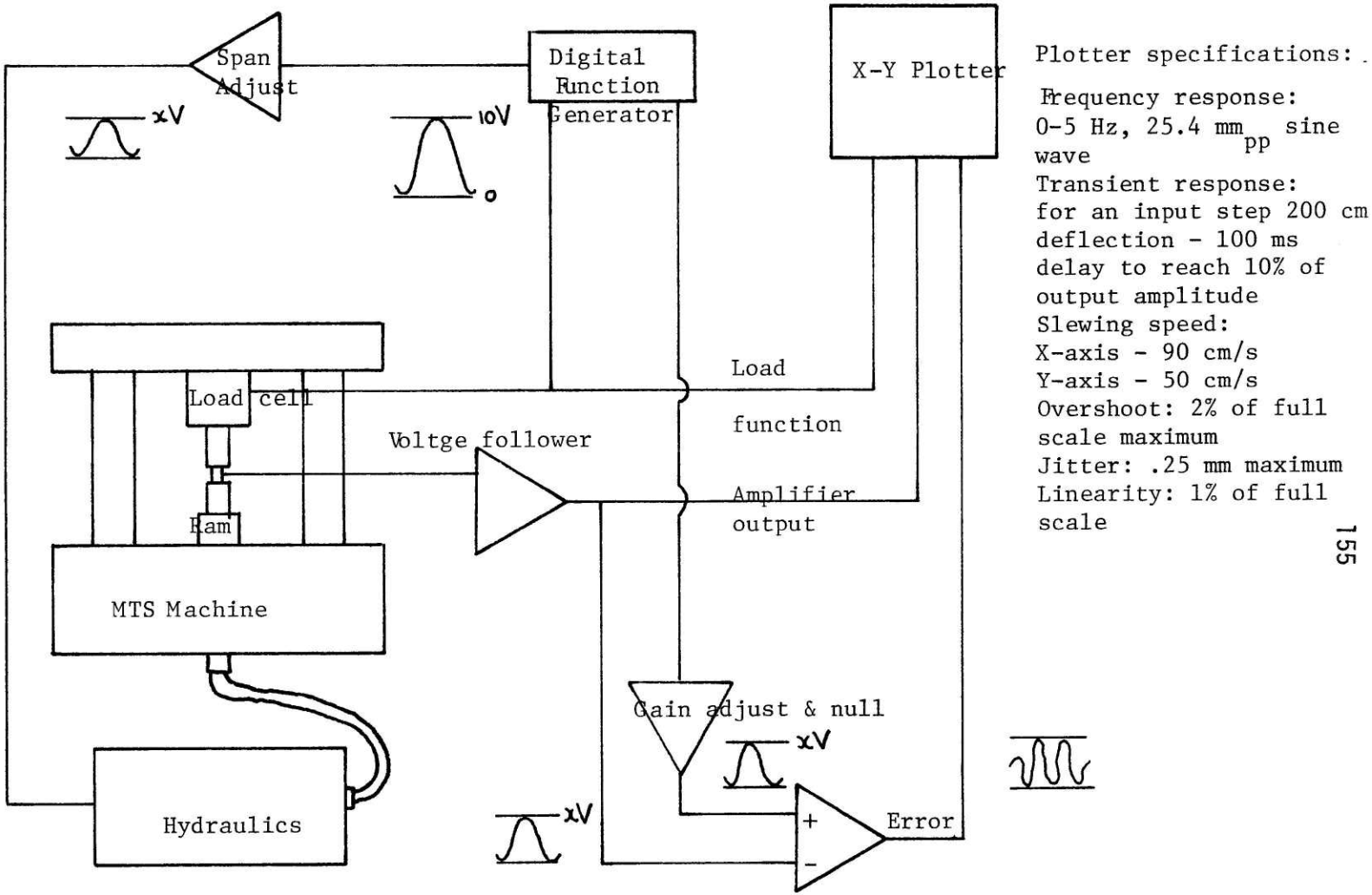

Plotter specifications:

Frequency response:
0-5 Hz, 25.4 mm_{pp} sine wave
Transient response:
for an input step 200 cm deflection - 100 ms delay to reach 10% of output amplitude
Slewing speed:
X-axis - 90 cm/s
Y-axis - 50 cm/s
Overshoot: 2% of full scale maximum
Jitter: .25 mm maximum
Linearity: 1% of full scale

Figure A-6 Experimental setup using the MTS machine.

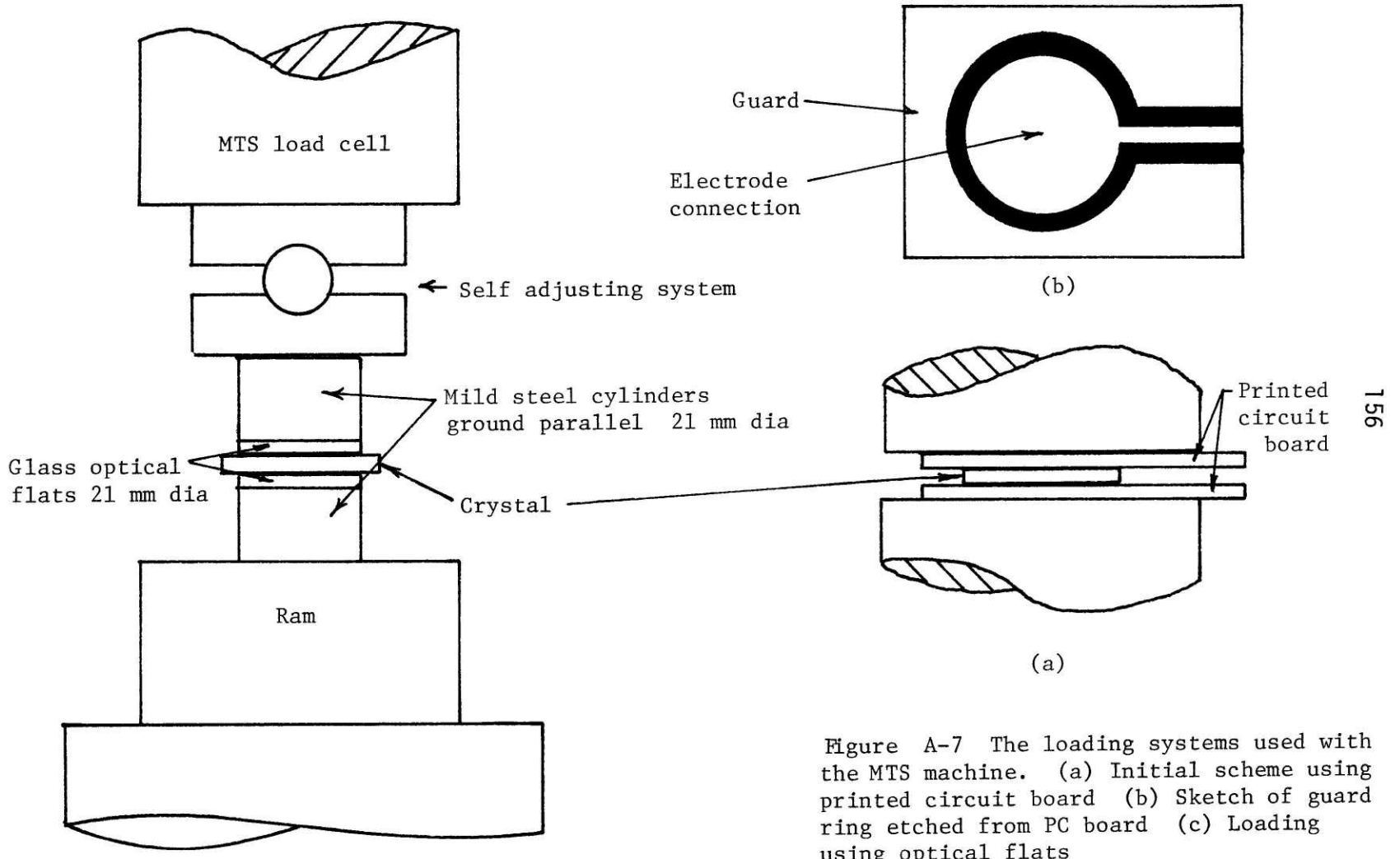

Figure A-7 The loading systems used with the MTS machine. (a) Initial scheme using printed circuit board (b) Sketch of guard ring etched from PC board (c) Loading using optical flats

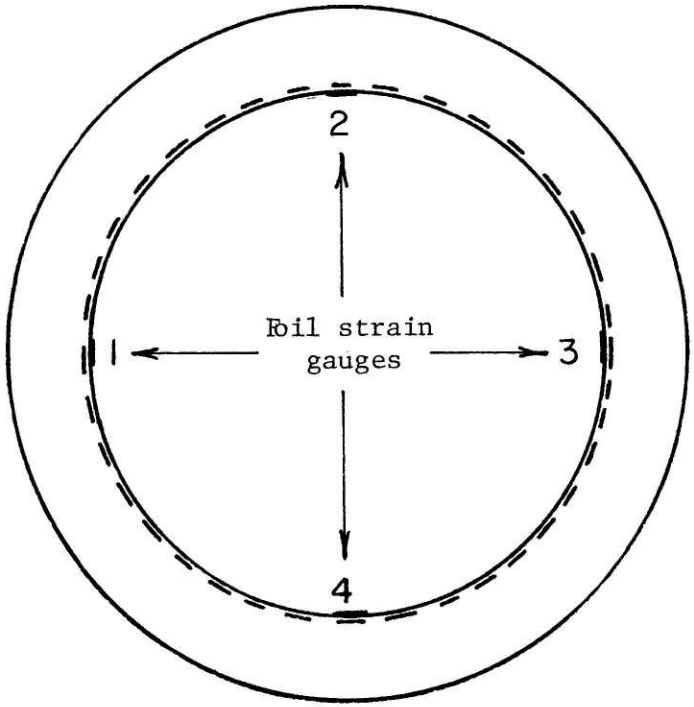

(a)

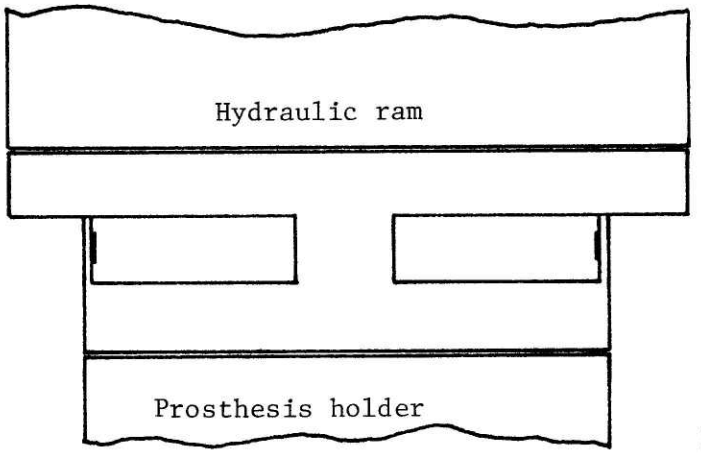

(b)

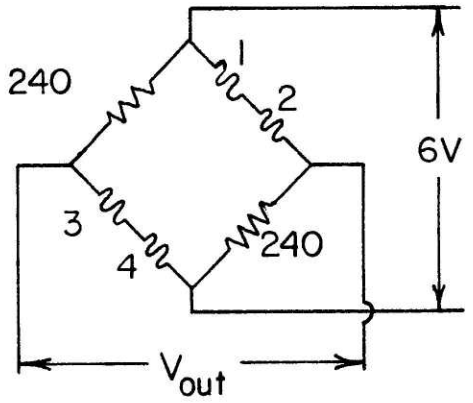

(c)

Figure A-8 A sketch of the HSM load cell.
(a) Top view (b) Side view (c) Bridge circuit

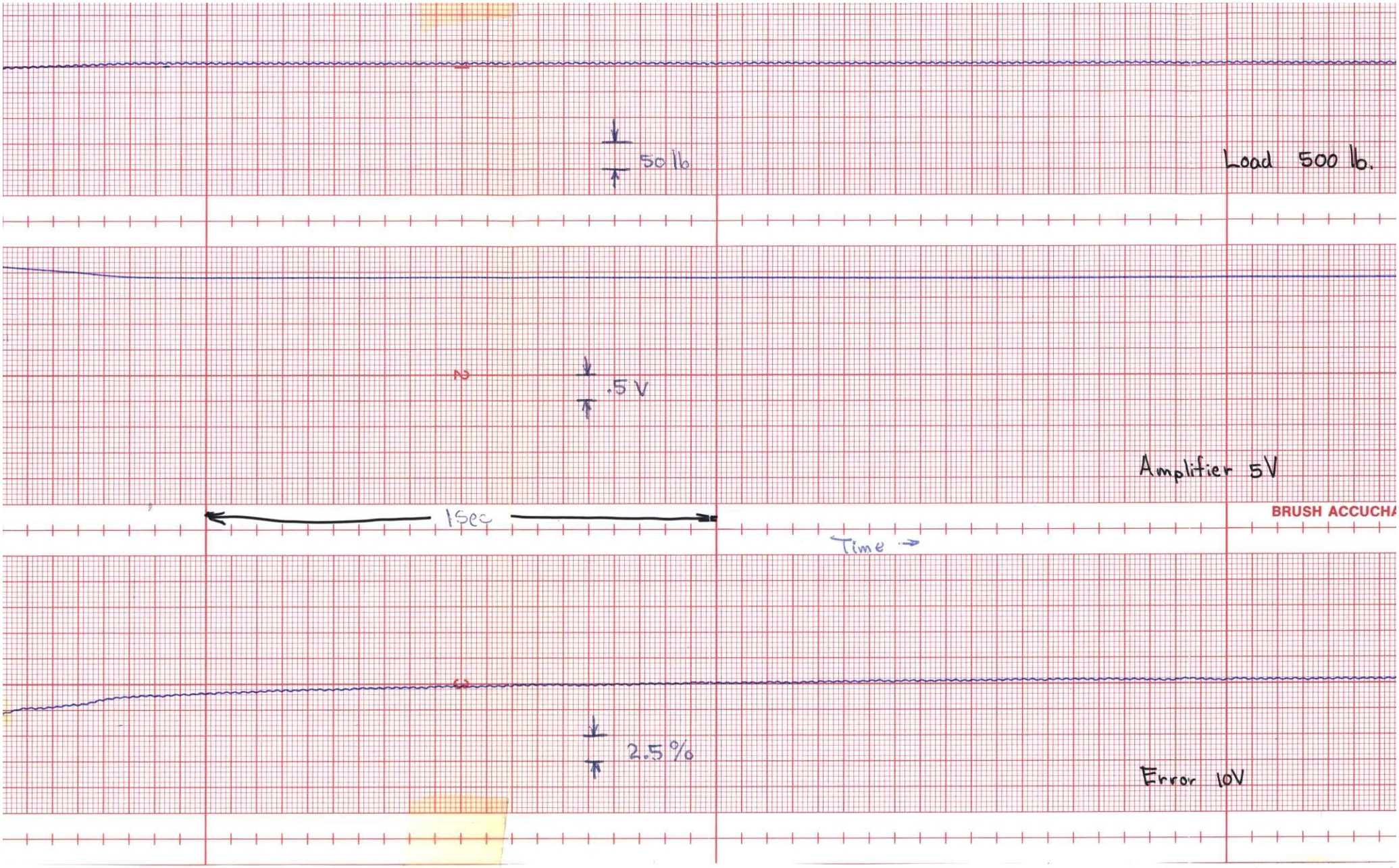

, crystal voltage and error versus
or a step input.

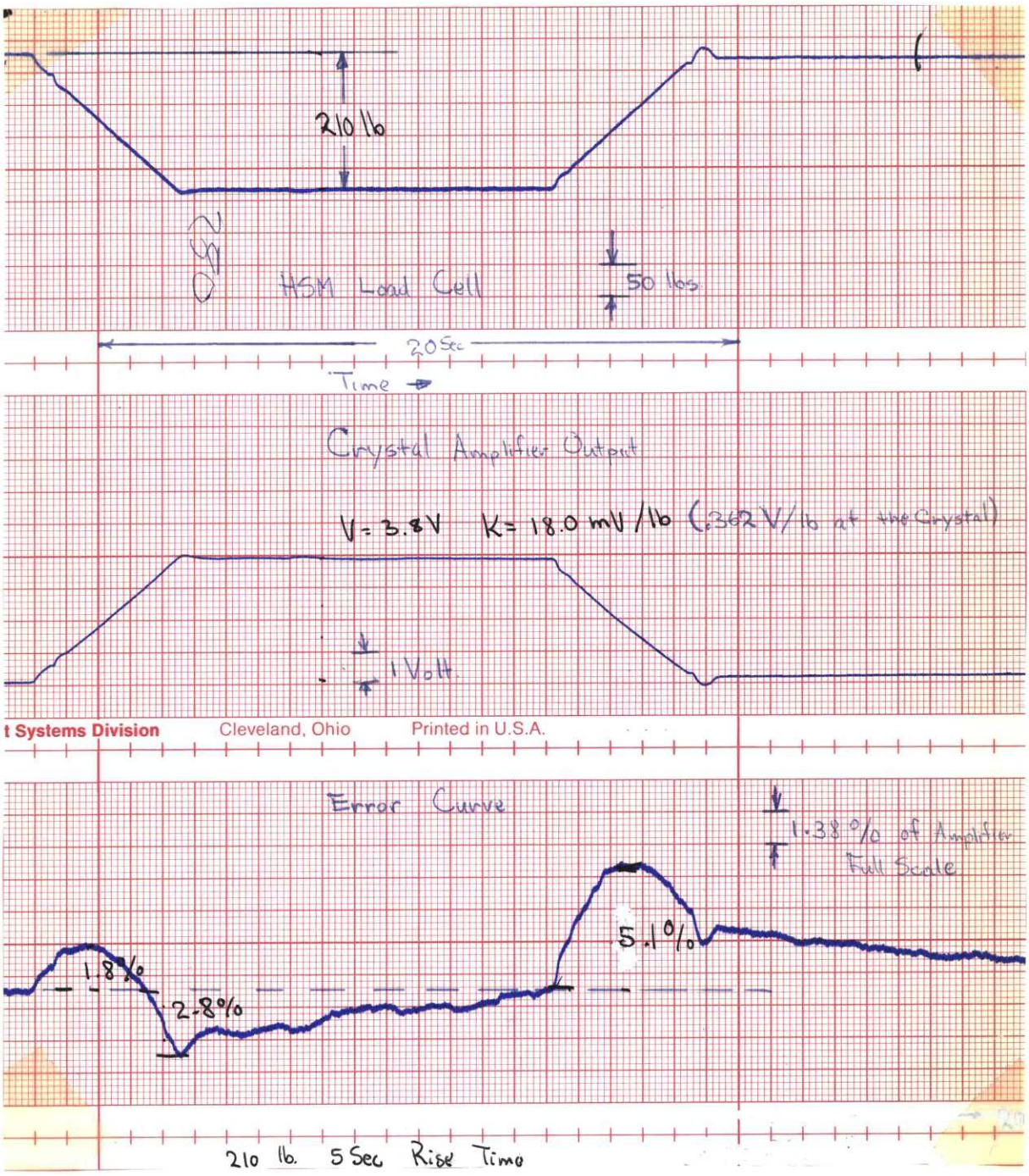

Figure A-10 Load, crystal voltage and error versus time for a slow rise input.

TABLE A-2

Sensitivity and voltage values for calibration run 12.

CALIBRATION RUN NUMBER 12 PZT-8 25.4 MM DIA 2.54 MM THK

SENSITIVITY VALUES AND VOLTAGE VALUES FOR THIS RUN

RATE LBS / MSEC	LOAD IN POUNDS 50	100	150	200	250	300	350	400	450	500
0.5	1.145	1.285	1.346	1.401	1.428	1.442	1.462	1.489	1.496	1.511
	1.191	1.312	1.366	1.413	1.441	1.469	1.474	1.537	1.507	1.531
	1.102	1.265	1.327	1.394	1.415	1.432	1.456	1.475	1.484	1.498
	0.090	0.048	0.039	0.018	0.026	0.037	0.019	0.062	0.023	0.032
	0.028	0.018	0.013	0.007	0.009	0.011	0.006	0.019	0.009	0.010
	0.873	0.778	0.743	0.714	0.700	0.694	0.684	0.672	0.668	0.662
	0.022	0.011	0.007	0.003	0.004	0.005	0.003	0.008	0.004	0.004
	0.060	0.131	0.207	0.284	0.362	0.440	0.520	0.600	0.679	0.761
	0.001	0.002	0.001	0.001	0.001	0.001	0.001	0.001	0.001	0.001
1.0	1.126	1.242	1.312	1.365	1.411	1.433	1.455	1.475	1.498	1.505
	1.148	1.254	1.333	1.386	1.437	1.446	1.469	1.486	1.555	1.519
	1.114	1.233	1.286	1.357	1.398	1.427	1.441	1.473	1.484	1.500
	0.034	0.020	0.047	0.029	0.039	0.019	0.028	0.014	0.071	0.019
	0.013	0.006	0.015	0.009	0.011	0.007	0.010	0.004	0.022	0.007
	0.888	0.805	0.763	0.732	0.709	0.698	0.687	0.678	0.668	0.664
	0.010	0.004	0.009	0.005	0.006	0.003	0.005	0.002	0.009	0.003
	0.061	0.130	0.203	0.280	0.358	0.438	0.517	0.597	0.576	0.762
	0.001	0.001	0.001	0.002	0.001	0.001	0.001	0.000	0.323	0.002
5.0	1.134	1.251	1.316	1.371	1.418	1.438	1.457	1.499	1.503	1.518
	1.189	1.290	1.341	1.407	1.438	1.460	1.467	1.531	1.527	1.537
	1.095	1.231	1.291	1.359	1.409	1.427	1.454	1.476	1.492	1.505
	0.095	0.060	0.050	0.048	0.029	0.034	0.012	0.055	0.035	0.032
	0.032	0.017	0.014	0.015	0.010	0.011	0.004	0.014	0.011	0.010
	0.882	0.800	0.760	0.729	0.705	0.696	0.686	0.667	0.665	0.659
	0.025	0.011	0.008	0.008	0.005	0.005	0.002	0.006	0.005	0.004
	0.062	0.131	0.204	0.279	0.359	0.437	0.518	0.599	0.681	0.764
	0.001	0.001	0.001	0.002	0.001	0.001	0.001	0.001	0.001	0.001

TABLE A-2 (cont'd)

```
10.0 1.137 1.251 1.316 1.370 1.411 1.433 1.460 1.489 1.502 1.515
     1.181 1.282 1.332 1.387 1.421 1.454 1.487 1.511 1.513 1.528
     1.088 1.232 1.294 1.359 1.401 1.424 1.454 1.476 1.495 1.505
     0.093 0.050 0.037 0.028 0.020 0.030 0.033 0.035 0.018 0.022
     0.027 0.019 0.011 0.011 0.008 0.011 0.010 0.012 0.006 0.008


     0.880 0.800 0.760 0.730 0.709 0.698 0.685 0.671 0.666 0.660
     0.021 0.012 0.007 0.006 0.004 0.005 0.004 0.006 0.003 0.004


     0.062 0.131 0.203 0.280 0.359 0.437 0.519 0.601 0.685 0.767
     0.001 0.001 0.001 0.001 0.001 0.001 0.001 0.001 0.001 0.001


20.0 1.157 1.231 1.304 1.367 1.404 1.433 1.462 1.490 1.501 1.516
     1.183 1.251 1.314 1.386 1.415 1.447 1.476 1.514 1.514 1.529
     1.103 1.221 1.297 1.354 1.398 1.427 1.457 1.482 1.497 1.507
     0.079 0.030 0.018 0.032 0.016 0.020 0.019 0.032 0.017 0.021
     0.026 0.011 0.006 0.010 0.005 0.006 0.006 0.011 0.005 0.007


     0.865 0.812 0.767 0.731 0.712 0.698 0.684 0.671 0.666 0.660
     0.020 0.007 0.004 0.005 0.003 0.003 0.003 0.005 0.002 0.003


     0.063 0.130 0.202 0.281 0.359 0.439 0.520 0.602 0.685 0.767
     0.001 0.001 0.000 0.001 0.001 0.001 0.000 0.001 0.001 0.001
```

THE FORMAT OF THE DATA IN EACH COLUMN IS:

SENSITIVITY(MV/LB):	AVERAGE VALUE
	MAXIMUM VALUE
	MINIMUM VALUE
	RANGE
	STANDARD DEVIATION
SENSITIVITY(LB/MV):	AVERAGE
	STANDARD DEVIATION
X-TAL VOLTAGE:	AVERAGE VALUE
	STANDARD DEVIATION

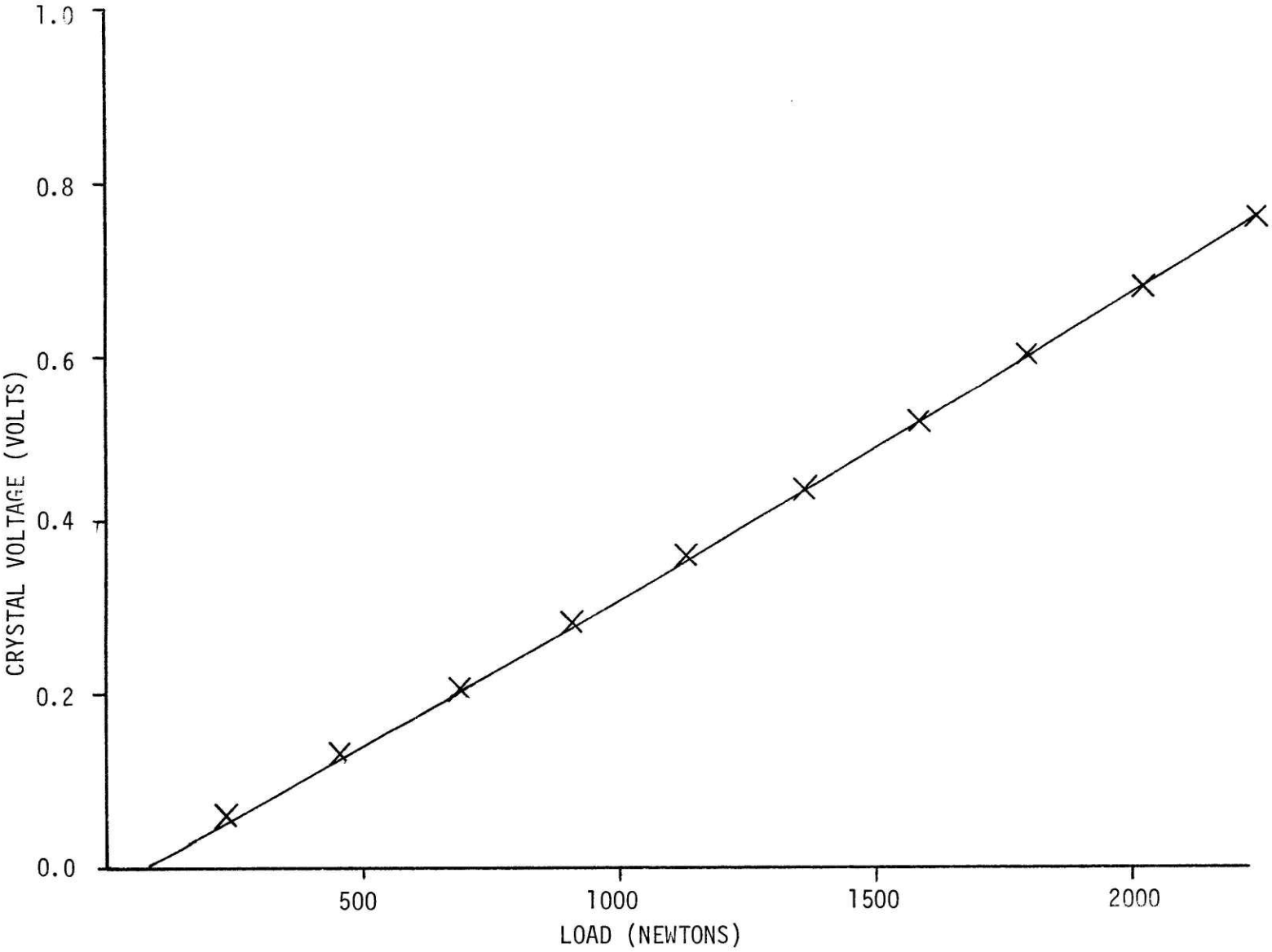

Figure A-11 Crystal voltage versus load, data points and fitted parabola.

TABLE A-3

Analysis of the curve fit for the Statham load cell.

CALIBRATION RUN USING STATHAM LOAD CELL

THE LARGEST LOAD WAS 505.6 POUNDS

THE FOLLOWING ARE THE COEFFICIENTS
FIT TO A POLYNOMIAL OF ORDER 1
GIVING LOAD IN POUNDS IN TERMS OF CRYSTAL VOLTAGE IN VOLTS

THE INTERCEPT = 5.29
THE COEFFICIENT OF X ** 1 = 446.47

THE STANDARD DEVIATION OF THE ABOVE CURVE FIT IS 1.6342
THIS CURVE FIT IS BASED ON 500 DATA POINTS

ANALYSIS OF LOAD CURVE COEFFICIENTS

THE FOLLOWING RESULTS WERE CALCULATED
TO CHECK THE EXPECTED VALUES AGAINST ACTUAL VALUES
USING THE DATA FROM THE CALIBRATION RUN AS INPUT

AVERAGE ERROR:	1.23	POUNDS(ABSOLUTE VALUE)
	0.24	PERCENT OF FULL SCALE
	0.57	PERCENT OF READING
RMS ERROR:	1.63	POUNDS
	0.32	PERCENT OF FULL SCALE
	0.89	PERCENT OF READING
LARGEST POSITIVE ERROR:	6.07	POUNDS
	1.20	PERCENT OF FULL SCALE
	3.04	PERCENT OF READING
LARGEST NEGATIVE ERROR:	-5.87	POUNDS
	-1.16	PERCENT OF FULL SCALE
	-7.21	PERCENT OF READING

ERROR VALUES HISTOGRAM

399	POINTS IN THE RANGE	0	LBS TO	2	LBS
91	POINTS IN THE RANGE	2	LBS TO	4	LBS
9	POINTS IN THE RANGE	4	LBS TO	6	LBS
1	POINTS IN THE RANGE	6	LBS TO	8	LBS

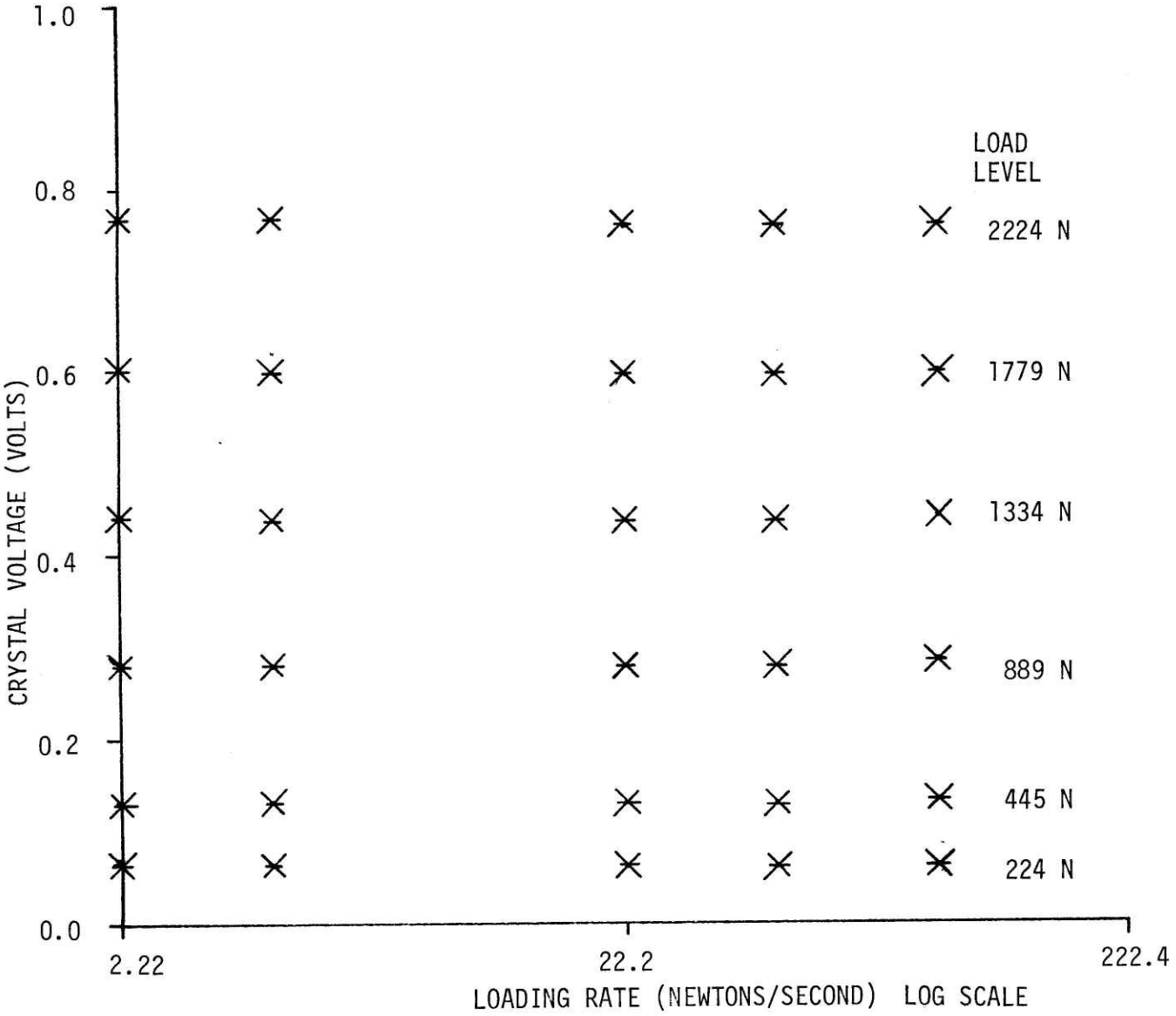

Figure A-12 Crystal voltage versus loading rate.

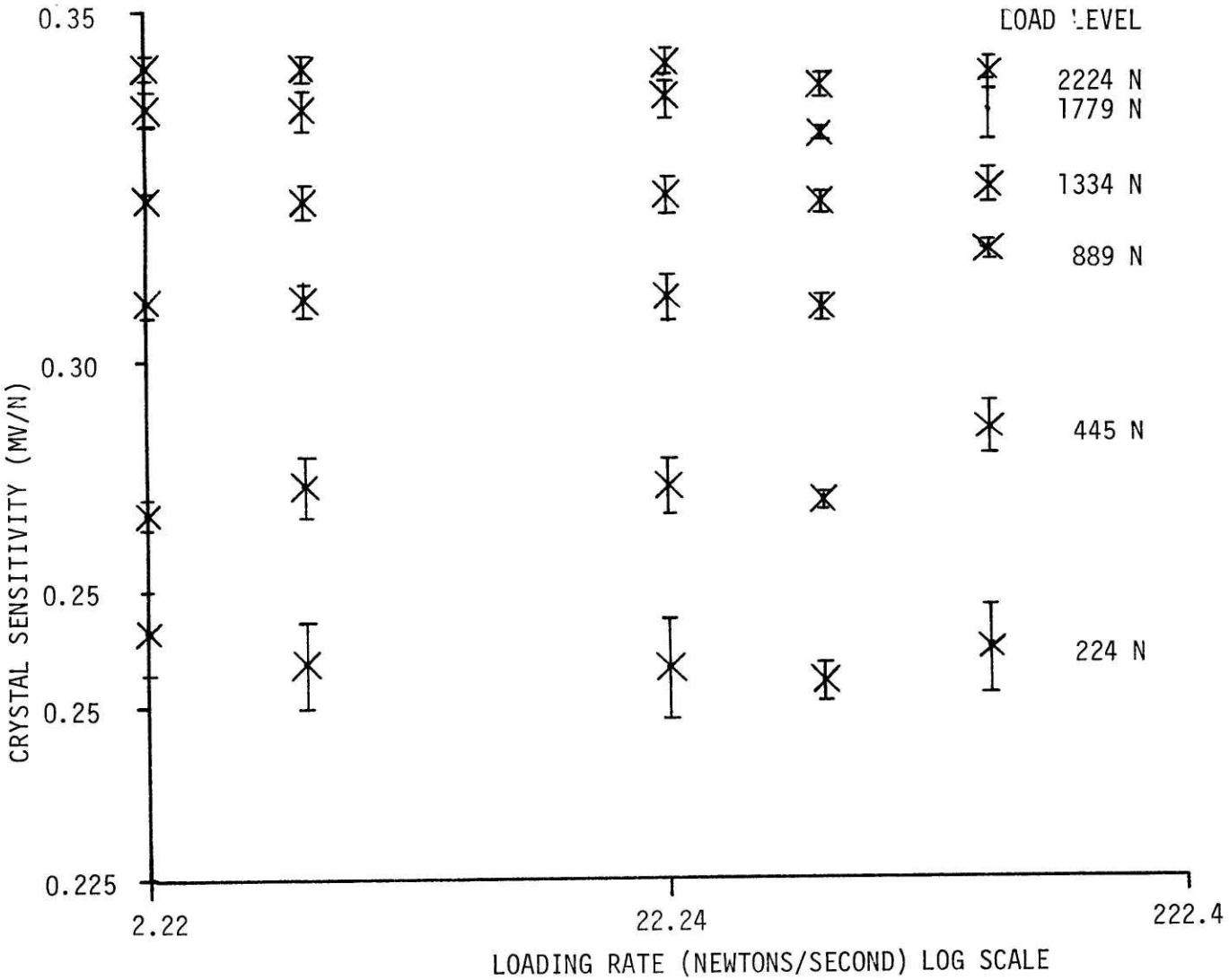

Figure A-13 Crystal sensitivity versus loading rate.

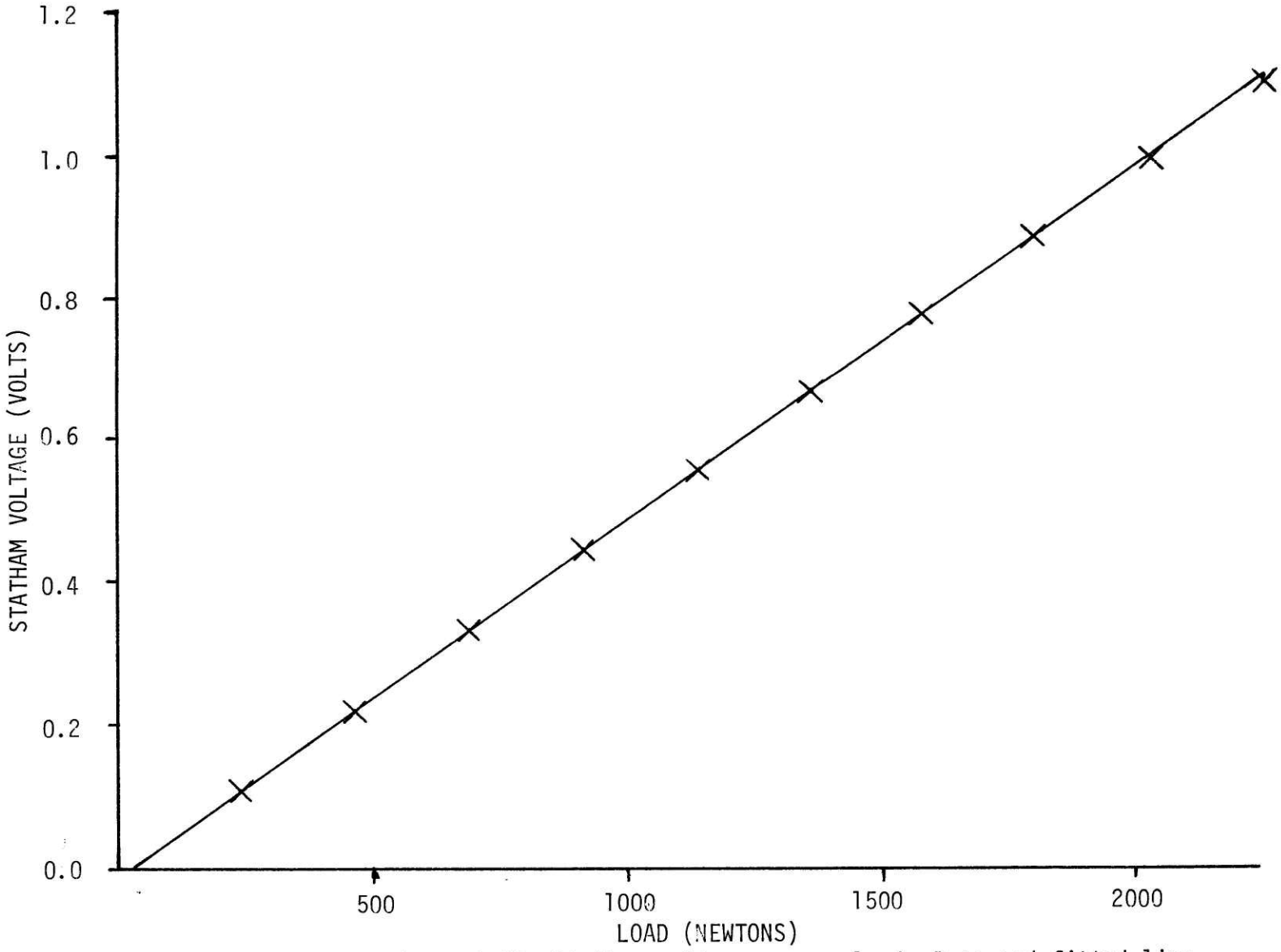

Figure A-14 Statham voltage versus load. Data and fitted line.

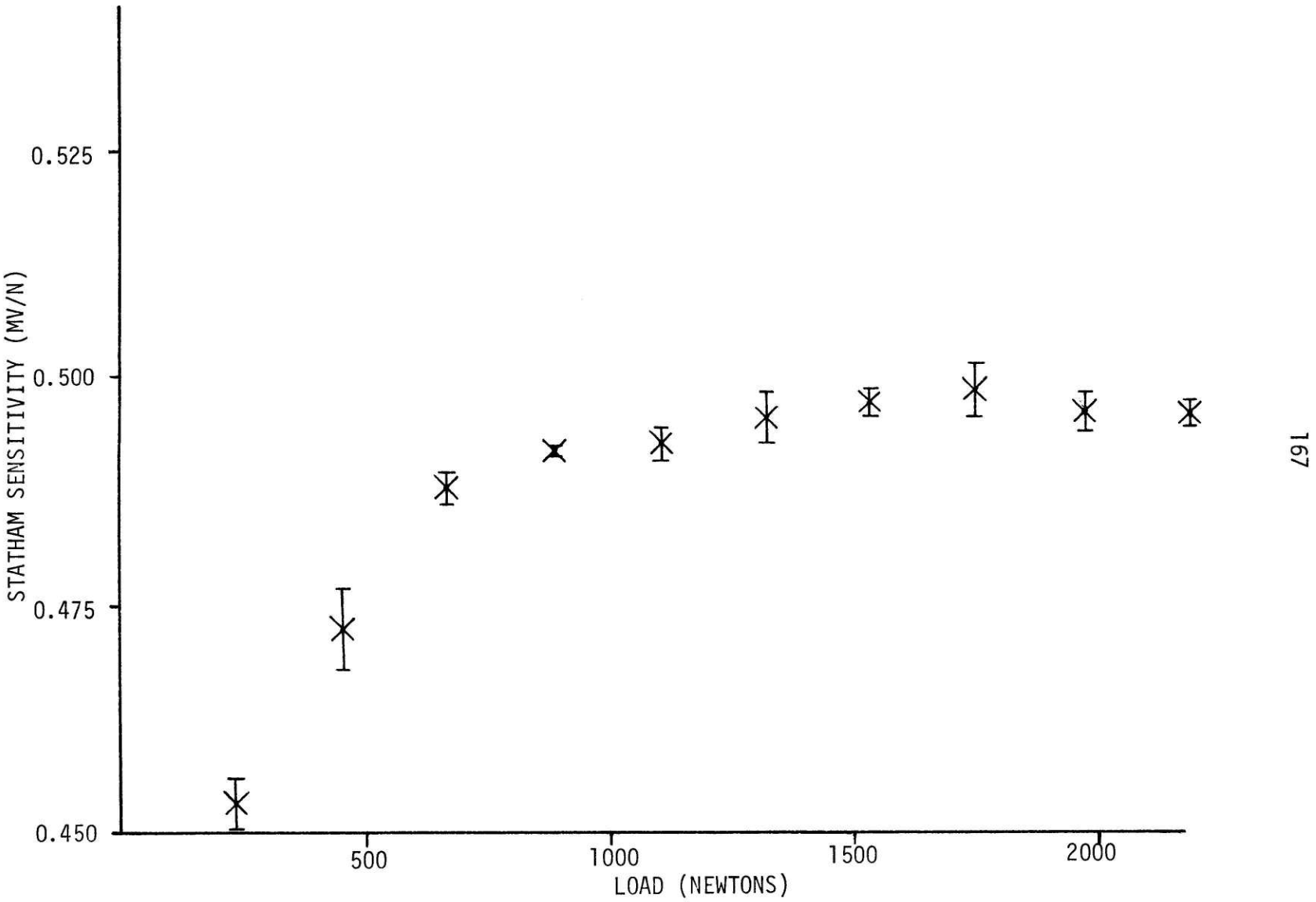

Figure A-15 Statham sensitivity versus load.

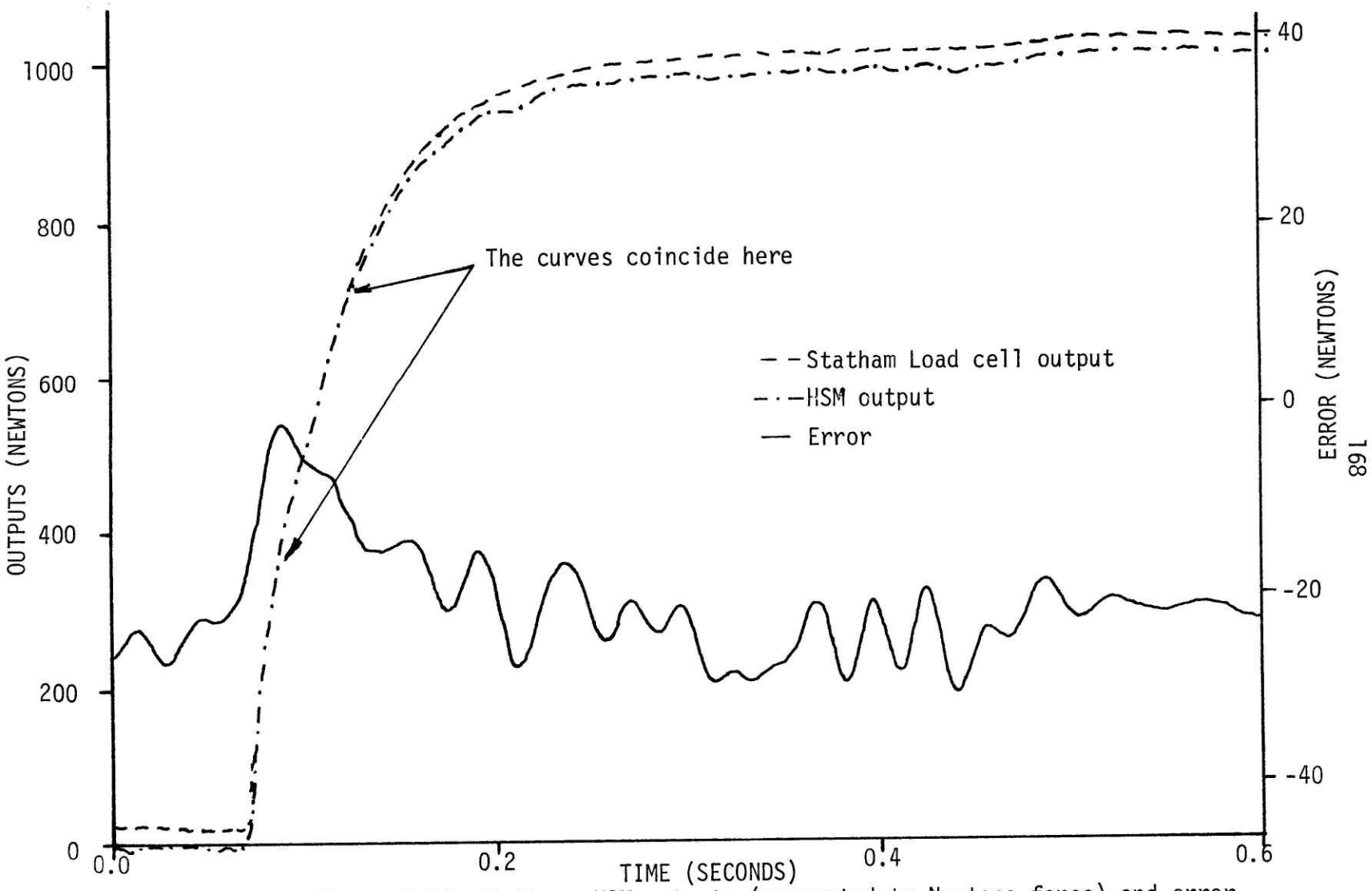

Figure A-16 Statham, HSM outputs (converted to Newtons force) and error versus time for a step load, both outputs filtered.

TABLE A-4

Sensitivity and voltage values for the Statham calibration.

STATHAM CALIBRATION RUN TO CHECK CALIBRATION METHOD

SENSITIVITY VALUES AND VOLTAGE VALUES FOR THIS RUN

RATE LBS --- MSEC	LOAD IN POUNDS 50	100	150	200	250	300	350	400	450	500
0.5	2.015	2.099	2.167	2.185	2.188	2.201	2.208	2.214	2.204	2.203
	2.048	2.117	2.178	2.189	2.197	2.218	2.225	2.244	2.222	2.221
	1.972	2.060	2.154	2.181	2.171	2.173	2.201	2.206	2.185	2.199
	0.075	0.057	0.024	0.008	0.025	0.045	0.024	0.038	0.037	0.022
	0.026	0.019	0.008	0.003	0.008	0.012	0.007	0.013	0.009	0.006
	0.496	0.477	0.461	0.458	0.457	0.454	0.453	0.452	0.454	0.454
	0.006	0.004	0.002	0.001	0.002	0.003	0.001	0.003	0.002	0.001
	0.108	0.217	0.332	0.444	0.555	0.668	0.778	0.889	0.999	1.109
	0.001	0.001	0.001	0.001	0.002	0.002	0.002	0.001	0.002	0.002
1.0	2.003	2.080	2.155	2.188	2.194	2.201	2.207	2.219	2.213	2.208
	2.068	2.121	2.164	2.193	2.217	2.211	2.226	2.236	2.231	2.210
	1.952	2.048	2.137	2.175	2.176	2.187	2.188	2.206	2.206	2.205
	0.115	0.073	0.027	0.018	0.041	0.024	0.038	0.030	0.025	0.005
	0.034	0.023	0.009	0.006	0.012	0.009	0.011	0.010	0.007	0.001
	0.499	0.481	0.464	0.457	0.456	0.454	0.453	0.451	0.452	0.453
	0.008	0.005	0.002	0.001	0.003	0.002	0.002	0.002	0.001	0.000
	0.108	0.217	0.329	0.441	0.555	0.668	0.779	0.891	1.001	1.109
	0.001	0.001	0.001	0.001	0.001	0.001	0.001	0.001	0.001	0.001
5.0	1.990	2.118	2.150	2.175	2.186	2.192	2.200	2.220	2.215	2.215
	2.083	2.136	2.169	2.193	2.196	2.198	2.205	2.236	2.224	2.242
	1.872	2.087	2.113	2.160	2.170	2.177	2.193	2.209	2.205	2.205
	0.211	0.049	0.057	0.032	0.026	0.021	0.012	0.027	0.019	0.037
	0.063	0.017	0.017	0.010	0.009	0.006	0.004	0.008	0.006	0.014
	0.503	0.472	0.465	0.460	0.457	0.456	0.455	0.450	0.452	0.451
	0.016	0.004	0.004	0.002	0.002	0.001	0.001	0.002	0.001	0.003
	0.109	0.220	0.329	0.440	0.552	0.663	0.774	0.891	1.001	1.112
	0.001	0.001	0.001	0.001	0.001	0.001	0.001	0.001	0.001	0.001

TABLE A-4 (cont'd)

```
10.0 2.018 2.137 2.171 2.191 2.203 2.201 2.216 2.219 2.214 2.206
     2.044 2.153 2.183 2.199 2.212 2.207 2.232 2.229 2.227 2.207
     1.985 2.113 2.158 2.183 2.186 2.195 2.206 2.215 2.206 2.204
     0.058 0.039 0.026 0.017 0.025 0.013 0.025 0.013 0.021 0.003
     0.020 0.012 0.009 0.006 0.007 0.004 0.009 0.004 0.006 0.001

     0.496 0.468 0.461 0.456 0.454 0.454 0.451 0.451 0.452 0.453
     0.005 0.003 0.002 0.001 0.001 0.001 0.002 0.001 0.001 0.000

     0.112 0.223 0.334 0.445 0.560 0.670 0.782 0.893 1.003 1.111
     0.001 0.000 0.001 0.001 0.002 0.001 0.002 0.001 0.002 0.001

20.0 2.018 2.127 2.173 2.198 2.202 2.206 2.219 2.223 2.217 2.213
     2.048 2.153 2.181 2.209 2.215 2.223 2.224 2.232 2.239 2.226
     1.948 2.052 2.158 2.176 2.184 2.193 2.200 2.210 2.207 2.205
     0.099 0.101 0.022 0.033 0.031 0.030 0.025 0.022 0.032 0.020
     0.034 0.030 0.006 0.012 0.012 0.009 0.007 0.006 0.009 0.008

     0.496 0.470 0.460 0.455 0.454 0.453 0.451 0.450 0.451 0.452
     0.008 0.007 0.001 0.003 0.003 0.002 0.001 0.001 0.002 0.002

     0.116 0.225 0.334 0.445 0.558 0.668 0.780 0.892 1.002 1.112
     0.001 0.001 0.000 0.001 0.001 0.001 0.001 0.001 0.001 0.001
```

THE FORMAT OF THE DATA IN EACH COLUMN IS:

SENSITIVITY(MV/LB):	AVERAGE VALUE
	MAXIMUM VALUE
	MINIMUM VALUE
	RANGE
	STANDARD DEVIATION
SENSITIVITY(LB/MV):	AVERAGE
	STANDARD DEVIATION
X-TAL VOLTAGE:	AVERAGE VALUE
	STANDARD DEVIATION

APPENDIX B
APPLIED FORCE CALCULATIONS FOR THE FORCE PLATE PATHWAY

B-1 Detailed Calculations

Figure B-1 is a 3-view sketch of a typical force plate giving the relevent dimensions and possible location of a point of application of force. The line A-A is the line which is midway between adjacent tiles, spaces included. The distance Y_1 is that from this datum to the transducer at the apex and Y_2 to the transducers at the base of the triangle. The value of X is the distance from the center of the triangles in the x-direction, line B-B, to the transducers along the base.

The transducers were assumed capable of resolving the force applied to them in three directions; z(normal force, x(fore-aft force), y(lateral force). The transducer used is indicated by the first subscript and the direction the force sensed was in, shown by the second subscript.

The values of Y_1, Y_2, X are

$$X = \frac{\ell}{2} - p \tan 60°$$

$$Y_1 = (\ell \sin 60° + s(1+.5))/2 - (s+2p)$$

$$Y_2 = (\ell \sin 60° + s(1+.5))/2 - (.5s+p).$$

To calculate the point of application of the force applied two equations are required. First using moments about the x-axis through

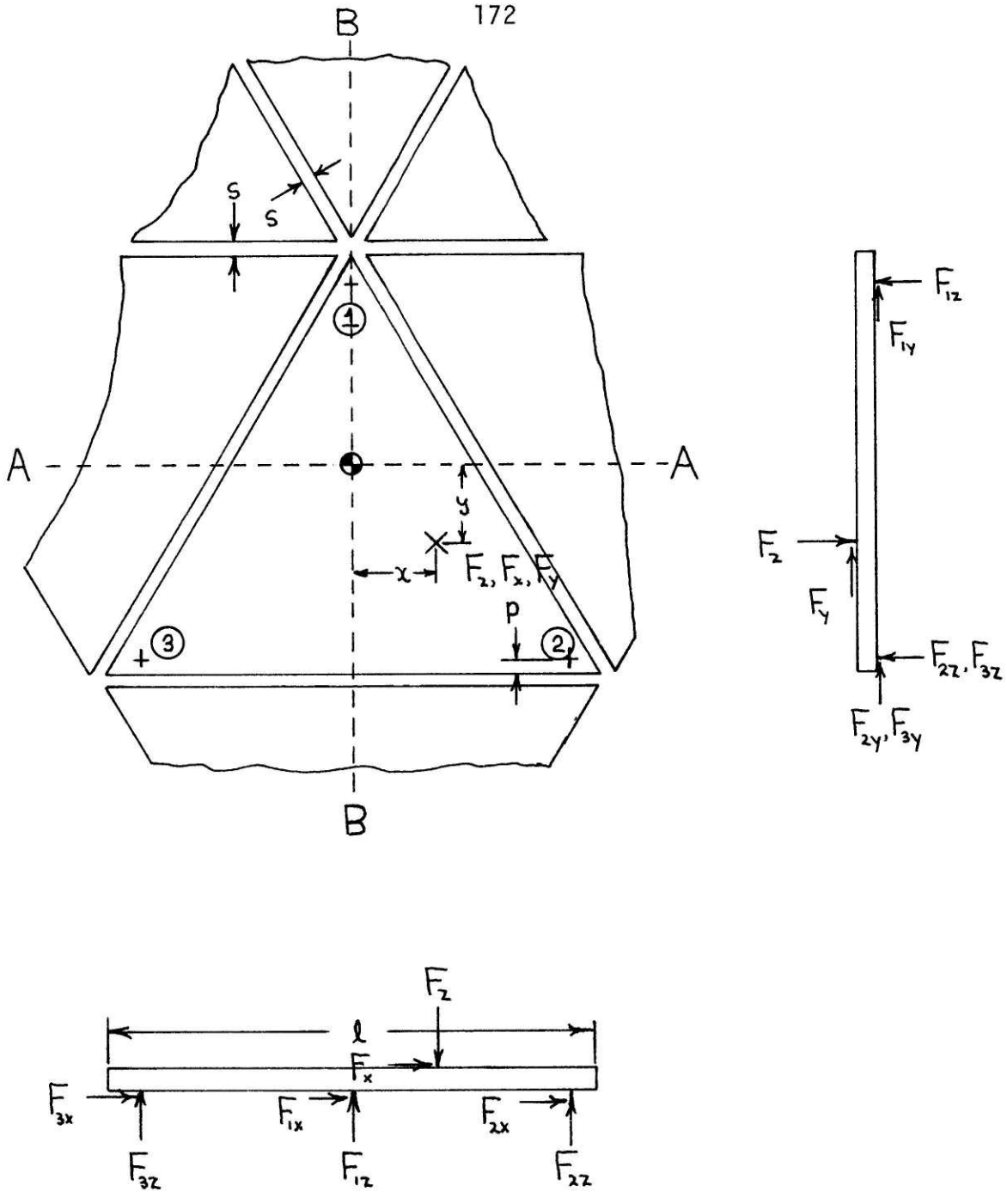

Figure B-1 A 3-view sketch of a force plate with a load applied.

the center of the plate the x value is given (refer to Figure B-2)

$$\Sigma F_y = 0 \quad \circlearrowleft \qquad -F_z x + F_{2z} X - F_{3z} X = 0$$

since $F_z = F_{1z} + F_{2z} + F_{3z}$,

$$x = \frac{(F_{2z} - F_{3z})X}{F_{1z} + F_{2z} + F_{3z}}$$

Next using Figure B-3 and moments about the y axis the value of y is calculated

$$\Sigma F_x = 0 \quad \circlearrowleft \qquad -F_z y - F_{1z} Y_1 + F_{2z} Y_2 + F_{3z} Y_2 = 0$$

$$y = \frac{(F_{2z} + F_{3z})Y_2 - F_{1z} Y_1}{F_{1z} + F_{2z} + F_{3z}}$$

The value of the moment about a line parallel to the z-axis, through the point of force application can be calculated using

$$\Sigma M_z = 0 \quad \circlearrowleft \qquad -F_{1x}(Y_1 - y) - F_{1y} x - F_{3y}(X + x) + F_{2y}(X - x)$$

$$+ F_{2x}(Y_2 + y) + F_{3x}(Y_2 + y) + M_z = 0$$

$$\therefore \quad M_z = F_{1x}(Y_1 - y) - (F_{2x} + F_{3x})(Y_2 + y) + F_{1y} x + F_{3y}(X + x) - F_{1y}(X - x).$$

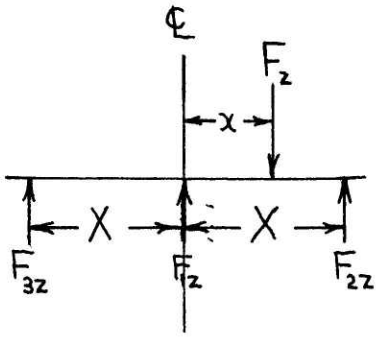

Figure B-2 Forces used to calculate x.

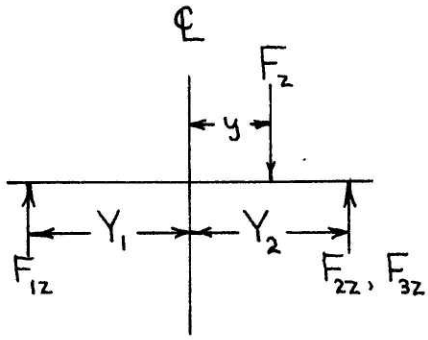

Figure B-3 Forces used to calculate y.

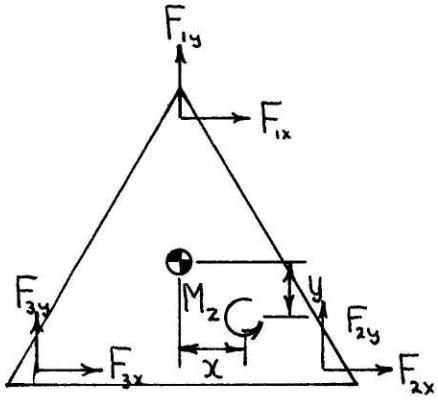

Figure B-4 Forces used to calculate the z-axis moment about the point of application.

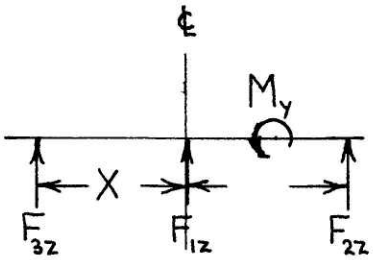

Figure B-5 Forces used to calculate the y-axis moment about the point of application.

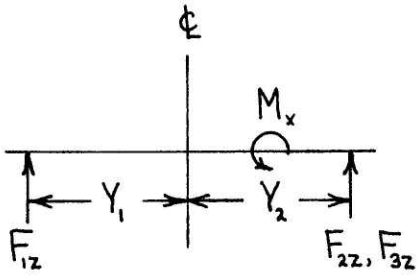

Figure B-6 Forces used to calculate the x-axis moment about the point of application.

Similarly, for the moments about the x, y-axes through the point of application

$$\Sigma M_x = 0 \quad \circlearrowleft \qquad M_x + (F_{2z} + F_{3z})(Y_2 + y) - F_{1z}(Y_1 - y) = 0$$

$$\therefore M_x = F_{1z}(Y_1 - y) - (F_{2z} + F_{3z})(Y_2 + y)$$

$$\Sigma M_y = 0 \quad \circlearrowleft \qquad M_y + F_{2z}(X - x) - F_{1z}x - F_{3z}(X + x) = 0$$

$$\therefore M_y = F_{3z}(X + x) + F_{1z}x - F_{2z}(X - x) .$$

Once these values are calculated for each plate, they are referred back to some datum to calculate the total forces and moments exerted on all plates and the resultant point of application. Figure B-7 shows 3 plates and the points of application of the forces and moments. For the total forces

$$F_{Total_z} = \bar{F}_{1z} + \bar{F}_{2z} + \bar{F}_{3z}$$

$$F_{Total_x} = \bar{F}_{1x} + \bar{F}_{2x} + \bar{F}_{3x}$$

$$F_{Total_y} = \bar{F}_{1y} + \bar{F}_{2y} + \bar{F}_{3y} .$$

For the point of application $\bar{X}$, $\bar{Y}$

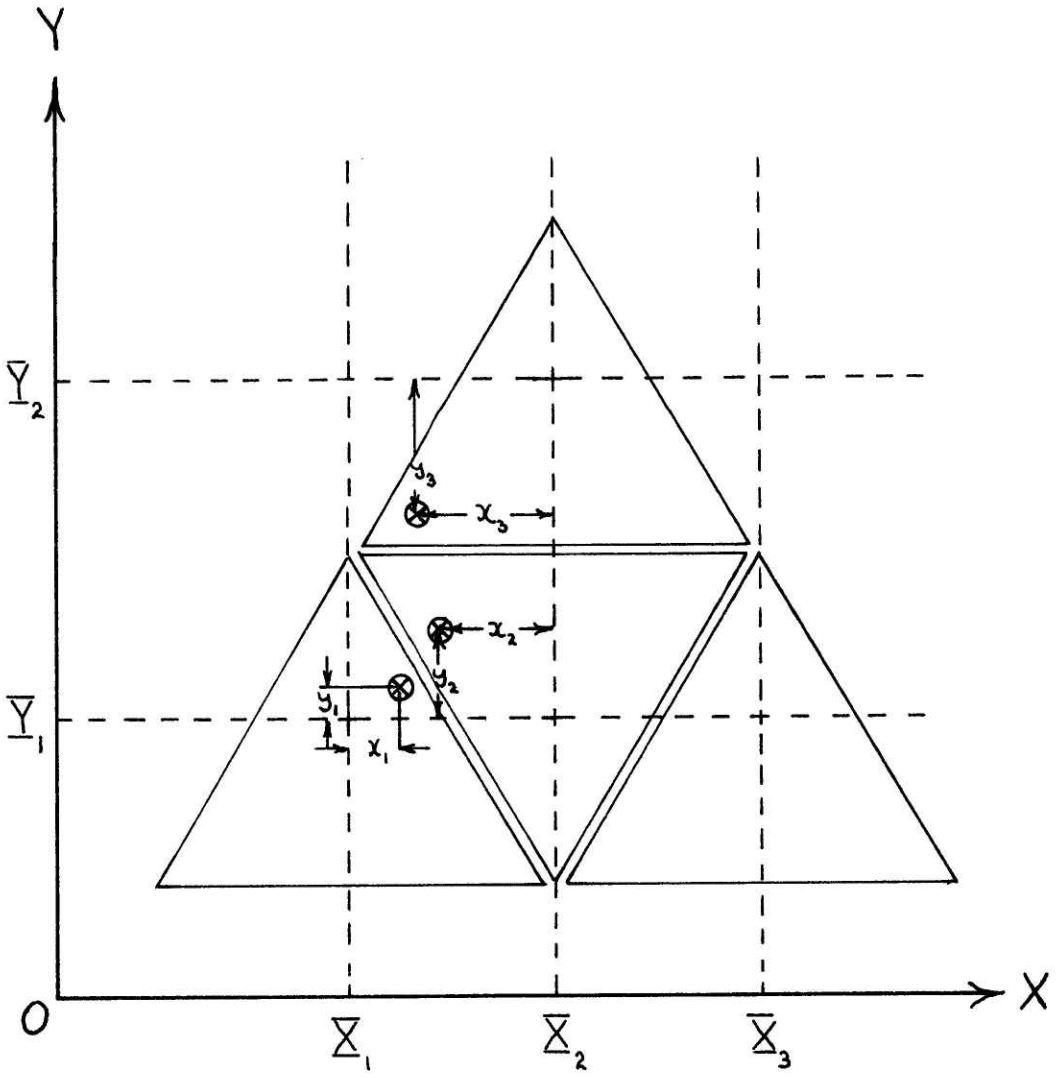

Figure B-7 Three plates showing the datum lines.

$$\bar{X} = \bar{F}_{1z}(x_1 + \bar{\underline{X}}_1) + \bar{F}_{2z}(x_2 + \bar{\underline{X}}_2) + \bar{F}_{3z}(x_3 + \bar{\underline{X}}_3)$$

$$\bar{Y} = \bar{F}_{1z}(y_1 + \bar{\underline{Y}}_1) + \bar{F}_{2z}(y_2 + \bar{\underline{Y}}_2) + \bar{F}_{3z}(y_3 + \bar{\underline{Y}}_3)$$

Note that the values of x_i, y_i may be negative and the values of $\bar{\underline{X}}_i$, $\bar{\underline{Y}}_i$ may be the same for different plates.

For the moments about the point of application, the total moment is the sum of the individual moment vectors from each plate.

$$M_{Total\,z} = \bar{M}_{1z} + \bar{M}_{2z} + \bar{M}_{3z}$$

$$M_{Total\,x} = \bar{M}_{1x} + \bar{M}_{2x} + \bar{M}_{3x}$$

$$M_{Total\,y} = \bar{M}_{1y} + \bar{M}_{2y} + \bar{M}_{3y}.$$

REFERENCES

1. Arcan, M., Brull, M.A.; "A Fundamental Characteristic of the Human Body and Foot, The Foot-Ground Pressure Pattern.", J. Biomechanics, Vol 9, 1976, pp 453-457

2. Baumeister, T, ed.; Standard Handbook for Mechanical Engineers: McGraw-Hill, New York, 1962

3. Bickle, L.W.; "The Use of Strain Gauges for the Measurement of Propagating Strain Waves", Proc. Tech. Comm. Strain Gauges, Oct. 1970, Soc. for Exp. Stress Anal., Westport, Conneticut

4. Biggs, J.M.; Structural Dynamics: McGraw-Hill, New York, 1964

5. Bressler, B., Frankel, J.P.; "The Forces and Moments in the Leg During Level Walking", ASME Transactions, January 1950

6. Cady, W.G.; Piezoelectricity: Dover Publications, New York, 1964

7. Carlsoo, S.A. "AMethod for Studying Walking on Different Surfaces", Ergonomics, Vol 5, 1962, pp 271-274

8. Cavanagh, P; Biomechanics Laboratory, Penn State University, Nittany, Pennsylvania

9. Clevite Corporation, Vernitron Division Bedford, Ohio 4416

10. Contini,R; "Body Segment Parameters, Part II", Artificial Limbs, Vol 16, No 1, Spring 1972, pp 1-19

11. Cooper, J.M., Ward, R., Taylor, P., Barlow, D.; "Kinesiology of the Long Jump", Medicine and Sport, Biomechanics III, Karger 1973, pp 381-386

12. Cooper,J.M., Bates,B.T.; "KInematic and KInetic Analysis of the Golf Swing", Medicine and Sport, Biomechanics IV, University Park Press, 1974

13. Cope, F.W.; "Problems in Human Vibration Engineering", Ergonomics, Vol 3, Jan 1960, pp 35-44

14. Cunningham, D.M., Brown, W.G.; "Two Devices for Measuring the Forces Acting on the Human Body During Walking", Proc. Soc. for Exp. Stress Anal., Vol 9, No2, 1952

15. Digital Equipment Limited, Maynard, Massachusetts

16. Doeblin, E.O.; Measurement Systems Application and Design: McGraw-Hill, New York, 1975

17. Donath, M.; "Human Gait Pattern Recognition for Evaluation, Diagnosis and Control", Phd Thesis, MIT, June 1978
Control", Phd Thesis, MIT, June 1978

18. Elftman,H; "The Measurement of the External Force in Walking", Science, Vol 88, pp 152-153

19. Elftman, H; "A Cinematic Study of the Distribution of Pressure in the Human Foot", The Anatomical Record, Vol 59, No 4, 1934, pp 481-487

20. Endo, B., Kimura, T.; "Dynamic Analysis of Human Walking", Proc. of the VIIth Internat. Cong. of Anthrop. & Ethn. Sci., Vol 1, 1968, pp 335-339

21. Fertis, P.G.; Dynamics and Vibration of Structures, Wiley, New York, 1973

22. Flowers, W.C., Personal Communication

23. Greene, J.H., Morris, W.H.; "The Design of a Force Platform for Work Measurement", Journal of Industrial Engineering, Vol 10, No 4, July 1959, pp 312-317

24. Hargraves, P., Scales, J.T.; "Clinical Assessment of Gait Using Load Measuring Footwear", Acta Orthopaedic Scandanavia, Vol 46, 1975, pp 877-895

25. Harris, C.M., Crede, C.E., eds; Shock and Vibration Handbook: McGraw-Hill, New York, 1976

26. Hearn, K.H., Konz, S.;"Equipment Note: An Improved Design for a Force Platform", Ergonomics, Vol 11, No 4, 1968, pp 383-389

27. Hennacy, R., Gunther, R.; "A Piezoelectric Crystal Method for Measuring Static and Dynamic Pressure Distribution in the Feet", J. of American Podiatry Association, Vol 65, No 5, May 1975, pp 444-449

28. Holden, T.S., Muncey, R.W.; "Pressures on the Human Foot During Walking", Australian Journal of Applied Science, Vol 4, 1953, pp 405-417

29. Jacobs, N.A., Skorecki, J., Charnley, J.; "Analysis of the Vertical Component of Force in Normal and Pathological Gait", J. Biomechanics, Vol 5, 1972, ppl1-34

30. Jaffe, B., Cook, W., Jaffe, H.; Piezoelectric Ceramics: Academic Press Inc, New York, 1971

31. Jona, F., Shrane, G.; Ferroelectric Crystals: Pergamon Press, New York, 1972

32. Kistler Corporation, 2475 Grand Island Blvd, Grand Island, New York, 14072

33. Kistler Specification Sheet, 9251-6

34. Kirkpatrick, G.S.; "A Study of Forces Developed in a Load Bearing Brace During Walking", MS Thesis, Univ. of Washington, 1967

35. Larau, L.; "Physiological Study of Motions", Advanced Management, Vol 22, No 3, March 1957, pp 17-24

36. Lebow Industries, Waltham Massachusetts, Model 661.23A-02

37. Leissa,A.W.; "Vibration of Plates", NASA-SP-160, NASA, 1969

38. Levin, R.; "Foot Force Transducer System", A Report to Rancho Los Amigos Hospital from Harvey Mudd College, June 1975

39. Mann, R.W.; "Technology and Human Rehabilitation: Protheses for Sensory Rehabilitation and/or Sensory Substitution", Adv. in Biomedical Engineering, Vol 4, 1974, Academic Press

40. Marsden, J.P., Montgomery, S.R.; "An Analysis of the Dynamic Characteristics of a Force Plate", Measurement and Control, Vol 5, March 1972

41. MTS Inc., Minneapolis, Minnesota, Model 916-04

42. Morton, J.; The Human Foot, Columbia University Press, 1936

43. Murray, M.P.; "Walking Patterns of Normal Men", J Bone and Jnt Surgery, Vol 46A, No 2, March 1964, pp 335-360

44. Murray, M.P.; "walking Patterns of Normal Women", Archives of Physical Medicine and Rehabilitation, Vol 51, Nov 1970

45. Neubert, H.; Instrument Transducers: Clarendon Press, Oxford, 1975

46. Patel, D.V.; "Supportive Forces on the Human Body During Underwater Activities", MS Thesis, Univ. of Wisconsin, Madison, Wisconsin, 1969

47. Paul, J.,Poulson, J.;"The Analysis of Forces Transmitted by Joints in the Human Body", Proc of the Vth Internat. Conf. of Stress Anal., Udine, Italy, 1974

48. Payne,A.H., Slater, W.J., Telford, T.; "The Use of a Force Platform in the Study of Athletic Activities. A Preliminary Investigation", Ergonomics, Vol 2, No 2, 1968, pp 123-143

49. Payne, A.H., "A Force Platform System for Biomechanics Research in Sport", Medicine and Sport, Biomechanics IV, University Park Press, 1974

50. Popov, E.P.; Introduction to Mechanics of Solids: Prentice-Hall, New Jersey, 1968

51. Ramey, M.R.; "Force Plate Designs & Applications", Exercise Sport Science Review, Vol 3, 1975, pp 303-319

52. Ramey, M.R.; "Use of Force Plates for Long Jump Studies", Medicine and Sport, Vol 8, Biomechanics III, University Park Press, 1973

53. Roarke, R.J., Young, W.C.; Formulas for Stress and Strain: McGraw-Hill, New York, 1975

54. Rushfeldt, P.D., Mann, R.W., Harris, W.H.; "Pressure Contour over the Human Ascetabulum", Biosigma '78, Paris, April 28, 1978

55. Rushfeldt, P.D., Mann, R.W., Palmer, D., Harris, W.H.; "In Vitro Hip Joint Pressure Distribution Testing Facility", AAMI 13th Annual Conference, March, 1978

56. Schaevitz Engineering, Camden, New Jersey 08101

57. Scranton, P. E., McMaster, J.H.; "Momentary Distribution of Forces Under the Foot", J. Biomechanics, Vol 9, 1976, pp 45-48

58. Shigley, J.E.; Mechanical Engineering Design: McGraw-Hill, New York, 1972

59. Skorecki,J; "The Design and Construction of an Apparatus for Measuring the Vertical Forces Exerted in Waliiking: A Gait Machine", J. of Strain Analysis, Vol 1, No 5, 1966

60. Simon, S.R., et al;"Peak Dynamic Force in Human Gait and its Attenuation by the Soft Tissues", J. of Bone and Jnt Surgery, Vol 59B, 1976

61. Spolek, C.A., Lippert, F.G., Kirkpatrick, G.S.; "An Instrumented Shoe System for Ambulatory Force Studies", Proceedings of Orthopaedic Research Society, San Fransico, March 1975

62. Statham Industries, Pasadena, California Model UL-4 & UR-5

63. Stokes, I.A.F., Stott, J.R.R., Hutton, W.C.; "Force Distributions Under the Foot A dynamic Measuring System", Biomedical Engineering, April 1974

64. Stott, J.R.R., Hutton, W.C., Stokes, I.A.F.; "Forces Under the Foot", J. of Bone and Joint Surgery, Vol 55B, No 2, May 1973

65. Thomson, W.T.; Vibration Theory and Applications: Prentice-Hall, 1965

66. Von Hippel, A.R.; Dielectrics and Waves: MIT Press, Cambridge, 1954

67. Whetsel, R.; "The Design and Mechanical Validation of a Portable Force Platform", MS Thesis, Purdue University, Lafayette, Indiana,1964

68. Whitney, R.J.; "The Strength of the Lifting Action in Man", Ergonomics, Vol 1, 1958, pp 101-127

69. Yamashita, T., Katoh, R.; "Moving Pattern of Point of Application of Vertical Resultant Force During Level Walking", J. Biomechanics, Vol 9, 1976, pp 93-99